Battelle Memorial Institute · COLUMBUS LABORATORIES

505 KING AVENUE COLUMBUS, OHIO 43201 · AREA CODE 614, TELEPHONE 299-3151 · CABLE ADDRESS: BATMIN

July 30, 1965

Gentlemen:

Final Report ASD-TDR-61-643, Part V
on Contract AF 33(615)-1311
Research on Elasto-Hydrodynamic Lubrication Effects
on High-Speed Rolling Contacts

The technical report is sent to you at the request of Research and Technology Division, United States Air Force. All correspondence pertaining to the material contained in or the distribution of this report should be directed to

Commander
Air Force Aero Propulsion Laboratory
Wright-Patterson Air Force Base
Ohio
Attention APFL

Sincerely yours,

J W Kannel

J. W. Kannel

JWK:js
Enc.

FOREWORD

This report was prepared by the Experimental Physics Division of the Battelle Memorial Institute under USAF Contract No. AF 33(615)-1311. This contract was initiated under Project No. 3044, "Aerospace Lubricants", Task No. 304401, "Turbine Engine Lubricants". The work was administered under the direction of the Fuels and Lubricants Branch, Air Force Aero Propulsion Laboratory, Research and Technology Division, with Mr. G. A. Beane, IV, acting as project engineer. This report was submitted by the authors March 18, 1965.

ABSTRACT

The effects of lubricants on the performance of heavily loaded rolling-contact elements have been studied experimentally and theoretically. Measurements of the deformations of lubricated rolling elements have been made using an X-ray technique for a range of loadings, temperatures, rolling speeds, and lubricants. A qualitative agreement appears to exist between variations in deformation profiles with lubricant types and variations in existing fatigue life with lubricant type. Efforts have been made to infer film pressures from the deformation measurements. Film pressures have been measured between steel as well as quartz disks using a manganin pressure transducer. For the heavily loaded conditions, a slight pressure spike appears in the measurements of pressures between steel disks. Stresses in the rolling elements have been inferred from the pressure measurements. The magnitudes of the maximum stresses do not deviate significantly from the Hertzian stresses although the location of the maximum shearing stress is much closer to the surface. The temperature on the surface of a pair of quartz disks has been measured using an evaporated resistance thermometer type transducer. The magnitude of the measured apparent temperature appears to be higher than anticipated resembling the peak temperature predicted assuming no heat loss from the lubricant to the disk for the pass of each fluid element through contact. Some rheology experiments have been conducted with a highly refined mineral oil.

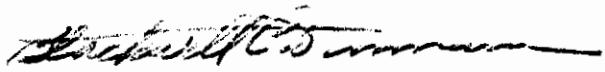

BLACKWELL C. DUNNAM, Chief
Fuels and Lubricants Branch
Technical Support Division
AF Aero Propulsion Laboratory

TABLE OF CONTENTS

	Page
INTRODUCTION	1
DEFORMATION PROFILE MEASUREMENTS	2
Technique for Measuring Deformation Profile	2
Discussion of Deformation Profile Experiments	4
Profile Measurements with a MIL-L-9236 Triester Lubricant	4
Profile Measurements with a Chlorinated Methyl Phenyl Silicone Lubricant	13
Deformation Profile Studies with a Highly Refined Mineral Oil	17
Analysis of Deformation Profile Data	17
Inferring Pressures from Deformations	23
A Sample Comparison of Lubricants	23
Observations Regarding Accuracy of Pressures Computed from Deformations	26
DIRECT CONTACT PRESSURE MEASUREMENTS	26
Contact Pressure Measurements (Glass Disks)	27
Contact Pressure Measurements (Steel Disks)	30
Development of Transducer	30
Preliminary Experiments	32
Preliminary Pressure Measurements	32
Discussion of Pressure Measurements Using Modified Technique	35
Modifications to Transducer Arrangement	35
Discussion of Pressure Experiments with an Ungrounded Circuit	35
ANALYSIS OF PRESSURE DATA	41
Computation of Deformation from Pressures	41
Comparison of Measured Deformations with Deformations Computed from Measured Pressures	44
Computations of Stresses from Measured Pressures	44
THE DETERMINATION OF THE TEMPERATURES IN THE LUBRICANT FILM	46
Discussion of Temperature Experiments	49
Analysis of the Preliminary Temperature Measurements	49
Detailed Analysis of Temperatures in Lubricant Films	54
RHEOLOGY EXPERIMENTS	54
Discussion of Experiments with a Highly Refined Mineral Oil	55
Analysis of Rheology Data	58
CONCLUSIONS	59
REFERENCES	61

TABLE OF CONTENTS
(Continued)

Page

APPENDIX A

ACCURACY OF PRESSURE FOUND FROM SURFACE DEFORMATION 62

A Method for Finding Pressure from Surface Deformation 62
Basic Theory. 62
Fitting of Polynomial Series of X-Ray Data. 64
Computation of Pressure Distributions 69
Examples of Pressure Calculations. 70
Data Selected for Analysis. 70
Analyses of Direct Experimental Data. 72
Effect of Smoothing and Interpolating 77
Calculations Based on Modified Clearance Patterns 78
A Pressure Spike 78
Minor Modifications. 81
Conclusions Concerning Accuracy of Pressure Calculations 83

LIST OF TABLES

Table		Page
1	Viscosity of Fluids Being Evaluated in Deformation Profile Studies.	6
2	Maximum Shearing Stresses in Rolling Disks Under Static and Lubricated Dynamic Conditions.	48
3	Variances Among Polynomial Fits to Experimental Data	77

LIST OF FIGURES

Figure		Page
1	Rolling-Disk Machine and X-Ray Equipment in Position for Film Measurements in Circumferential Direction	3
2	Static Profile of Unloaded Disks as Measured by X-ray Technique with a Triester Lubricant Pumped Through Contact Zone	5
3	Circumferential Profile of Rolling-Contact Disks Lubricated with a Triester Fluid, T = 175 F, RS = 2600 fpm	7
4	Circumferential Profile of Rolling-Contact Disks Lubricated with a Triester Fluid, T = 150 F, RS = 4500 fpm	8
5	Circumferential Profile of Rolling-Contact Disks Lubricated with a Triester Fluid, T = 175 F, RS = 4500 fpm	9
6	Circumferential Profile of Rolling-Contact Disks Lubricated with a Triester Fluid, T = 225 F, RS = 4500 fpm	10
7	Circumferential Profile of Rolling-Contact Disks Lubricated with a Triester Fluid, T = 175 F, RS = 6800 fpm	11
8	Circumferential Profile of Rolling-Contact Disks Lubricated with a Triester Fluid, T = 175 F, RS = 9100 fpm	12
9	Static Profile of Disks as Measured by the X-Ray Technique with a Silicone Fluid Pumped Through the Contact Region	14
10	Circumferential Profile of Rolling-Contact Disks Lubricated with a Silicone Fluid, T = 175 F; RS = 6800 fpm; P_h = 100,000, 140,000 psi (Hertz)	15
11	Circumferential Profiles of Rolling-Contact Disks Lubricated with a Silicone Fluid, T = 175 F; P_h = 100,000 psi Hertz; RS = 4500 fpm and 6800 fpm	16
12	Circumferential Profiles of Rolling-Contact Disks Lubricated with a Highly Refined Mineral Oil, T = 175 F; P_h = 80,000 psi, 100,000 psi, and 140,000 psi Hertz; RS = 6800 fpm	18
13	Circumferential Profiles of Rolling-Contact Disks Lubricated with a Highly Refined Mineral Oil, T = 175 F; P_h = 100,000 psi Hertz; RS = 2600, 4500, 6800 fpm	19
14	Circumferential Profiles of Rolling-Contact Disks Lubricated with a Highly Refined Mineral Oil, T = 150 F, 225 F; P_h = 100,000 psi, RS = 6800 fpm	20
15	Static Profile of Disks as Measured by the X-Ray Technique with a Highly Refined Mineral Oil Pumped Through the Contact Region	21

LIST OF FIGURES
(Continued)

Figure		Page
16	Comparison of Circumferential Profiles of Rolling Disks when Lubricated with Various Fluids, T = 175 F; RS = 6800 fpm; P_h = 100,000 psi (calculated maximum Hertz stress)	22
17	Corrected Circumferential Profiles of Rolling Disks when Lubricated with Various Fluids, T = 175 F; RS = 6800 fpm (9000 rpm); maximum Hertz stress = 107,000 psi.	24
18	Pressures Calculated from Circumferential Profiles for Three Lubricants, T = 175 F; RS = 6800 fpm (9000 rpm); maximum Hertz stress = 107,000 psi	25
19	Schematic Diagram of Lubricant Film Pressure-Measuring Device	28
20	Preliminary Film-Pressure Measurements (Glass Disks) for T $\tilde{-}$ 100 F and a Loading of 200 lb/in.	29
21	Preliminary Film-Pressure Measurements (Glass Disks) for T $\tilde{-}$ 100 F and a Loading of 344 lb/in.	29
22	Manganin Pressure Transducer Located on Steel Disk.	31
23	Preliminary Film Pressure Profiles Obtained Using Averaging Process for Four Loading Conditions, T = 110 F; RS = 1400 fpm	33
24	Lubricant Film Pressure Profile Obtained Using Averaging Process, P_h = 99,000 psi Hertz; T = 175 F; RS = 2520 fpm	34
25	Diagram of Modification to Pressure Measuring System (Steel Disks) to Accommodate Ungrounded Electrical Circuitry	36
26	Pressure Measurements Between Steel Disks Using Improved Pressure Measurement Technique, T = 115 F; P_h = 104,000, 116,000, and 128,000 psi Hertz; RS = 950 fpm	37
27	Pressure Measurements Between Steel Disks Using Improved Pressure Measurement Technique, T = 115 F; P_h = 104,000, 116,000, and 128,000 psi Hertz; RS = 1400 fpm.	38
28	Pressure Measurements Between Steel Disks Using Improved Pressure Measurement Technique, T = 115 F; P_h = 104,000, 116,000, and 128,000 psi Hertz; RS = 2100 fpm.	39
29	Comparison of Preliminary Pressure Profile Obtained with the Aid of an Averaging Process with a Profile by Direct Measurements, T = 115 F; RS = 1400 fpm	40
30	Measured Variation in Pressure Profile with Disk Loading, T = 115 F; RS = 1400 fpm	42

LIST OF FIGURES
(Continued)

Figure		Page
31	Variation in Pressure Profile with Rolling Speed, T = 115 F; P_h = 128,000 psi.	43
32	Comparison of Deformation Profile Computed from the Measured Pressures of Figure 17 and Measured Deformation Profile	45
33	Variation of Maximum Shearing Stress Below Surface in Rolling Elements as Calculated from Pressure Measurements, T = 115 F; RS = 1400 fpm	47
34	Preliminary Film-Temperature Measurements Using a Copper Transducer with Quartz Disks, T(ambient) = 110 F, Rolling Speed = 1400 fpm, and Loading of 149 and 246 lb/in.	50
35	Preliminary Film-Temperature Measurements Using a Copper Transducer with Quartz Disks, T(ambient) = 110 F, Rolling Speed = 1400 fpm, and a Loading of 390 lb/in. (30,000 psi Hertz).	51
36	Comparison of Measured Temperature Profile with Profile Computed Using an Adiabatic Analysis	53
37	Traction-Shear Rate Data for Highly Refined Mineral Oil, P_h = 140,000 psi Hertz; T = 175 F.	56
38	Traction-Shear Rate Data for Polyphenyl Ether, P_h = 140,000 psi, T = 175 F	57
39	Static Profile of Unloaded Disks Used for Calibration of X-Ray Measurements of Disk Separation by a Film of Highly Refined Mineral Oil	71
40	Circumferential Clearance Profile Data Used in Pressure Accuracy Study	73
41	Calculated Pressure Distributions Based on 11-Term Fits to 37-Point Tables of Particular Experimental Data, Averaged Data, and Smoothed Data.	75
42	Calculated Pressure Distributions Based on 21-Term Fits to 37-Point Tables of Particular Experimental Data, Averaged Data, and Smoothed Data.	76
43	Modified Circumferential Clearance Profile Used for Pressure Sensitivity Study	79
44	A Pressure Distribution Containing a Spike, as Computed from Series of Various Lengths Based on a Smooth 289-Point Table (Modification 1).	80
45	Effect of Minor Clearance Changes on Calculated Pressure Distribution.	82

NOMENCLATURE

a	Half width of reference region or minor axis of contact ellipse
a_h	Half width of Hertz contact pressure region
b	Minor axis of contact ellipse
c	Specific heat
E	Defined by $\frac{1 - \nu_1^2}{E_1} + \frac{1 - \nu_2^2}{E_2}$
E_1, E_2	Moduli of elasticity of disks
F_T	Tractive Force
h	Film thickness
J	Factor for converting heat into its mechanical equivalent
K	Thermal conductivity
P	Pressure
P_h	Maximum Hertz contact pressure
q	$2R\ (1 - \nu^2)P/aE$
R.S.	Rolling speed
R	Defined by $1/R = 1/R_1 + 1/R_2$
R_1, R_2	Radii of disks
T	Temperature
T_n	Tchebyshev polynomial of first kind
U_n	Tchebyshev polynomial of second kind
u	Surface velocity of disks
W'	Disk loading
x	Coordinate variable in direction of rolling
X	x/a_h
α	Defined by $\mu = \mu_o\ e^{-\alpha T}$
α_n	Fourier coefficient
β	Coefficient of thermal expansion
δ	Elastic displacement
ξ	x/a
μ	Viscosity
μ_o	Base viscosity
γ	Defined by $\mu = \mu_o\ e^{\gamma P}$
$\nu_1 \nu_2$	Poisson's ratio of disks
σ_x, σ_y	Normal stresses
τ_{xy}	Shear stress
ρ	Lubricant density

RESEARCH ON ELASTOHYDRODYNAMIC LUBRICATION EFFECTS ON HIGH-SPEED ROLLING CONTACTS

by

J. W. Kannel, J. C. Bell, J. A. Walowit,
O. A. Ullrich, and C. M. Allen

INTRODUCTION

Research is being conducted to determine the influence of lubricants on the performance of high-speed, heavily loaded, lubricated rolling contacts. The objective of the study is to determine the relationship between the endurance of lubricated rolling-contact elements such as rolling-element bearings and the properties of the lubricants employed. The study is being conducted on a continuing basis; the efforts reported here represent the research completed during the year ending in February, 1965.

Early in the research program, an X-ray technique was developed[1]* for measuring the thickness of the lubricating film between a pair of crowned, rolling disks designed such that their contact zone simulated the contact region in a typical engine bearing. From the film measurements, it was found that bearing-lubrication theories were valid for predicting the thickness of the film between rolling elements for moderately low rolling speeds; at higher rolling speeds, the theories consistently predicted films that were thicker than were observed.

One reason postulated for the disagreement between the experimental and theoretical film thicknesses at high rolling speeds is that the lubricant does not follow the simple Newtonian model as typically assumed in the theories. A film-thickness theory was subsequently devised under the program incorporating a non-Newtonian (Ree-Eyring) lubricant[2] model. Also, a technique was developed for measuring the rheological properties of a lubricant under rolling-contact conditions[3] employing a rolling-disk-type viscometer.

More recently, efforts have been directed towards determining the effect of the lubrication process on the deformation and fatigue-inducing stresses in the rolling elements. The stresses are being inferred from film-pressure measurements. Two techniques have been devised for these pressure measurements; one technique consists of determining the deformations of the rolling disks by measuring circumferential film profiles, using the X-ray technique, and then inferring the pressures from the deformations. The second method for determining film pressures consists of using a manganin-pressure transducer located on the surface of one of the rolling disks.

In the study reported here, deformations of the rolling disk when lubricated with various fluids under several operating conditions have been obtained using the X-ray technique. Film pressures have been inferred from these deformations. Film pressures have been measured between steel disks using the manganin-pressure transducer. Disk stresses have been inferred from these measurements. Experimental and theoretical studies have been made to determine the temperatures in the lubricating film. Rheology experiments of the type discussed in Reference 3 have been conducted.

---

*References on page 61.

DEFORMATION PROFILE MEASUREMENTS

The stresses in cylindrical elements, heavily loaded together under lubricated rolling contact, can be significantly altered from the stress-patterns which exist when the elements are simply loaded together in dry static contact. This alteration in the stress patterns can vary notably with the rolling condition and type of lubricant employed. The deformed shape of the surfaces of the rolling elements, too, will deviate considerably from the flat dry contact shape concomitantly with this alteration of the stress pattern. Since the stresses in rolling-contact elements should be expected to control the fatigue life of those elements, a measure of the deformations can provide data which, by careful analysis, can be used for predicting the life of rolling contacts.

Technique for Measuring Deformation Profile

The rolling-disk machine used in the deformation profile studies has been described previously[4] and is shown schematically in Figure 1.

An X-ray beam passes through an 0.003-in.-wide aperture in a tantalum plate located near the contact region of the disks. The X-rays which then pass through the contact region are related to the gap between the disks and are detected by a scintillation counter. This gap (film thickness) can be determined as a function of circumferential position by moving the slit across the contact region with the micrometer adjustment. The deviation of the film thickness profile from the initial (cylindrical) shape of the disks is a manifestation of the pressures in the lubricant film. These profiles can be interpreted in terms of the film pressures acting on the disks and from them can be derived the stresses in the disks which are significant to the fatigue life of the disks.

The disks used in the study are 2.88 inches in diameter and contain 36-inch-radii transverse crowns. These disks are driven by high-frequency induction motors with the rotors mounted on the same shaft as the disks. Speed is controlled in the apparatus by varying the input frequency to the motors by a special high-frequency generator system (the speed of each disk can be controlled independently).

The disk temperature is monitored by a thermocouple located 0.005 inch from the disk surface.[5] A vacuum is used to aspirate the lubricant clinging to the disk surface over the thermocouple. The principal means of attaining specified temperatures in the disks is by means of induction-heating coils surrounding the disks' driving shafts in the contact zone. Good temperature control is obtained with this system. However, since the X-ray detection equipment also detects the output from the induction heating apparatus, the X-ray counting and the disk heating cannot be done concurrently.

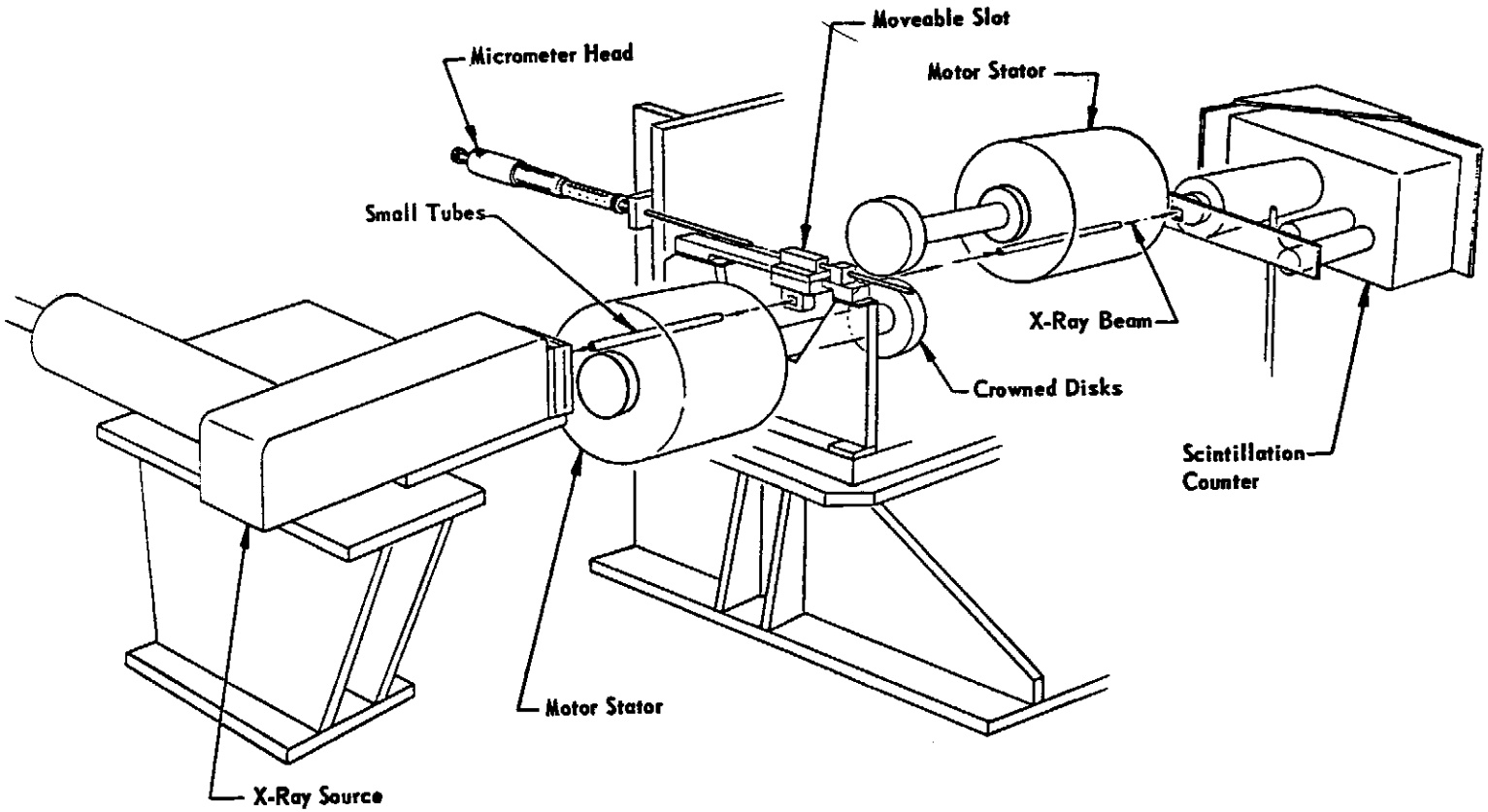

FIGURE 1. ROLLING-DISK MACHINE AND X-RAY EQUIPMENT IN POSITION FOR FILM MEASUREMENTS IN CIRCUMFERENTIAL DIRECTION

Since X-rays are emitted at a random rate, the X-ray level for each micrometer setting must be determined by time-averaging the detected X-rays. During an experiment, first the X-rays corresponding to each micrometer setting are averaged over a 30-sec interval, then the temperature-control unit is actuated for 25 sec. A 5-sec lag time occurs between heating and X-ray counting to eliminate residual noise due to the heating unit. Sixty seconds are thus required to measure the X-ray level (corresponding to the film thickness) for each micrometer setting.

The calibration of the X-ray system to convert the measurements from X-ray counts to microinches of film thickness is obtained by using a measured X-ray profile of the disks in an unloaded, static condition. The known shape of the disks is compared with this sequence of X-ray counts. A typical measured static profile of the disks is given in Figure 2. During the measurement of the calibration profile, lubricant is pumped into the contact zone in the same manner as during rolling-contact experiments, so as to maintain the same attenuation of the X-rays by the lubricant. One error not accounted for in this method of calibration occurs as a result of cavitation of the lubricant, causing the X-ray absorption to vary somewhat with position.

Discussion of Deformation Profile Experiments

Film profile measurements are being obtained for several fluids as supplied by the Air Force Aero Propulsion Laboratory including

polyphenyl ether (5P4E)
triester, MIL-L-9236, fluid
highly refined mineral oil
chlorinated methyl phenyl silicone fluid
diester MIL-L-7808 fluid.

Viscosity temperature data as obtained with a capillary tube viscometer are given in Table 1. Previously, data have been obtained with the polyphenyl ether[4]. This report presents data for the triester, the silicone, and the highly refined mineral oil fluids.

Profile Measurements with a MIL-L-9236 Triester Lubricant

A series of dynamic profiles of the contact region of the rolling disks in lubricated rolling contact are given in Figures 3 through 8 with a triester (MIL-L-9236) fluid as the lubricant; the average values of the X-ray count-rate level for each micrometer setting are presented as points in these data. The calibration of the data from X-ray count rate to film thickness was taken from the curve of Figure 2. The location of the vertical scale was taken as the micrometer setting (on the micrometer-slit adjustment) for the center of the contact region as determined from the static profile. The data are essentially recorded X-ray counts as a function of position subjected only to a linear calibration for film thickness. No corrections for X-ray beam width, variation in X-ray intensity, or variations in X-ray absorption by the lubricant have been made in these data.

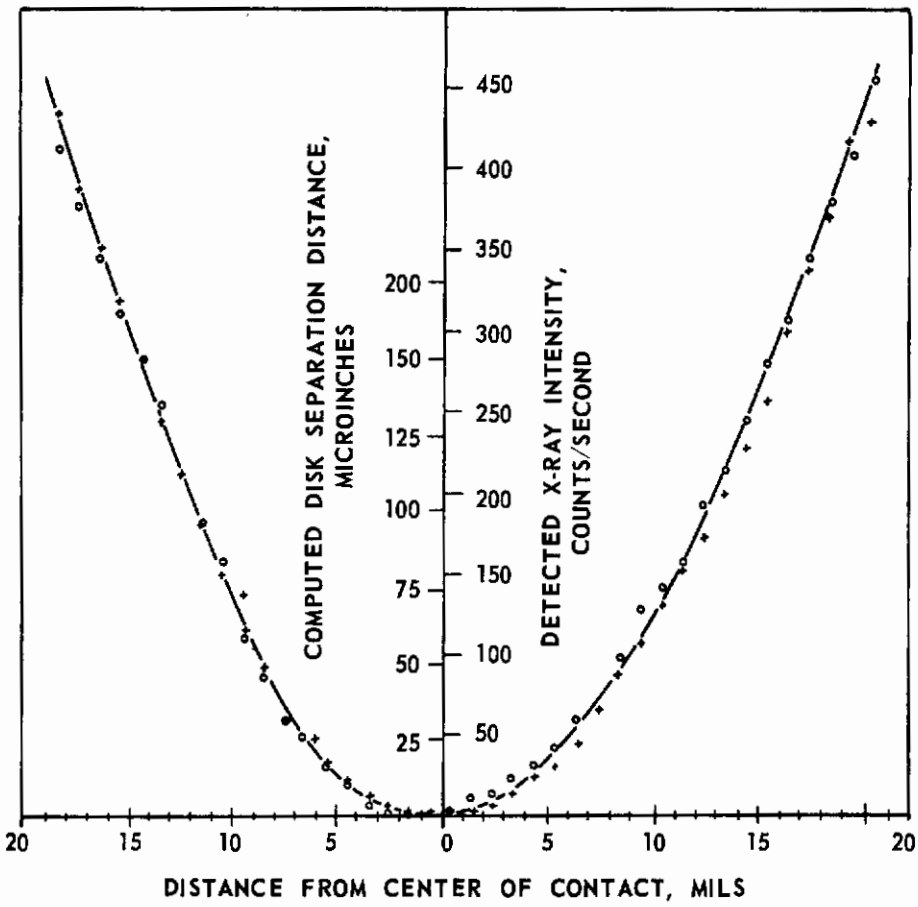

FIGURE 2. STATIC PROFILE OF UNLOADED DISKS AS MEASURED BY X-RAY TECHNIQUE WITH A TRIESTER LUBRICANT PUMPED THROUGH CONTACT ZONE

TABLE 1. VISCOSITY OF FLUIDS BEING EVALUATED IN DEFORMATION PROFILE STUDIES

Fluid	Kinematic Viscosity, cs	
	100 F	210 F
Polyphenyl Ether	306.0	11.5
Triester (MIL-L-9236)	15.4	3.5
Highly Refined Mineral Oil	50.8	6.8
Chlorinated Methyl Phenyl Silicone Fluid	56.6	18.5
Diester (MIL-L-7808)	12.9	3.3

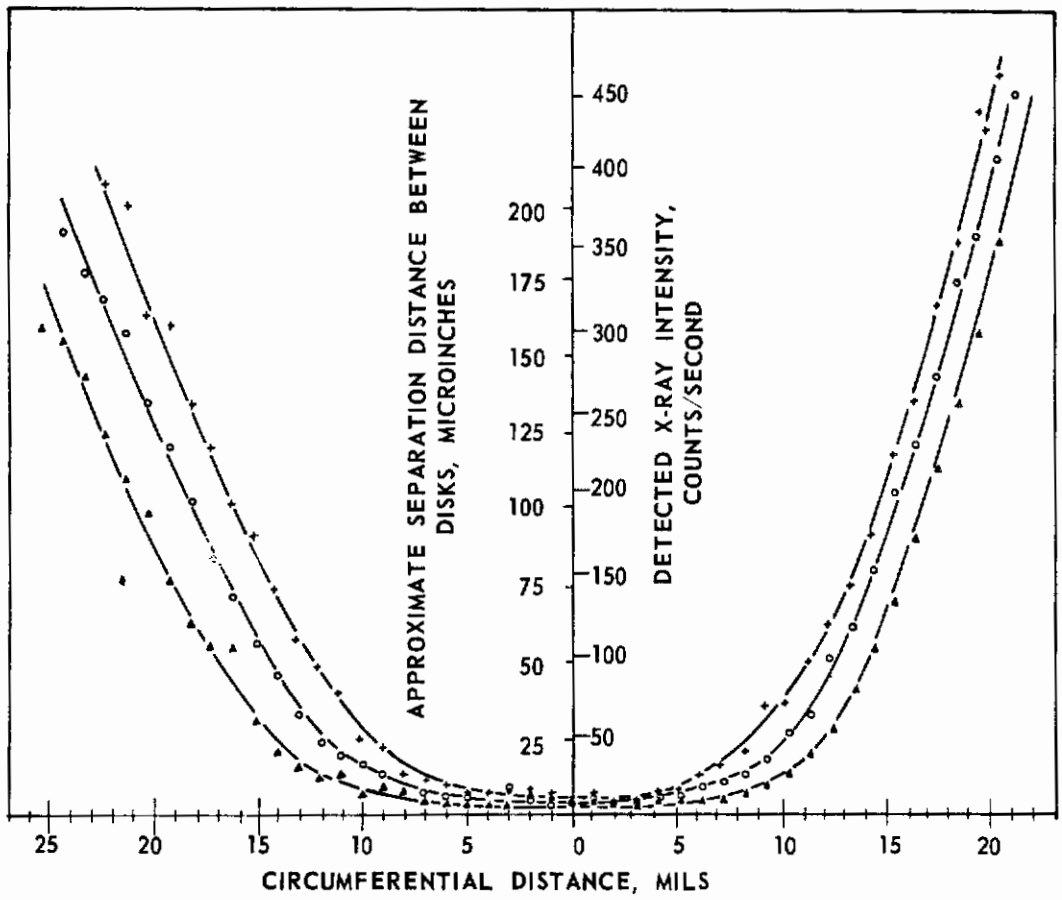

FIGURE 3. CIRCUMFERENTIAL PROFILE OF ROLLING-CONTACT DISKS LUBRICATED WITH A TRIESTER FLUID

T = 175 F, RS = 2600 fpm.

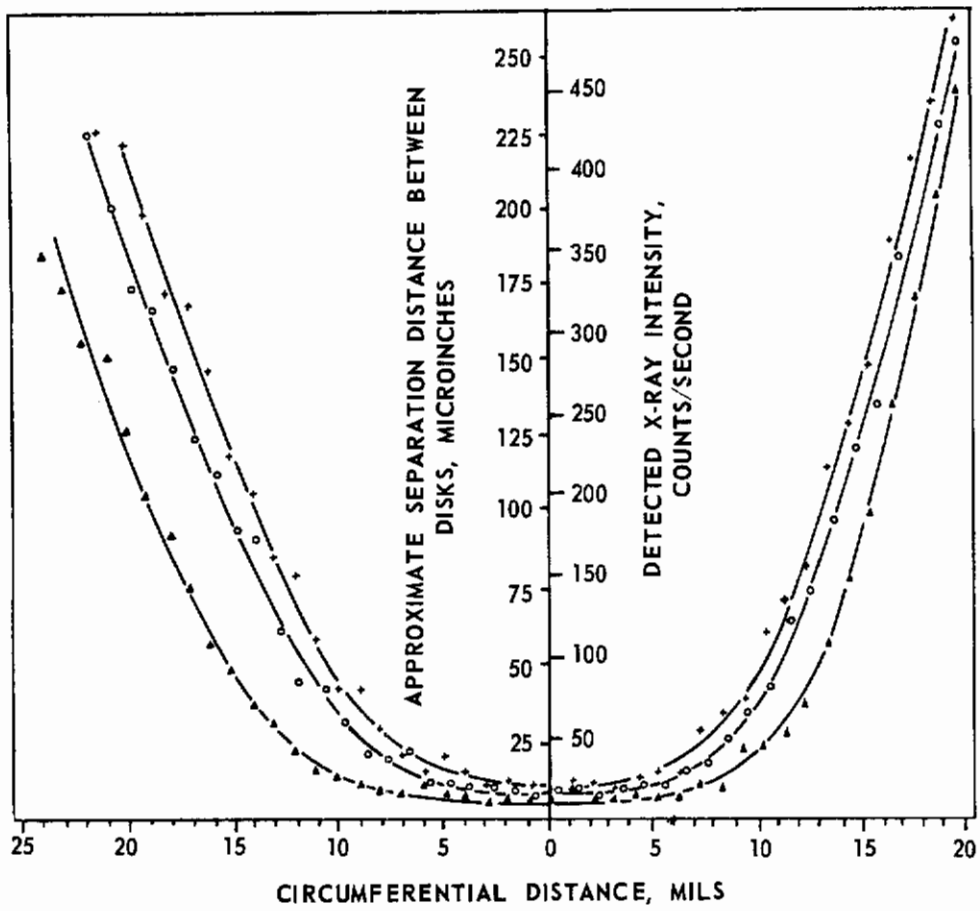

FIGURE 4. CIRCUMFERENTIAL PROFILE OF ROLLING-CONTACT DISKS LUBRICATED WITH A TRIESTER FLUID

T = 150 F, RS = 4500 fpm.

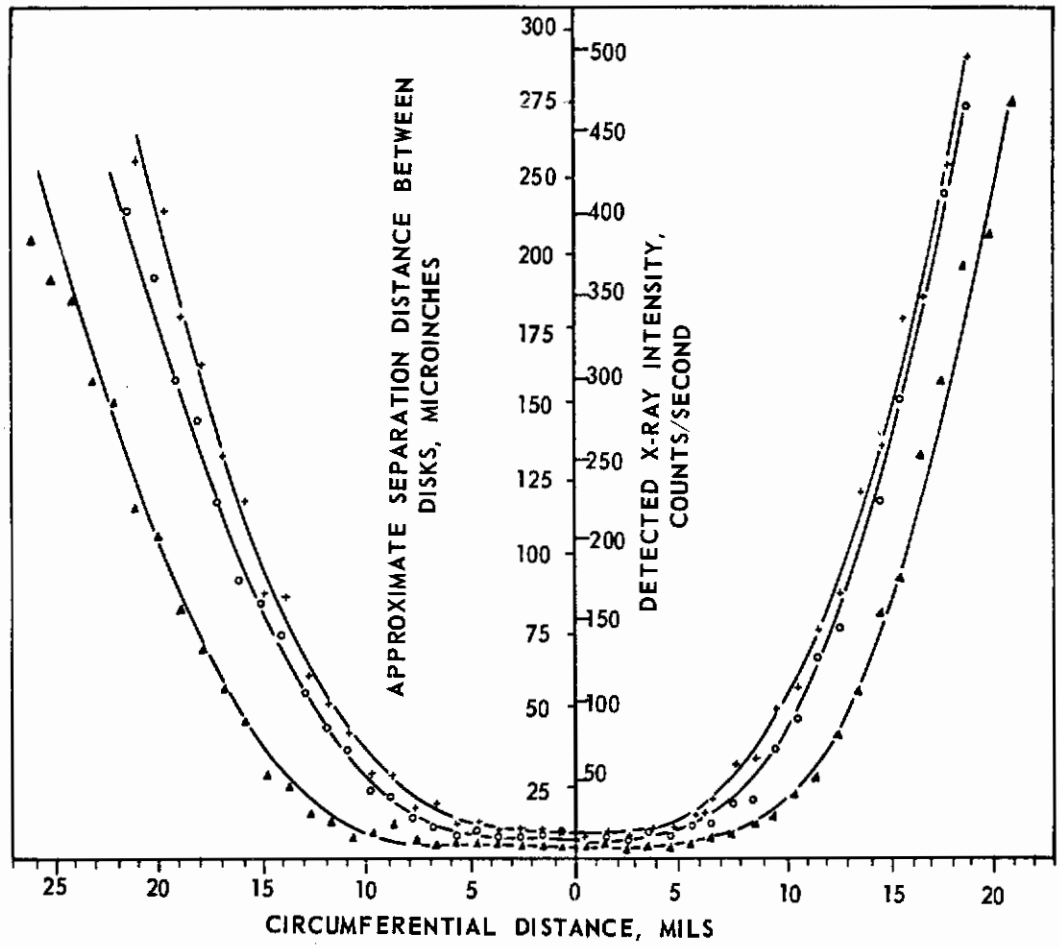

FIGURE 5. CIRCUMFERENTIAL PROFILE OF ROLLING-CONTACT DISKS LUBRICATED WITH A TRIESTER FLUID

T = 175 F, RS = 4500 fpm.

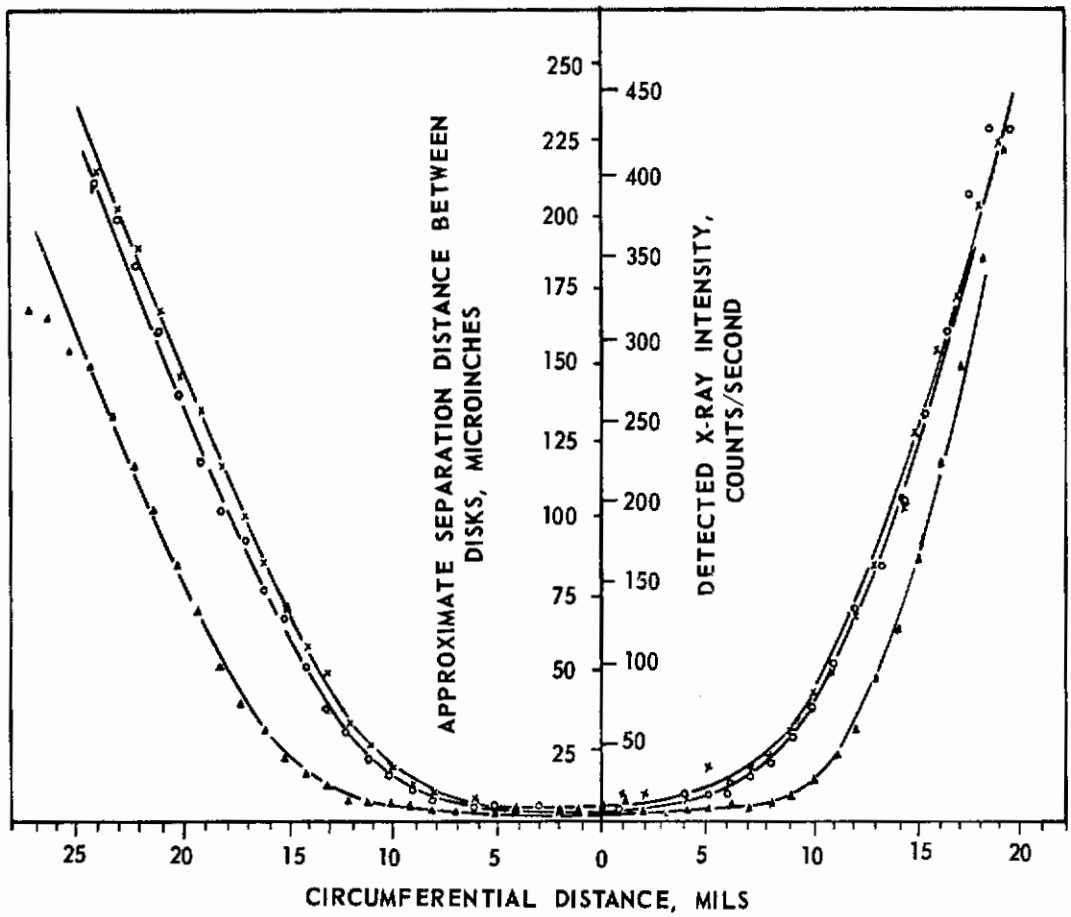

FIGURE 6. CIRCUMFERENTIAL PROFILE OF ROLLING-CONTACT DISKS LUBRICATED WITH A TRIESTER FLUID

T = 225 F, RS = 4500 fpm.

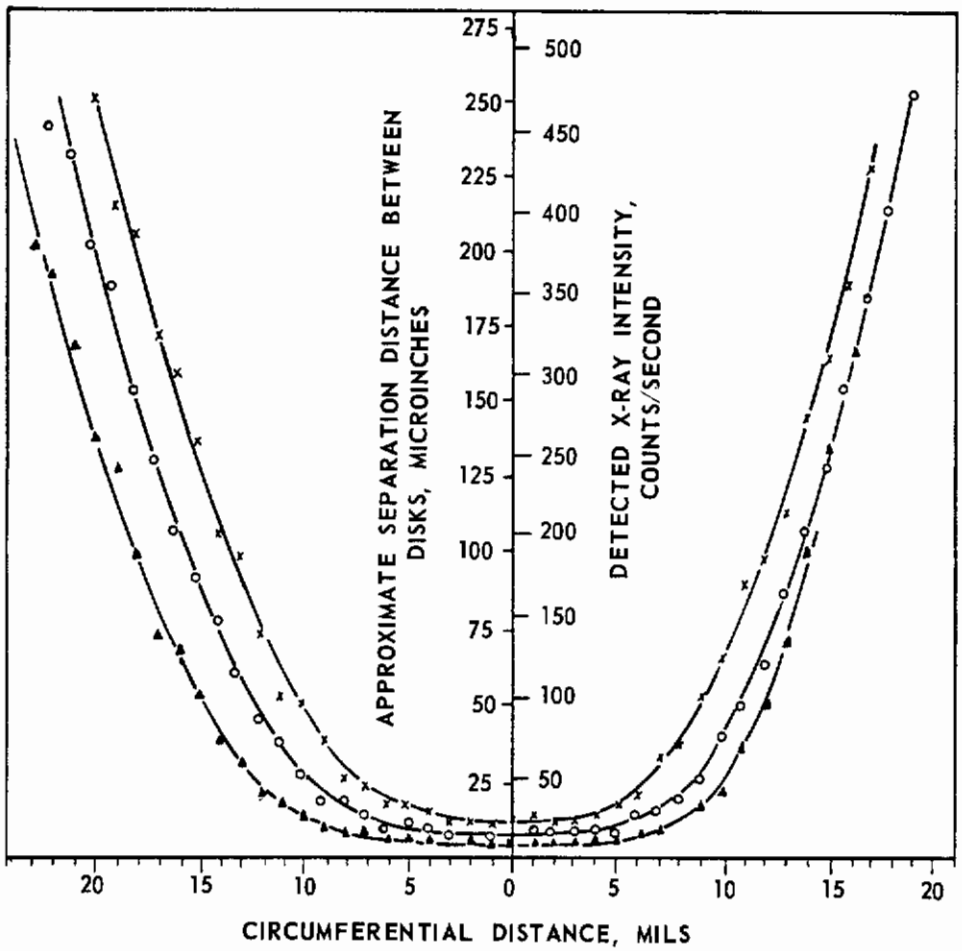

FIGURE 7. CIRCUMFERENTIAL PROFILE OF ROLLING-CONTACT DISKS LUBRICATED WITH A TRIESTER FLUID

T = 175 F, RS = 6800 fpm.

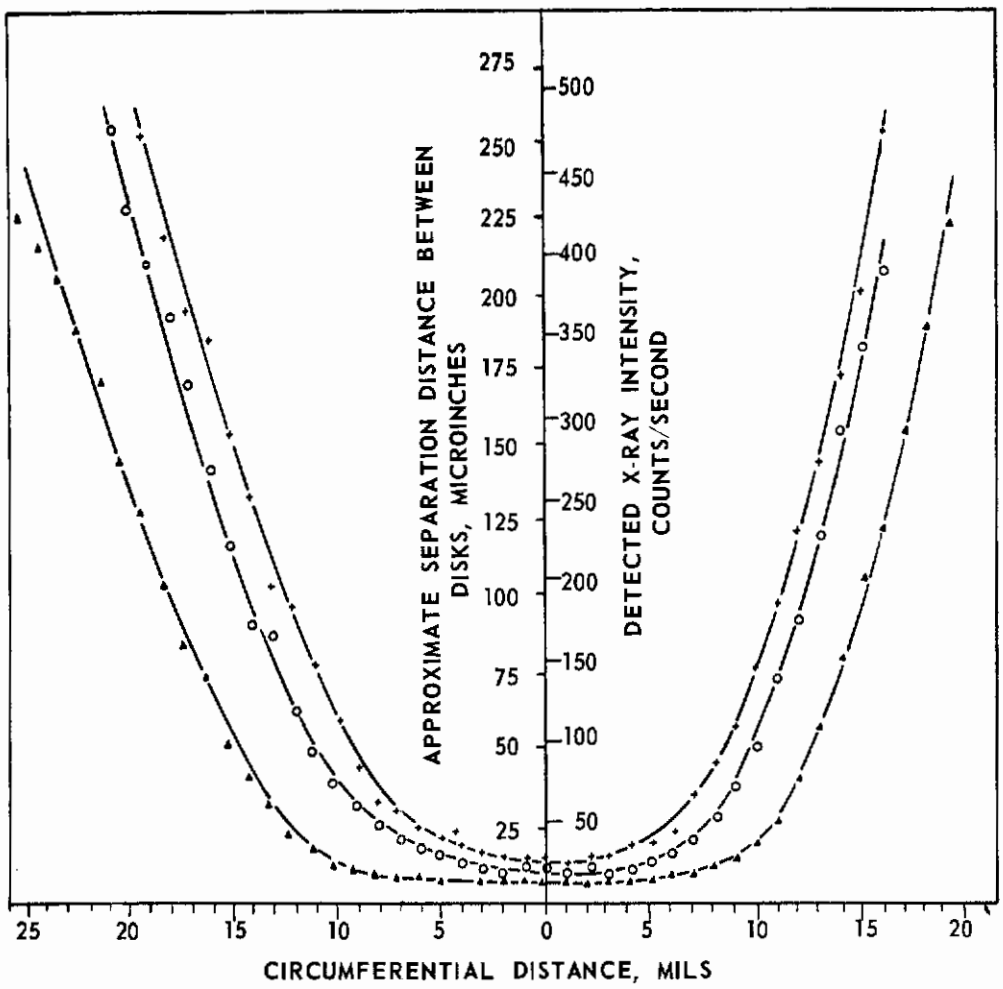

FIGURE 8. CIRCUMFERENTIAL PROFILE OF ROLLING-CONTACT DISKS LUBRICATED WITH A TRIESTER FLUID

T = 175 F, RS = 9100 fpm.

The data presented do appear to be consistent in that

(1) An increase in loading (maximum calculated Hertz stress) causes a thinning of the lubricant film and a spreading of the profile for data taken under otherwise identical conditions. Presumably the size of the contact area should increase with increasing load.

(2) As the temperature increases, some decrease in the film thickness and spreading of the profiles (at least in the center region) can be observed for data taken under otherwise identical operating conditions. In that an increase in temperature is accompanied by a decrease in viscosity, such trends might be anticipated (at least qualitatively).

(3) As the rolling speeds are increased, the film thickness increases and the profiles become more narrow (at least in the center region) for the data with otherwise identical operating conditions. This is consistent with the results of References 4 and 5 and the theoretical work such as reported in Reference 6.

Profile Measurements with a Chlorinated Methyl Phenyl Silicone Lubricant

Some difficulties have been encountered in obtaining deformation profile data by the X-ray technique with the silicone fluid as a lubricant because of the high degree of absorption of the X-rays by this fluid. The other lubricants evaluated thus far typically decreased the intensity of the X-rays being transmitted through the gap between the disks by about 65 per cent; the silicone fluid decreases the intensity by almost 99 per cent. One problem associated with this high absorption characteristic of the silicone fluid is that a very high gain setting on the X-ray detection unit is required to detect the film thickness signal and hence, difficulties associated with background interference are manifestly increased. The relationship between film thickness and X-ray count rate shown in the calibration profile for the silicone fluid, Figure 9, in comparison with this same relationship as shown for the triester fluid in Figure 2, demonstrates the extremely high rate of X-ray absorption by the silicone fluid. The scatter in the data of Figure 9 versus the scatter in Figure 2 demonstrates the uncertainties attributed to the required high gain settings.

The absorption of the X-rays by the fluids introduces uncertainties in the calibration of the data in the region where the lubricant cavitates near the exit end of the contact zone, because in this region the absorption of the X-rays by the fluids diminishes to almost zero. The larger the absorption factor of the fluid the greater these uncertainties due to cavitation would be expected to be. The cavitation, then, is a very serious problem associated with the silicone fluid.

The difficulties associated with X-ray absorption tend to make quantitative interpretation of the deformation profile data using a silicone lubricant very difficult. Some profiles have been, however, obtained to determine qualitative information on the effect of a silicone fluid on the performance of rolling-contact elements and are given in Figures 10 and 11.

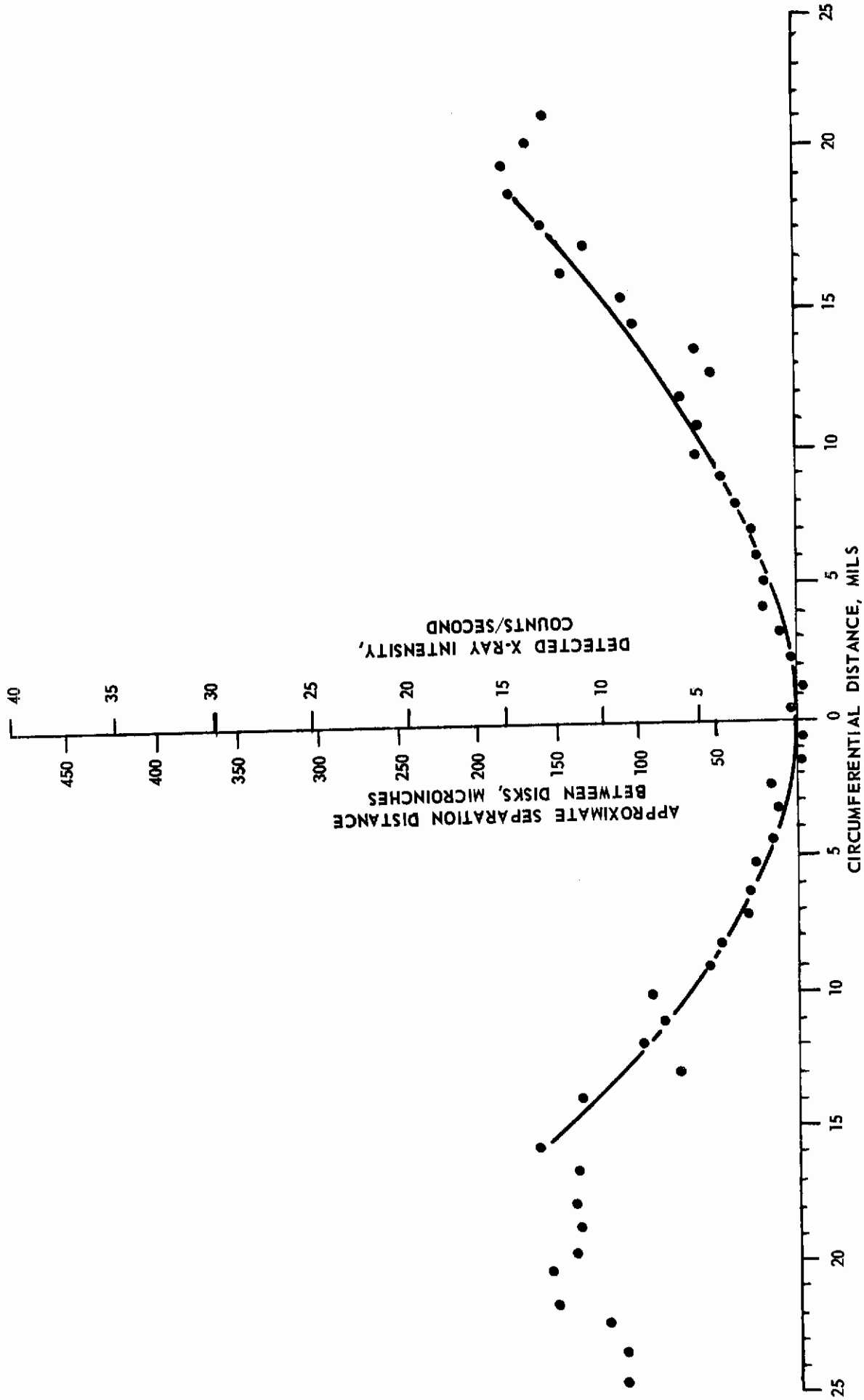

FIGURE 9. STATIC PROFILE OF DISKS AS MEASURED BY THE X-RAY TECHNIQUE WITH A SILICONE FLUID PUMPED THROUGH THE CONTACT REGION

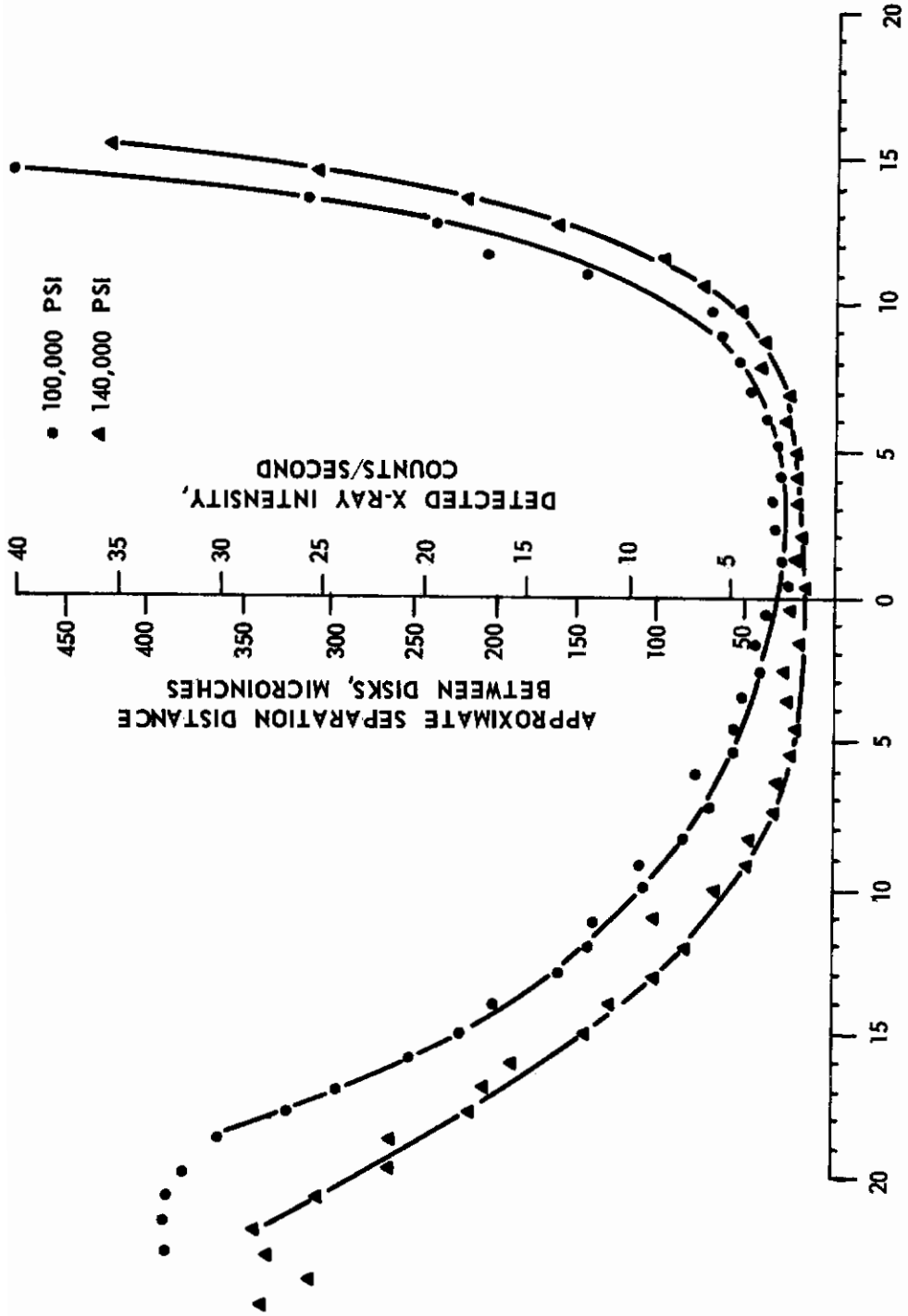

FIGURE 10. CIRCUMFERENTIAL PROFILE OF ROLLING CONTACT DISKS LUBRICATED WITH A SILICONE FLUID

T = 175 F; RS = 6800 fpm; P_h = 100,000, 140,000 psi (Hertz).

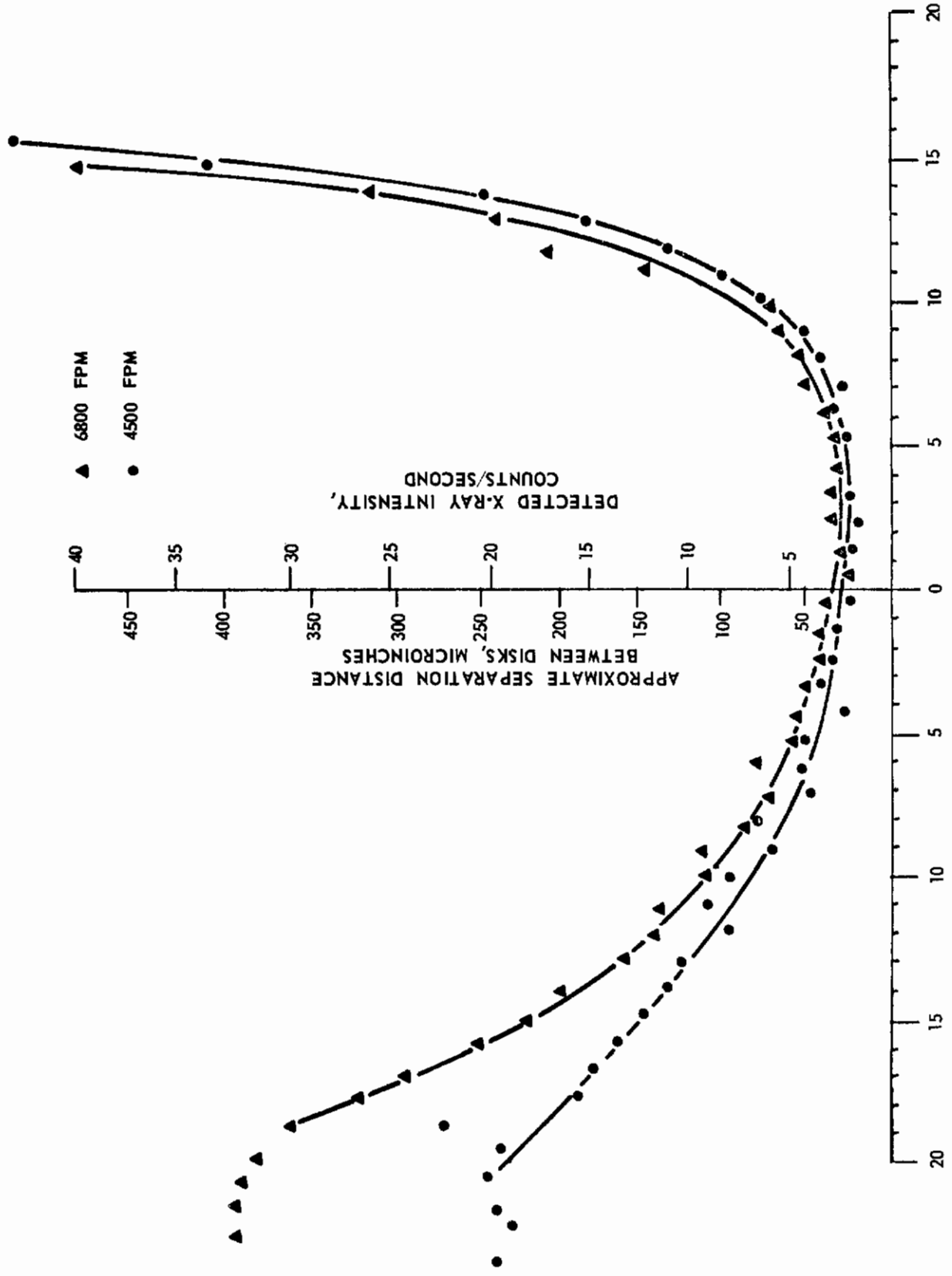

FIGURE 11. CIRCUMFERENTIAL PROFILES OF ROLLING-CONTACT DISKS LUBRICATED WITH A SILICONE FLUID

T = 175 F; P_h = 100,000 psi Hertz; RS = 4500 fpm and 6800 fpm.

Deformation Profile Studies with a Highly Refined Mineral Oil

The highly refined mineral oil is an SAE 20 straight mineral oil (paraffinic)*. Deformation profile data recorded with the mineral oil are given in Figures 12-14. The static calibration profile is given in Figure 15. The experiments conducted with this fluid have been quite reproducible and the data have appeared reasonable.

Analysis of Deformation Profile Data

The measured deformation profiles of the rolling disks furnish an indication of the stresses that exist in the rolling elements as well as an indication of the pressures in the lubricant film. A qualitative correlation between the performance of rolling elements lubricated with various fluids should be possible simply by comparing the profiles of the lubricated rolling elements. For example, the more the profiles are flattened out the more concentrated the film pressures might be expected to be and hence the more severe the stresses. The more rounded the profiles are the more spread out the pressure profile should be and the lower the stresses should be with the exception of any severe very localized effects such as high-pressure spikes as predicted by various theories such as Dowson.[6]

The effects of four lubricants (polyphenyl ether[4], a triester, a silicone, and the highly refined mineral oil) on the deformation of the rolling disks are shown in Figure 16; here temperature, T = 175 F, rolling speed, RS = 6800 fpm, and the loading is 100,000 psi Hertz. The uncertainties associated with the calibration due to cavitation(especially with the silicone fluid) near the trailing edge of the contact zone make completely accurate comparisons of these data difficult. Also it should be remembered that absorption of the X-rays makes the profile using the silicone fluid somewhat questionable. However, based on the relative minimum film thicknesses and the curvatures at the inlet and center regions, it appears that the performance ranking of rolling (only) contact elements lubricated with these fluids (starting with the best) might be the silicone, the polyphenyl ether, the highly refined mineral oil, and the triester fluids.

More exact comparisons of the effects the lubricants exert on rolling-contact elements, using the measured deformation profile data, can be made least theoretically by inferring the film pressures and contact-disk stresses from the measurements and comparing the pressure and stresses. Computed film pressures have been reported from the polyphenyl ether data[2] and some computations have been made to determine pressures from other data (avoiding, however, the silicone fluid data).

---

*A different batch of this same oil was described in Reference 7, 1963.

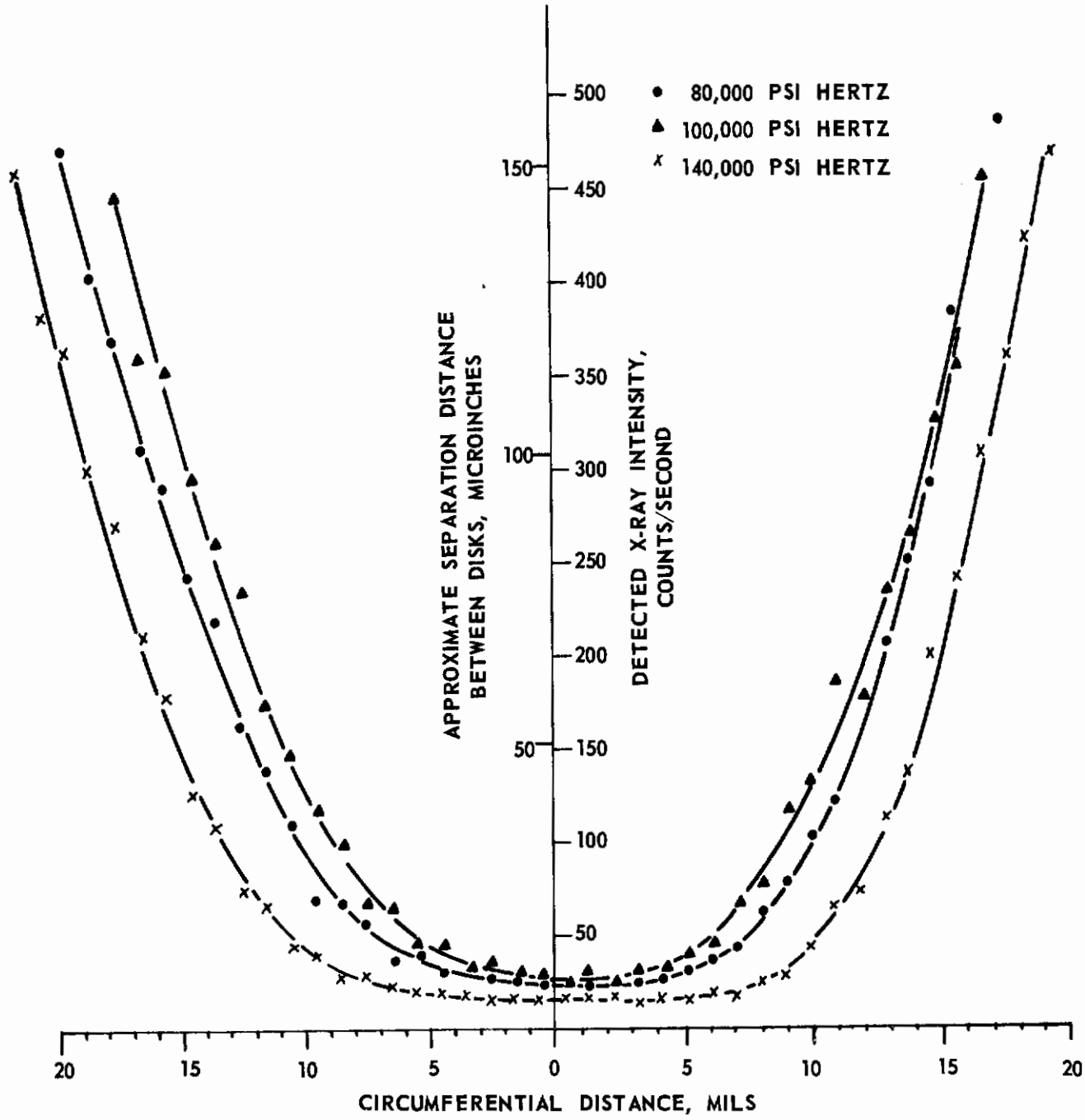

FIGURE 12. CIRCUMFERENTIAL PROFILES OF ROLLING-CONTACT DISKS LUBRICATED WITH A HIGHLY REFINED MINERAL OIL

T = 175 F; P_h = 80,000 psi, 100,000 psi, and 140,000 psi Hertz; RS = 6800 fpm.

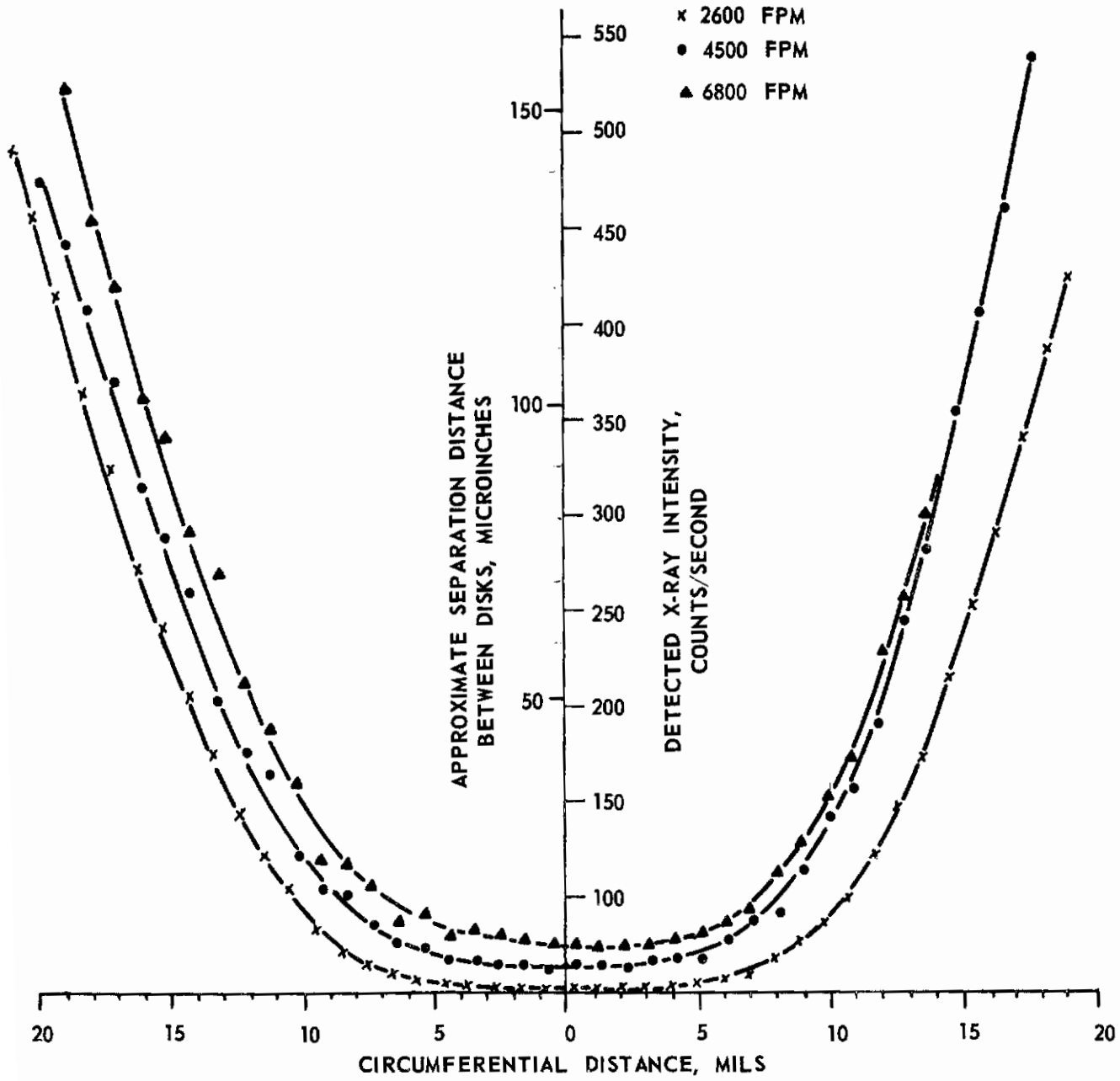

FIGURE 13. CIRCUMFERENTIAL PROFILES OF ROLLING-CONTACT DISKS LUBRICATED WITH A HIGHLY REFINED MINERAL OIL

T = 175 F; P_h = 100,000 psi Hertz; RS = 2600, 4500, 6800 fpm.

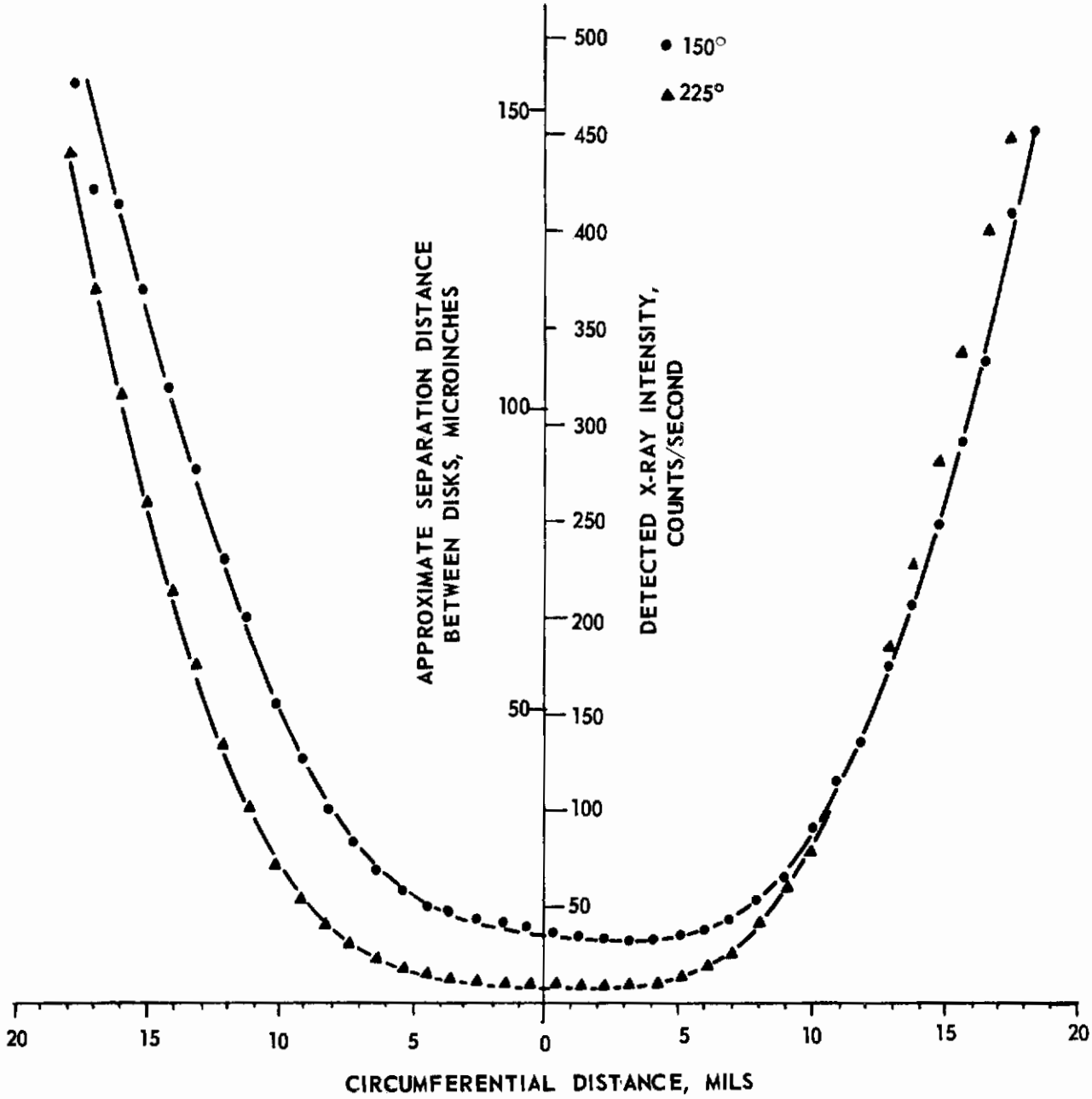

FIGURE 14. CIRCUMFERENTIAL PROFILES OF ROLLING-CONTACT DISKS LUBRICATED WITH A HIGHLY REFINED MINERAL OIL

T = 150 F, 225 F; P_h = 100,000 psi; RS = 6800 fpm.

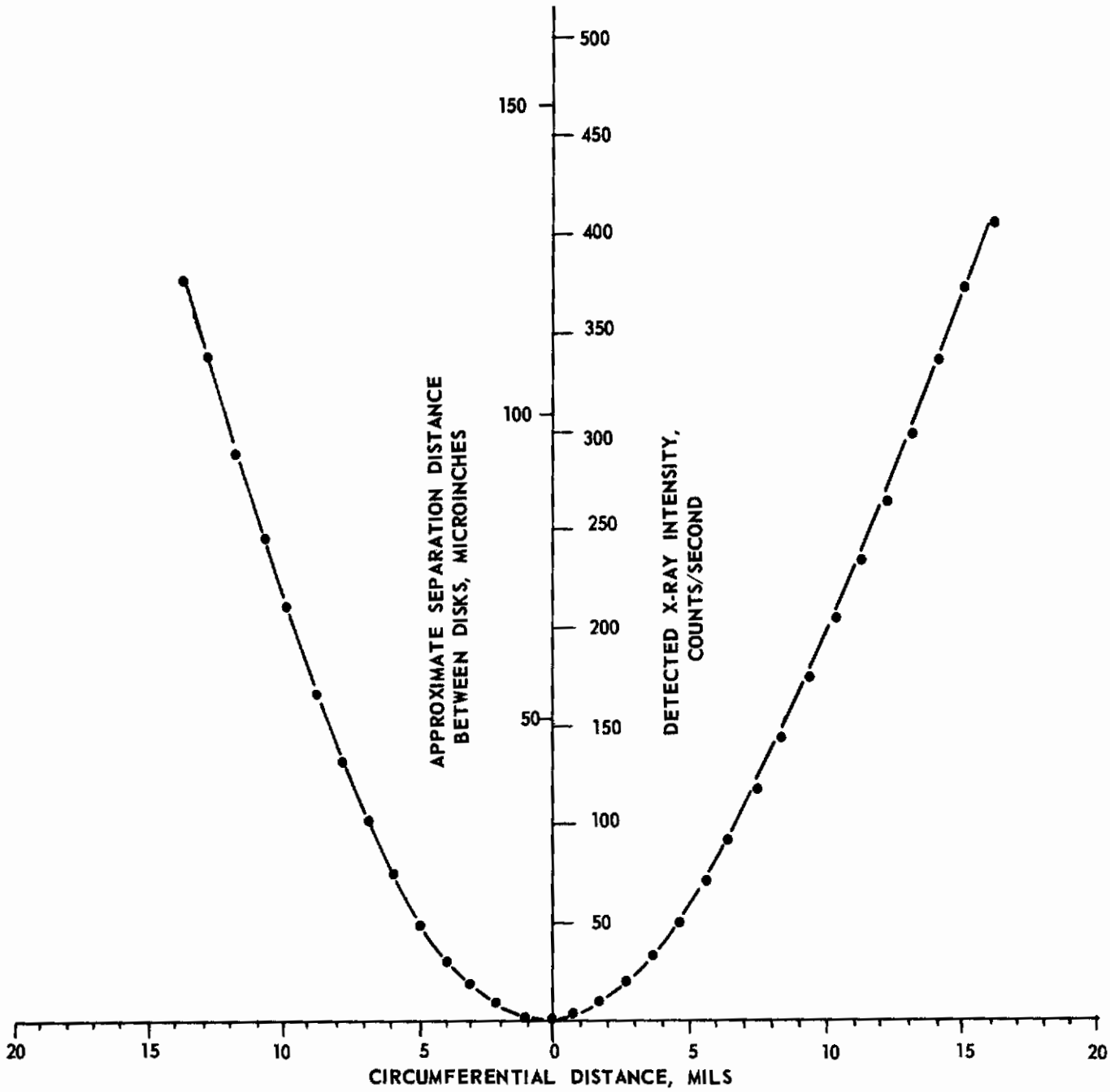

FIGURE 15. STATIC PROFILE OF DISKS AS MEASURED BY THE X-RAY TECHNIQUE WITH A HIGHLY REFINED MINERAL OIL PUMPED THROUGH THE CONTACT REGION

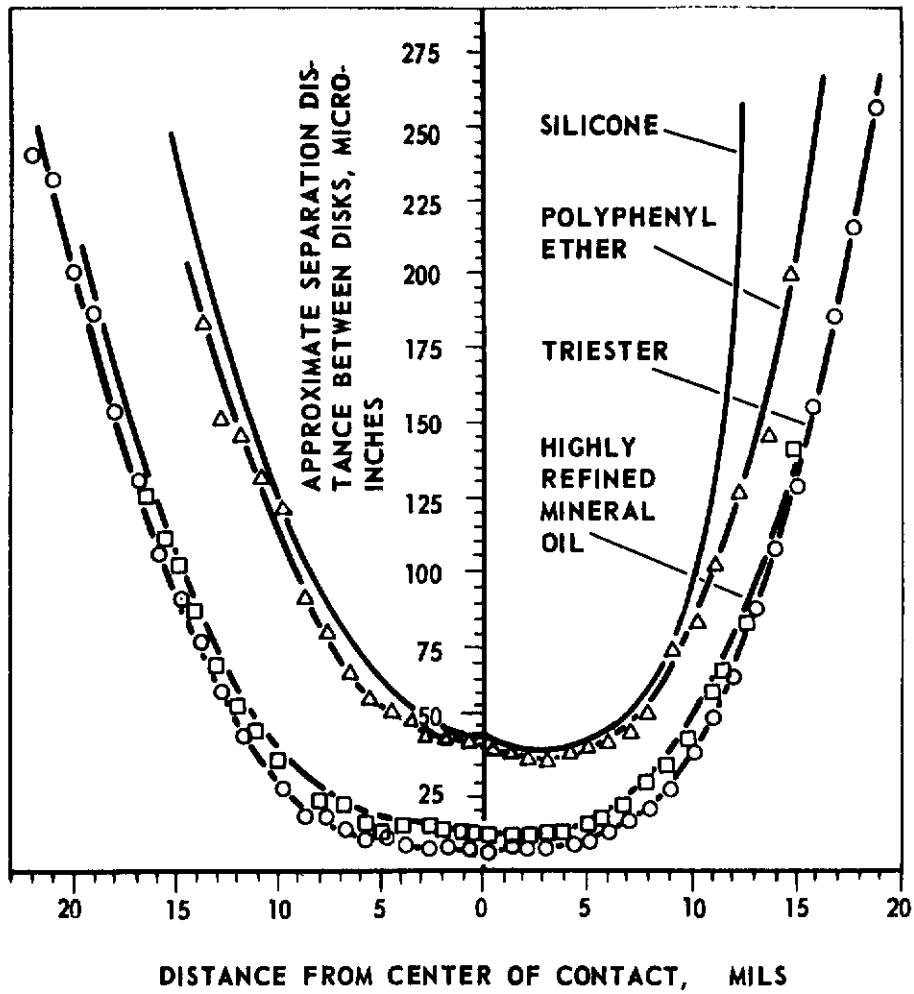

FIGURE 16. COMPARISON OF CIRCUMFERENTIAL PROFILES OF ROLLING DISKS WHEN LUBRICATED WITH VARIOUS FLUIDS

T = 175 F; RS = 6800 fpm; P_h = 100,000 psi (calculated maximum Hertz stress).

Inferring Pressures from Deformations

A Sample Comparison of Lubricants

Formulas to be used in inferring film pressures from deformation data have been provided in earlier publications.(4) These formulas depend on the knowledge of actual disk separation profiles, that is to say on profiles unconfused with variations of X-ray beam intensity or X-ray absorption by the lubricant. Therefore, a necessary preliminary step in deducing pressures from data such as those in Figure 16 is to correct them for those two variations in the X-ray measuring system. A method for doing this has been prepared and is described in Appendix A. Applying it to the data shown in Figure 16 yields corrected disk separation measurements shown in Figure 17. (Further correction accounting for finite width of the X-ray beam might be applied, but this is omitted for the present. Note also that the estimate of maximum pressure has also been refined.) It can be seen here that the profiles for the highly refined mineral oil and for the triester are nearly the same except for a small translation to one side, so they suggest nearly equal pressure distributions. The profile for polyphenyl ether is narrower, suggesting a more nearly uniform pressure distribution, hence one with a lower maximum pressure.

Use of data such as those in Figure 17 for pressure calculations has been reduced to a process which is quite mechanical except for choice of the number of terms to be used in a series representation of the pressure, and also except for possible revisions of the table of disk separations. This method is described in Appendix A. Applying it to the discrete clearance measurements shown in Figure 17 and using 11-term Tchebyshev polynomial series to represent the clearance data, pressure distributions were calculated which are shown in Figure 18. It is interesting to observe that, in ascending order, the maximum pressures attained for the three lubricants are those for polyphenyl ether, for highly refined mineral oil, and for the triester. This is the same as the order of merit that was deduced qualitatively from Figure 16.

Actually, the order of merit suggested by Figure 18 is not as clear as it seems at first glance. Calculations of this sort converge irregularly with increasing length of their series, and intermediate representations often predict an erroneous total load. In this instance, the 11-term series that were used lead to theoretical loads that were respectively for the polyphenyl ether, the highly refined mineral oil, and the triester were 96,122, and 119 per cent of the known applied load. Since the indicated maximum loads were about 78,000, 102,000, and 104,000 psi in these three cases, reduction of these maxima in proportion to the percentage of loads predicted would make the corrected maxima be 81,000, 84,000, and 88,000 psi, respectively. Thus, even after this adjustment, the order of merit among these lubricants remains the same. However, the change in the difference between the quantitative rating here shows the danger in making loose evaluations of orders of merit on the basis of casual inspection of disk separation data.

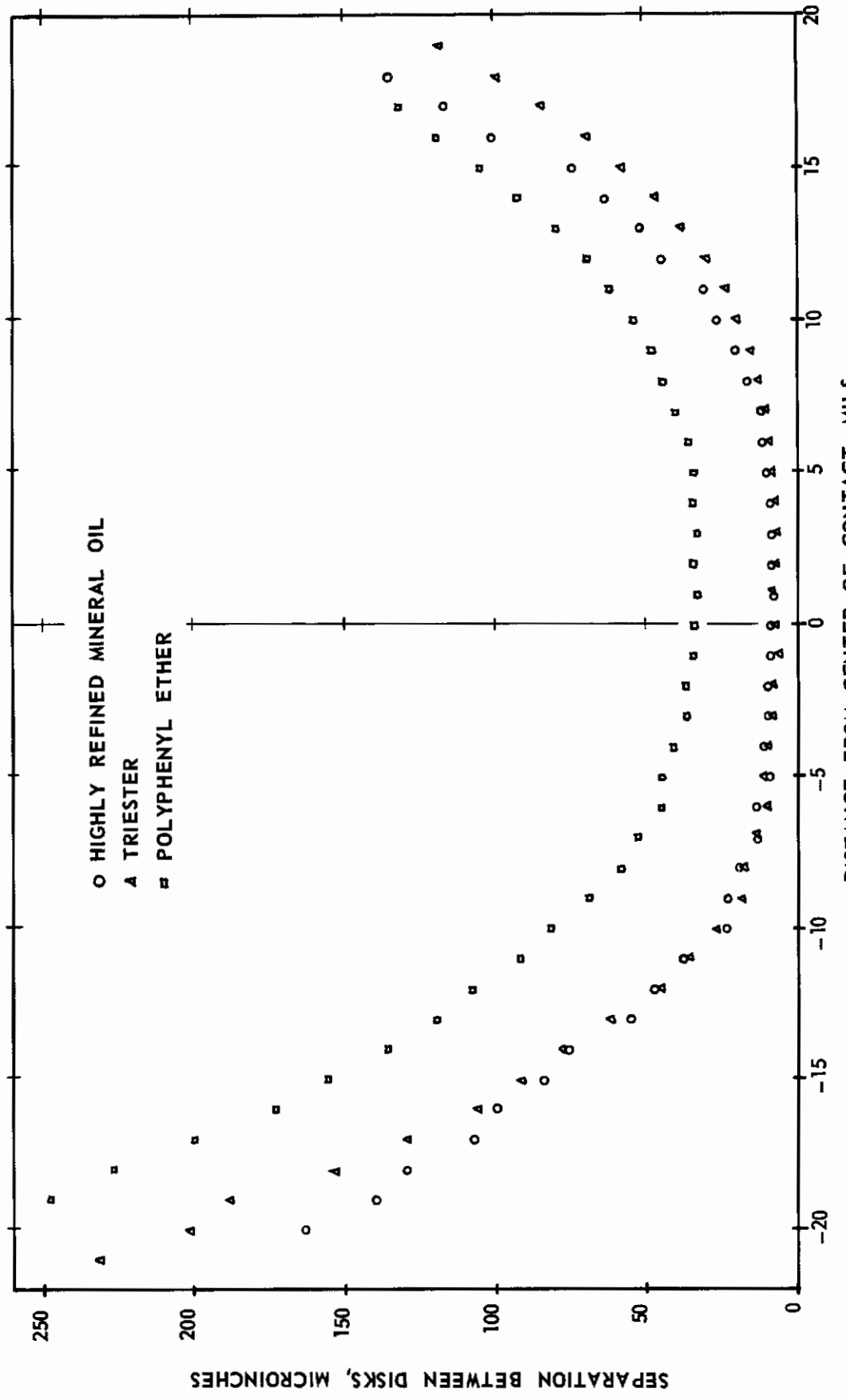

FIGURE 17. CORRECTED CIRCUMFERENTIAL PROFILES OF ROLLING DISKS WHEN LUBRICATED WITH VARIOUS FLUIDS

T = 175 F; RS = 6800 fpm (9000 rpm); maximum Hertz stress = 107,000 psi.

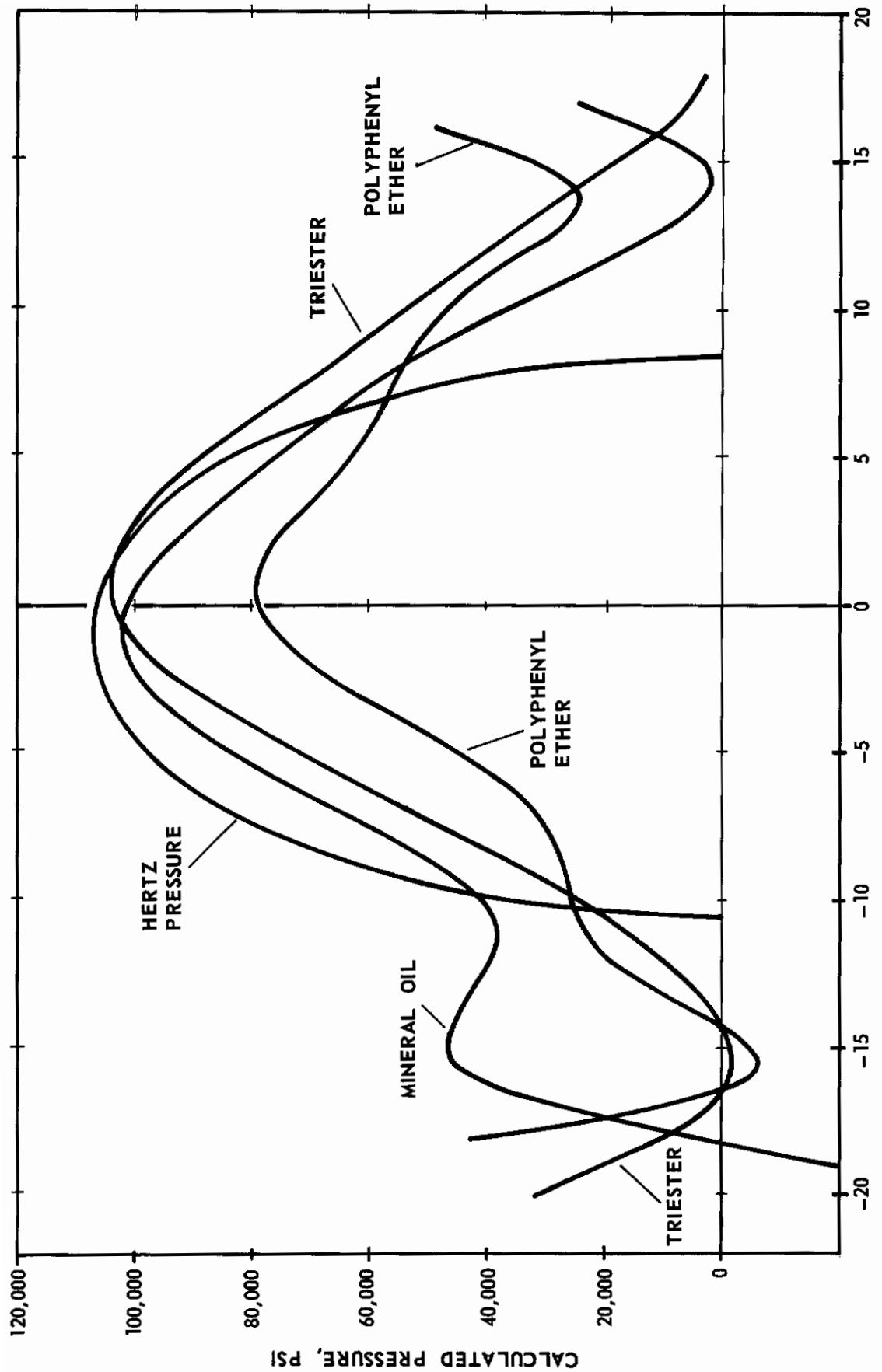

FIGURE 18. PRESSURES CALCULATED FROM CIRCUMFERENTIAL PROFILES FOR THREE LUBRICANTS

T = 175 F; RS = 6800 fpm (9000 rpm); maximum Hertz stress = 107,000 psi.

Observations Regarding Accuracy of Pressures Computed from Deformations

The somewhat irregular shapes of the pressure distributions shown in Figure 18 raises again the question of how accurately pressure distribution can be derived from disk separation profiles found by X-rays. The validity of calculating pressures from X-ray measured deformations is demonstrated in a case discussed in Appendix A, for which there were three replicate experiments (see Figure 40). Analyses that were sufficiently modest (that is using 11-term series) showed excellent agreement over their central regions (see Figure 41). This then demonstrates that accurate pressures can be inferred. The fine detail in these pressure computations will depend, of course, on the detail in the experimental data. One method for obtaining more detail in the pressures would be to use more closely spaced experimental data points than those reported here or of improving the accuracy of the measurements.

As matters now stand, a mechanized procedure has been developed which can be used for rapid estimation of pressure distribution from a given set of deformation data and far more: it can be used in studying the accuracy attainable from given data or from idealized data. Thus, it can be used to study the matter of accuracy as a whole by using simulated data. The study of pressure accuracy by this method up to now is quite limited, but the results indicate that useful accuracy should indeed be attainable by this whole method for pressure evaluation. First order estimates of the pressure distributions can be had by analyzing current data, and improved estimates showing greater detail should be attainable by making feasible improvements in both the experiments and the analysis.

Improvements of the experimental technique may be had, for example, by using a stronger X-ray source, so that a narrower beam could be tolerated. If also a more penetrating beam were used (and the $K\alpha$ beam from a silver target should be), or if the X-ray path were shortened by use of narrower disks, then less correction would be needed for the effects of lubricant cavitation on X-ray absorption. Again, better coordination between heating and X-ray reading cycles has been thought promising for reducing the scatter among X-ray counts. On the analytical side, fuller attention to weighting of clearance readings, in accordance with the expected accuracy of readings in individual localities, should improve the amount of information that can be derived from those readings. Several such improvements could be incorporated into future use of this method for pressure evaluation between rolling surfaces.

DIRECT CONTACT PRESSURE MEASUREMENTS

A knowledge of the pressures that exist in the lubricant film are of paramount importance to the elastohydrodynamic study for two reasons:

(1) The pressures provide information which can be used to compute the state of stress in a bearing which, in turn, affects the bearing

performance. A knowledge of the film pressures existing between rolling elements for different operating conditions can provide data for comparing bearing performance under specific conditions as influenced by lubricant types.

(2) A knowledge of the pressures is required to interpret rheology data on fluids obtained from a rolling-disk type of viscometer.[3]

A second method for determining film pressures pursued in the study consists of using a manganin-pressure transducer located on the surface of one of a pair of rolling-contact disks.

Contact Pressure Measurements (Quartz Disks)

The disk machine used in the pressure measurements has been described previously[4,5] and is shown schematically in Figure 19. A thin ($\sim 10^{-6}$ in. x 0.002 in.) band of Manganin is located (by vapor deposition) in the axial direction on the outside surface of a disk. The change in resistance of the band as it passes through the contact region is detected and displayed on an oscilloscope. The preliminary experiments have been conducted with a pair of 3-in.-diameter by 5/8-in.-wide glass cylindrical disks.

The disks are driven by conventional (60 cps) induction motors with the disks mounted on the same shafts as the motor rotors. The high-frequency generator system used to develop the power for the apparatus used in the X-ray profile measurements has recently been modified so that some speed fluctuation can be obtained for the pressure measurements. Also induction heating coils have been added to the apparatus to control the disk temperature. A disk temperature-measuring scheme similar to the one used on the X-ray disk apparatus has been installed. Here a thermocouple is located 0.005 inch from the surface of the upper disk. A vacuum is used to aspirate the lubricant clinging to the disk over the couple.

Some pressure measurements are given in Figures 20 and 21 for a temperature of 95 F and for rolling speeds of 1090 and 1400 fpm and loadings of 200 and 344 lb/in. of face width (Hertz maximum calculated contact pressures of 21,000 and 28,000 psi, respectively) with polyphenyl ether as the lubricant. The pressure calibration factor is inferred from the loading. For the small range of speeds covered in this series of experiments, no notable change in the profile was observed. The spreading of the profiles at the lower rolling speed is due to the change in the time the manganin band is in the contact zone. The data presented here were developed to demonstrate that consistent pressure profiles, such as given in ref. (4 and 5), could be obtained with quartz disks and to evaluate the effect of speed on the pressure profile. The basic interest of the study is, of course, associated with steel rolling elements; efforts have therefore been given to applying the pressure measurement technique to steel disks.

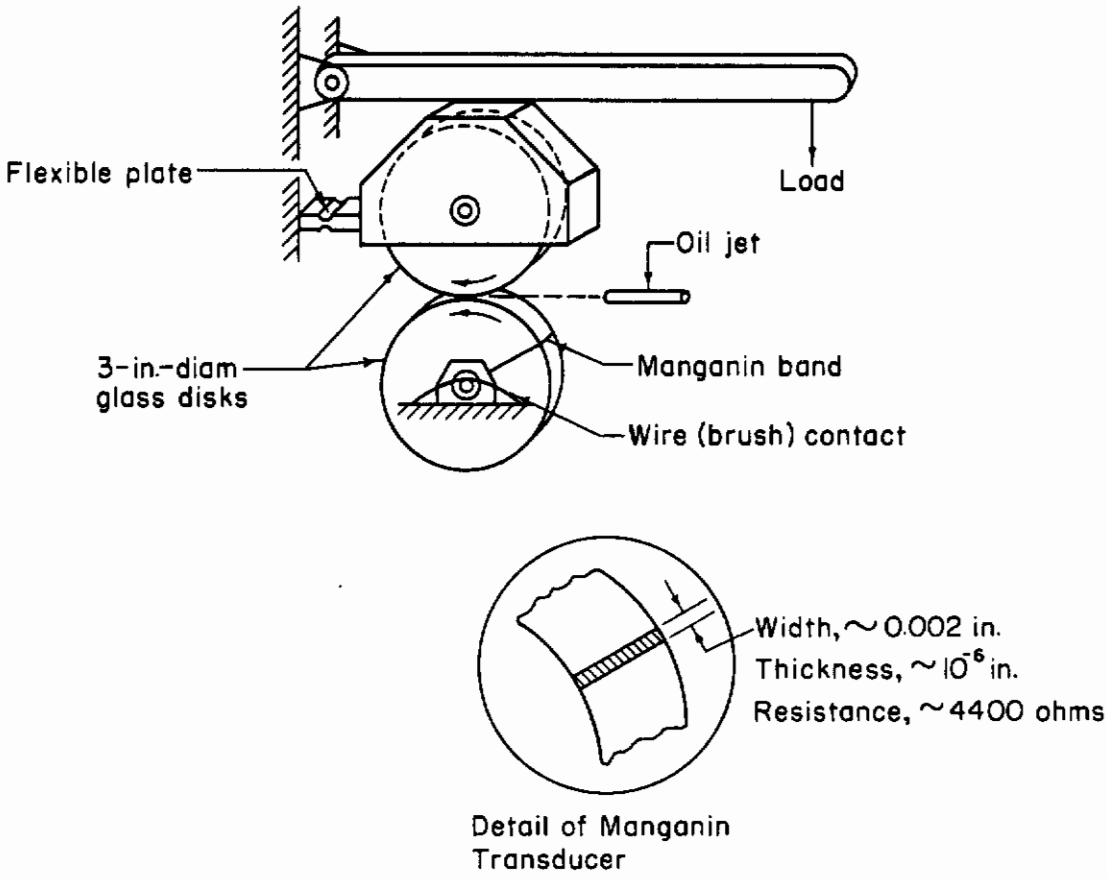

FIGURE 19. SCHEMATIC DIAGRAM OF LUBRICANT FILM PRESSURE-MEASURING DEVICE

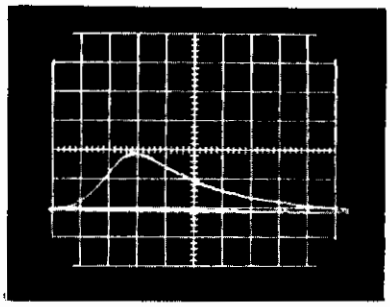

←——— Direction of Rolling

a. Rolling Speed 220 In. /Sec

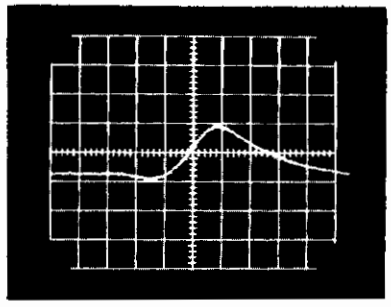

←——— Direction of Rolling

b. Rolling Speed 280 In. /Sec

FIGURE 20. PRELIMINARY FILM-PRESSURE MEASUREMENTS (GLASS DISKS) FOR T ≈ 100 F AND A LOADING OF 200 LB/IN.

Oscilloscope sweep speed 20 μsec/div; estimated pressure ~700 psi/div.

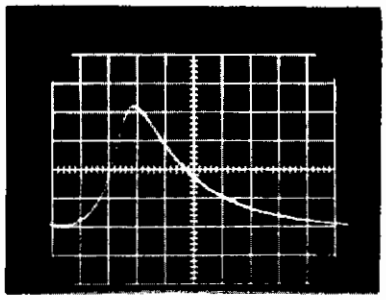

←——— Direction of Rolling

a. Rolling Speed 220 In. /Sec

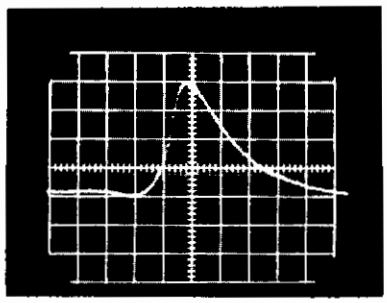

←——— Direction of Rolling

b. Rolling Speed 280 In. /Sec

FIGURE 21. PRELIMINARY FILM-PRESSURE MEASUREMENTS (GLASS DISKS) FOR T ≈ 100 F AND A LOADING OF 344 LB/IN.

Oscilloscope sweep speed 20 μsec/div; estimated pressure 7000 psi/div.

Contact Pressure Measurements (Steel Disks)

Development of Transducer

A technique for measuring film pressures between steel disks has been developed. Here a layer of an insulating material is required between the Manganin and the steel disks.

A pair of AISI 52100 (through-hardened) cylindrical steel disks 3 inches in diameter have been fabricated and polished with manganese dioxide. The polished disks in their bearings run true within <0.0001 inch total indicated runout. A special technique has been developed for obtaining evaporated coating.

The disk is located in a vacuum chamber and the pressure brought to approximately 10^{-2} torr. An ion cleaning process is now used to remove contaminant particles clinging to the disk surface. The pressure is next reduced to 2 to 5 x 10^{-5} torr. Silicon monoxide is heated above its vapor pressure in the vacuum chamber and allowed to vaporize and deposit onto the steel disks. With the vacuum maintained, a shield containing a 0.002-inch slit is positioned remotely between the disk and a resistance heating element. The heating element is heated to a temperature above the vapor pressure of Manganin. The Manganin is fed into this heating element and allowed to vaporize through the slit onto the steel disks forming a thin band of Manganin to be used as the pressure transducer. Since the deposition of the coatings is all done in one operation, there is no opportunity for contamination to form between the silicon oxide layer and the Manganin coating which should insure as strong a bond as possible.

As might be anticipated, using a manganin pressure transducer with steel disks introduces many complexities not encountered in using the transducer with quartz disks. Extreme care must be taken in depositing the transducer to insure that the SiO_2 layer is of sufficient thickness to completely insulate the Manganin from the steel. Conversely, if the SiO_2 is too thick, then cracking of this coating will occur. After several attempts, it was found that a thickness corresponding to about 30 microinches was sufficient; this thickness was determined by observing changes in apparent color of the normally transparent SiO_2 coating due essentially to light refraction as the layers built up during deposition. Extreme care must also be taken in making electrical contact with the Manganin coating to keep from shorting to the steel. The initial technique used is illustrated in Figure 22. A radius is machined on one side of the steel disk and a plexiglass plate bonded to that side. A brass tab is mounted onto the plexiglass plate and loaded against the Manganin band. Silver paint is spread around the junction to insure a stable electrical contact. The other side of the Manganin band is grounded to the disk. Some difficulties were incurred in obtaining uniform coatings on this radius; consequently, (as will be discussed) in later experiments a different arrangement for the electrical contacts has been used.

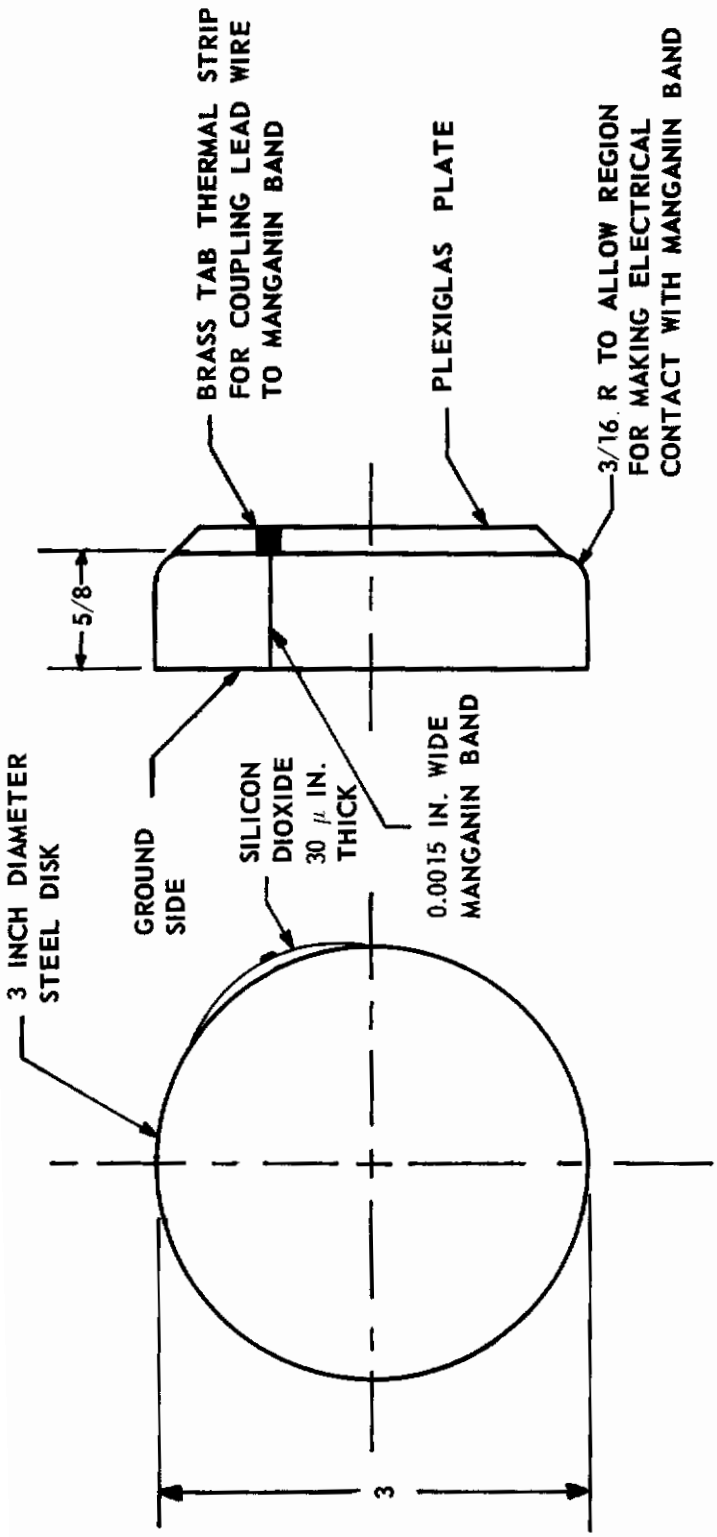

FIGURE 22. MANGANIN PRESSURE TRANSDUCER LOCATED ON STEEL DISK

Preliminary Experiments

In the initial pressure experiments, it was observed that an electrical voltage was developed in the Manganin as it passed through contact, which tended to obscure the pressure measurements. Studies have been made to determine the nature of the background voltage. A glass disk containing a manganin band was run in lubricated rolling contact with both a steel and a glass disk; no background signal was detected with this band. The steel disk containing a Manganin band was run with a glass disk; the background voltage did exist. The signal then appears to be associated with the SiO_2 coating possibly from piezoelectric features of this coating.

Several methods for eliminating the background voltage from the pressure measurements were investigated. One method for partially eliminating the errors in the pressure measurements resulting from the background voltage is to increase the ratio of the pressure signal to the background signal by simply increasing the voltage applied across the Manganin. Unfortunately, however, it was found that increasing the voltage above 3 volts caused a breakdown in the SiO_2 coating. A second method for compensating for the background voltage consists of applying 3 volts dc to the bridge and observing the apparent pressure; then, of reversing the direction of the input voltage and again observing the apparent pressures. To one trace the background voltage is added; from the other it is subtracted. The actua pressure trace is the average of these two traces. A third method for eliminating the effect of the background voltage is to measure the difference in the voltage level above ground for each side of the Manganin rather than using the one-side grounded circuit shown in Figure 22. With this arrangement, an induced voltage would be nulled out in the electronic differencing process.

Preliminary Pressure Measurements

The preliminary pressure measurements were made using the grounded circuit employing the averaging process to account for the background voltage. In Figure 23, pressure traces obtained by this process are presented. The calibration for the pressure measurements was obtained by comparing the integral of the recorded trace with the known loading. This type of calibration was done for the four loading conditions given in Figure 23 and the agreement between the calibration factors was very good within about 5 per cent. The precise location of the center of contact in the measured pressures is somewhat difficult to determine. Theoretically[6], the pressures should be expected to follow the Hertzian for a large portion of the inlet region. In Figure 23, the circumferential axis of the measured pressures were shifted to give the best fit of the measured pressures with the Hertzian on the inlet side. This provides an estimate for the position of the line of centers.

In addition to the pressure data presented for T = 110 F and rolling speed of 280 in./sec., a pressure profile for T = 175 F and a rolling speed of 2530 fpm is given in Figure 24. The Manganin-transducer used in obtaining these pressure traces was a different one than the one used for the data of Figure 23 and the calibration factor is slightly different. Also given in Figure 24 is a Hertzian pressure profile for the same loading conditions as the dynamic profile.

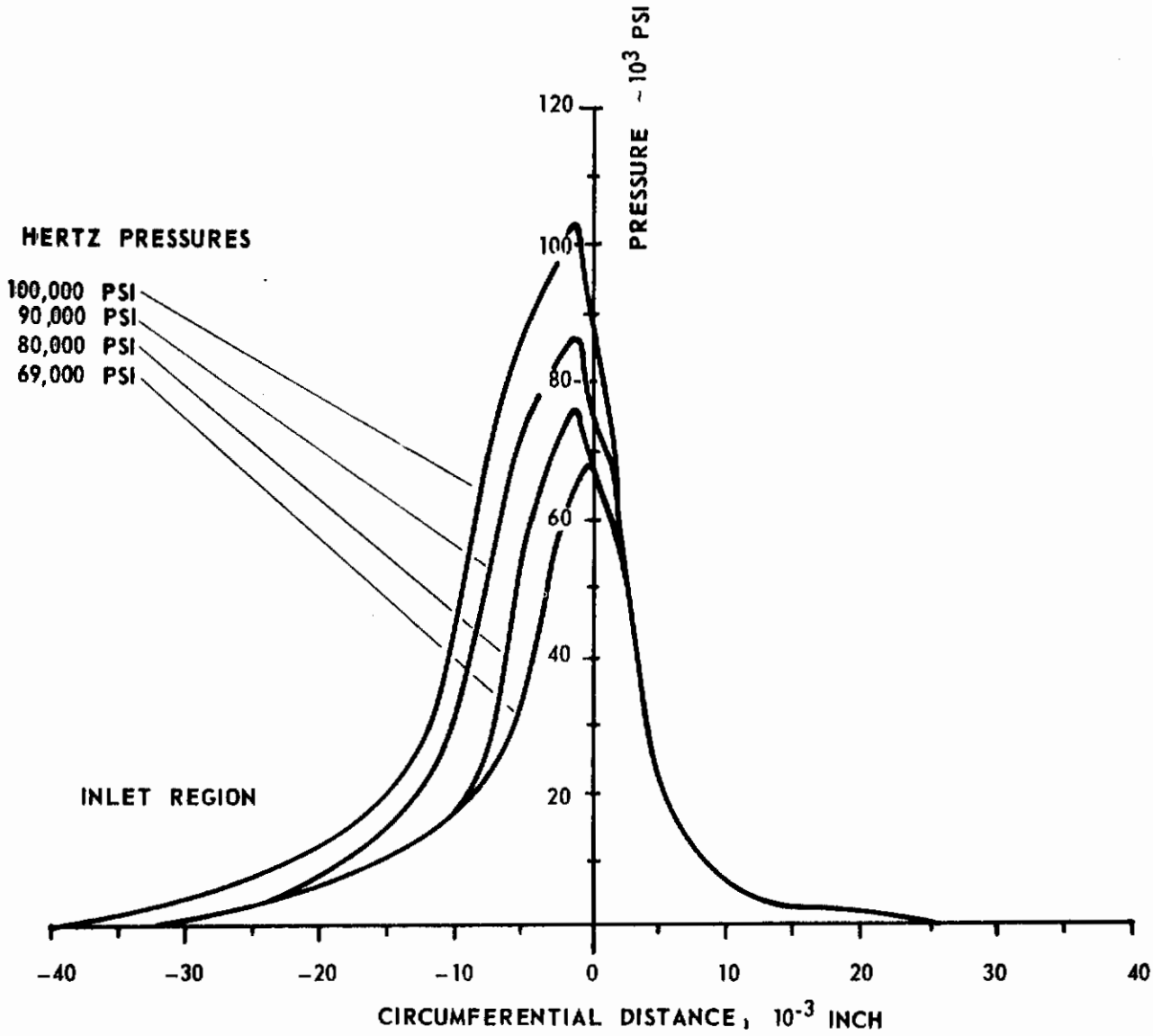

FIGURE 23. PRELIMINARY FILM PRESSURE PROFILES OBTAINED USING AVERAGING PROCESS FOR FOUR LOADING CONDITIONS

T = 110 F; RS = 1400 fpm.

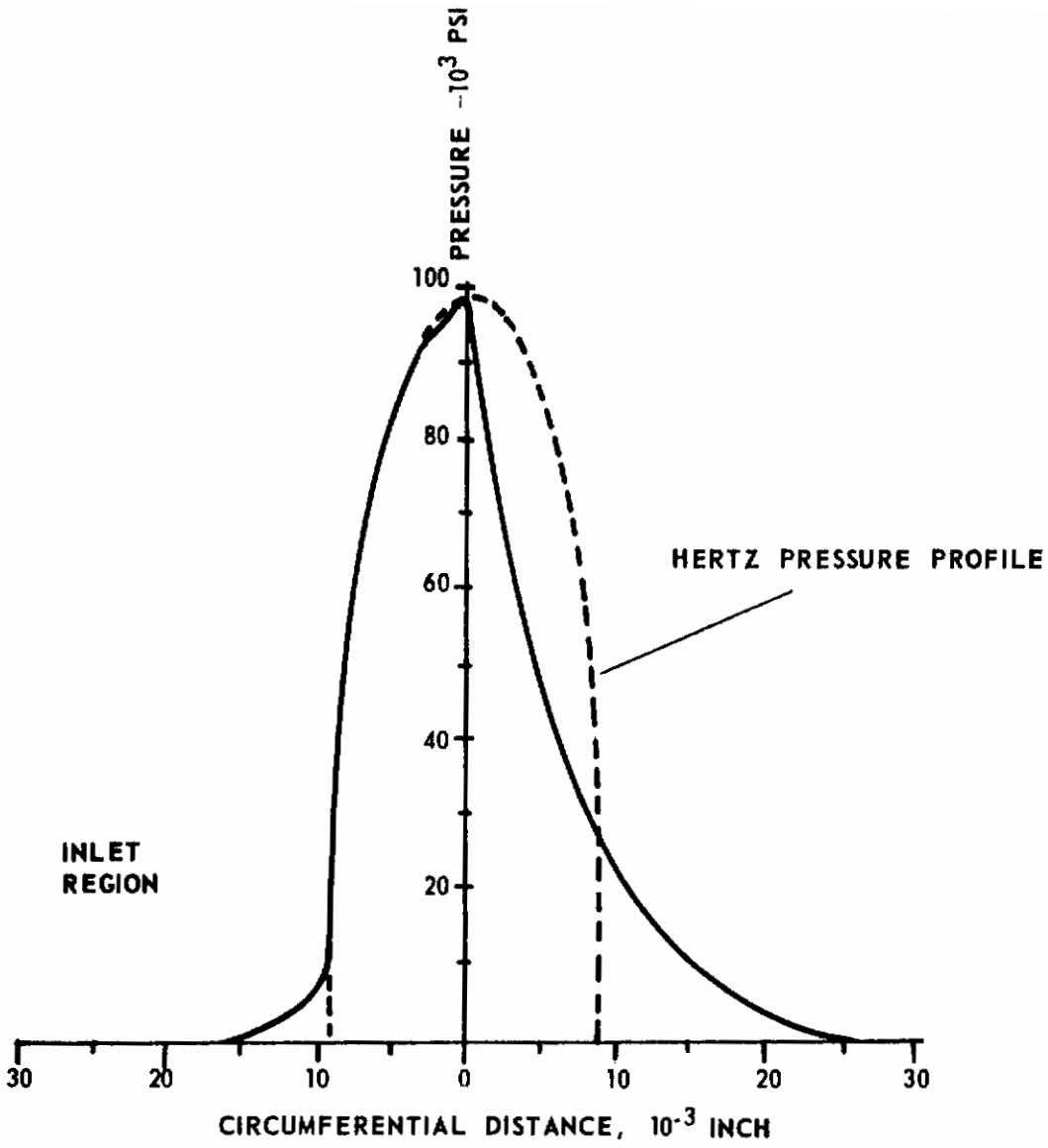

FIGURE 24. LUBRICANT FILM PRESSURE PROFILE OBTAINED USING AVERAGING PROCESS

P_h = 99,000 psi Hertz; T = 175 F; RS = 2520 fpm.

Discussion of Pressure Measurements Using Modified Technique

Modifications to Transducer Arrangement. The pressures obtained by using the manganin transducer along with the averaging process have appeared to be quite self consistent in their dependence on loading. However, it is possible that details in the pressure data (such as pressure spikes) could easily be lost in the averaging process; hence the pressure measuring system has been modified in an attempt to completely eliminate the background voltage. The one method which appeared quite promising is to use an ungrounded Manganin strip with a differential-type input to the oscilloscope. That is, to use an oscilloscope to measure the difference in the voltage level above ground on one terminal of the manganin strip from the voltage level on the other terminal.

The disks used in the pressure studies have been modified to accommodate the ungrounded electrical circuit as shown in Figure 25. Here the upper disk is considerably narrower than the lower one containing the transducer, and the electrical connections are made on top (rather than on the sides) of the disks to eliminate the difficulties associated with the nonuniform coatings on the corners of the disks.

Discussion of Pressure Experiments with an Ungrounded Circuit

Film pressures between lubricated steel rolling disks have been measured for a series of disk operating conditions using the modified manganin-transducer arrangement. Photographs of oscilloscope traces for these pressure measurements are given in Figures 26-28; the range of conditions covered here is T = 115 F, R.S. = 950-2100 fpm, and loading = 104,000 psi - 128,000 psi Hertz.

The pressure trace for the condition where T = 115, R.S. = 1400 fpm, and a loading of 104,000 psi Hertz obtained using the modified apparatus is compared in Figure 29 with the measurement for a loading of 99,000 psi obtained by the aforementioned averaging process of data using the original transducer arrangement to demonstrate the consistency in the pressure measurements using the two slightly different techniques.

For the measurement of film pressures for the 116,000 and 128,000 psi loadings, the pressure peak occurs almost as a truncated pressure spike. Following the peak, the pressure drops very rapidly. This possible pressure spike, although distinctive, is not large in magnitude. However, since the pressures detected by the transducer are actually the average pressures over the width of the transducer, any anomaly in the data such as pressure spike would be naturally truncated.

Although pressure spikes between rolling contacts have been predicted by various elastohydrodynamic theories[6,8,9], the data reported here are believed to be the first experimental evidence of such pressure concentration. Severe pressure concentrations would be expected to develop severe stress concentrations in the rolling elements which would greatly influence the performance of lubricated rolling elements.

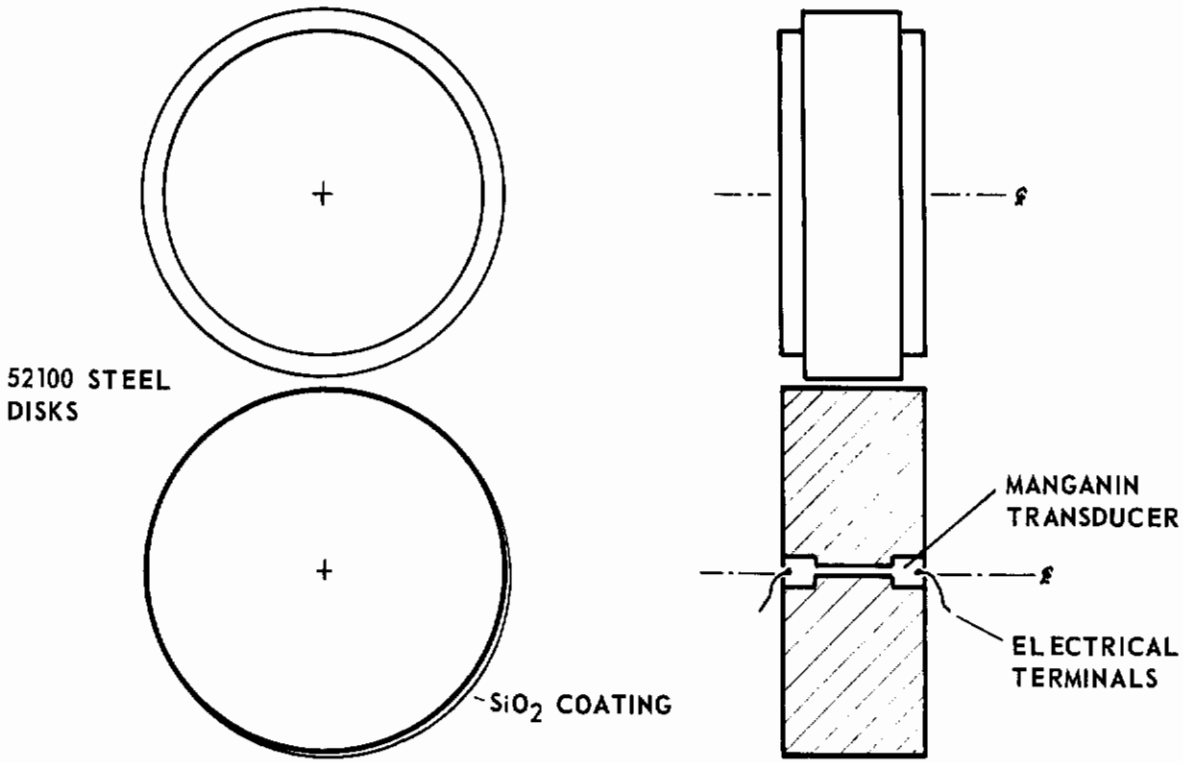

FIGURE 25. DIAGRAM OF MODIFICATION TO PRESSURE MEASURING SYSTEM (STEEL DISKS) TO ACCOMMODATE UNGROUNDED ELECTRICAL CIRCUITRY

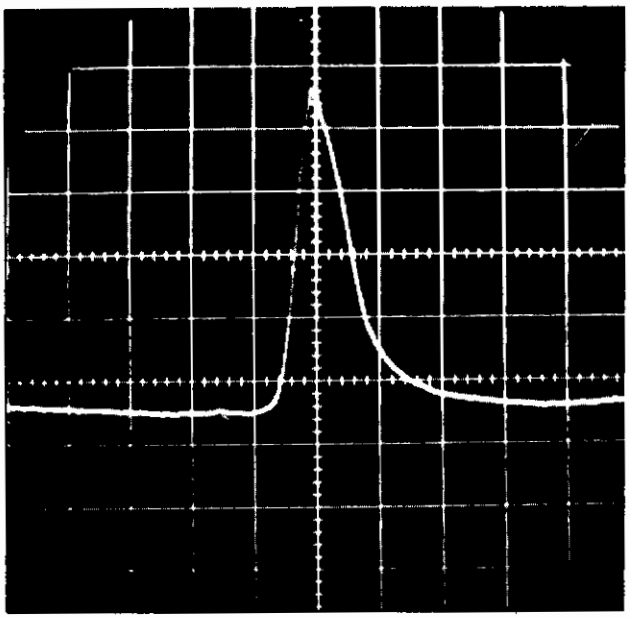

(a) P_h = 104,000 psi Hertz
Abscissa scale = 0.0093 in./div
Ordinate scale ≈ 20,000 psi/div
← Direction of Rolling

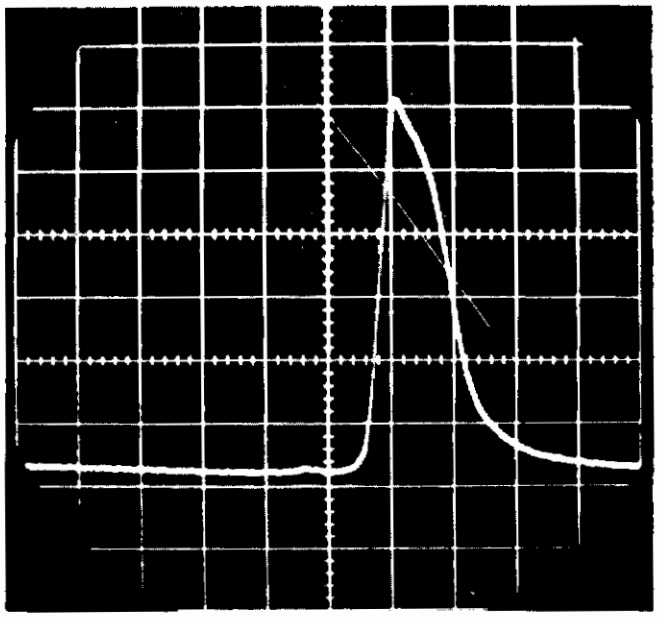

(b) P_h = 116,000 psi Hertz
Abscissa scale = 0.0093 in./div
Ordinate scale ≈ 20,000 psi/div
← Direction of Rolling

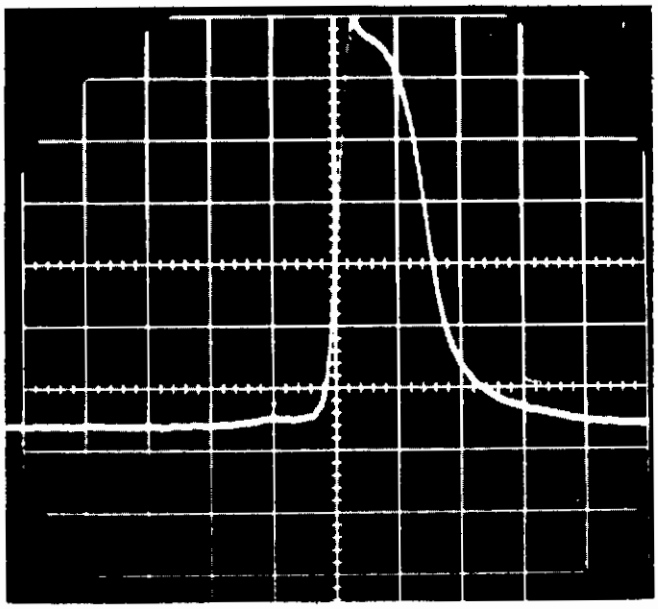

(c) P_h = 128,000 psi Hertz
Abscissa scale = 0.0093 in./div
Ordinate scale ≈ 20,000 psi/div
← Direction of Rolling

FIGURE 26. PRESSURE MEASUREMENTS BETWEEN STEEL DISKS USING IMPROVED PRESSURE MEASUREMENT TECHNIQUE

T = 115 F; P_h = 104,000, 116,000, and 128,000 psi Hertz; RS = 950 fpm.

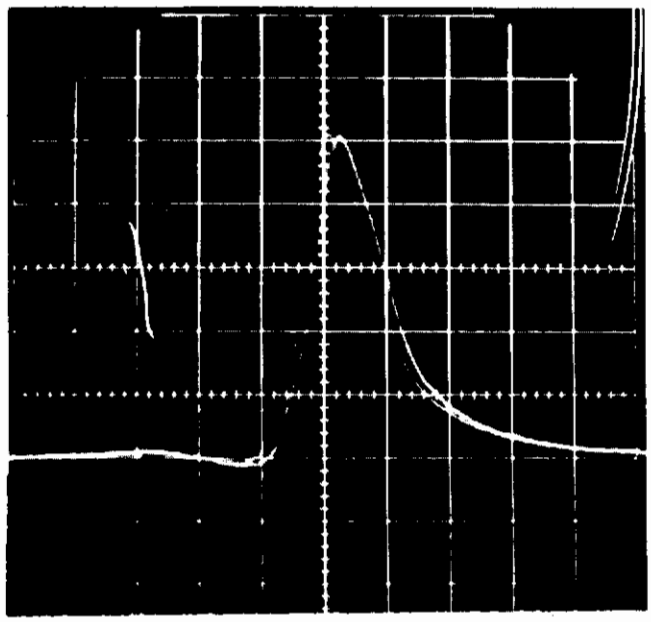

(a) P_h = 104,000 psi
Abscissa scale = 0.007 in./div
Ordinate scale ≈ 20,000 psi/div
← Direction of Rolling

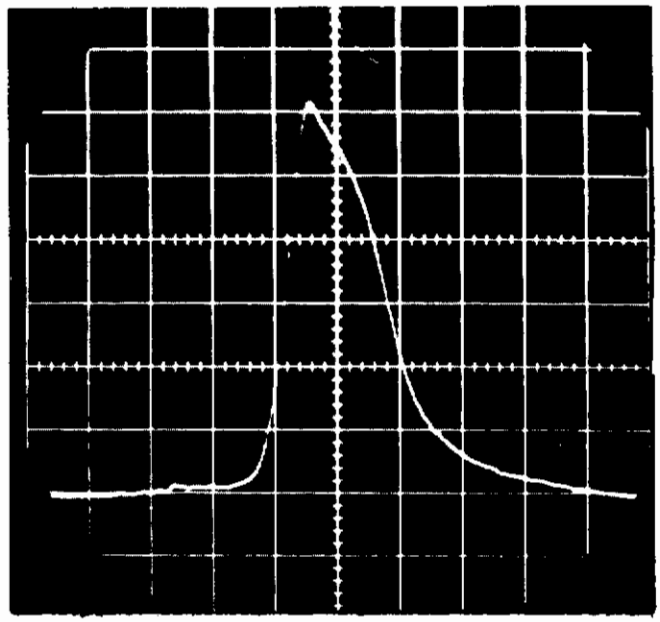

(b) P_h = 116,000 psi
Abscissa scale = 0.007 in./div
Ordinate scale ≈ 20,000 psi/div
← Direction of Rolling

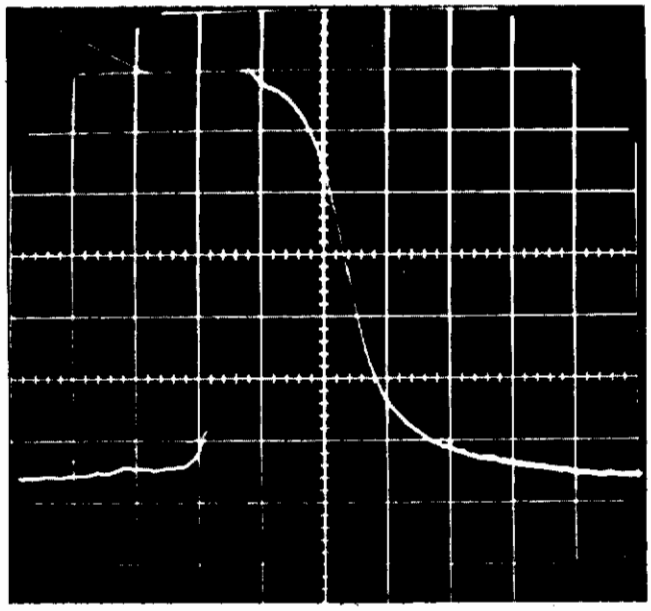

(c) P_h = 128,000 psi
Abscissa scale = 0.007 in./div
Ordinate scale ≈ 20,000 psi/div
← Direction of Rolling

FIGURE 27. PRESSURE MEASUREMENTS BETWEEN STEEL DISKS USING IMPROVED PRESSURE MEASUREMENT TECHNIQUE

T = 115 F; P_h = 104,000, 116,000, and 128,000 psi Hertz; RS = 1400 fpm.

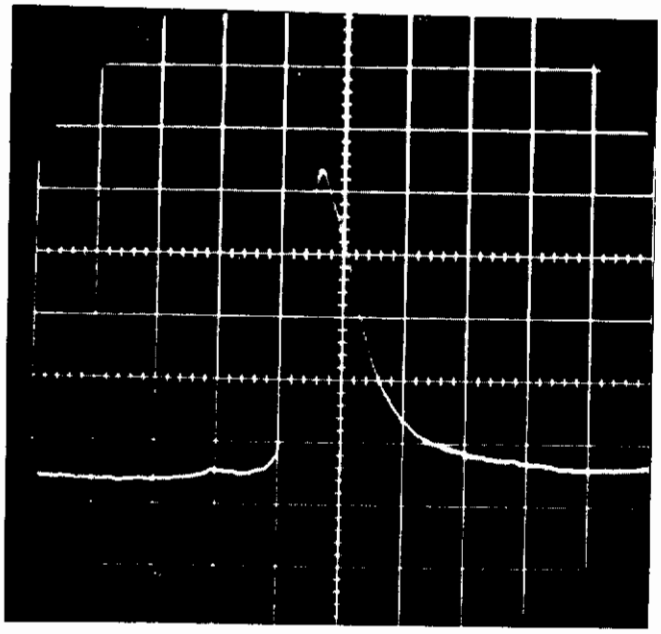

(a) P_h = 104,000 psi
Abscissa scale = 0.0085 in./div
Ordinate scale ≈ 20,000 psi/div
← Direction of Rolling

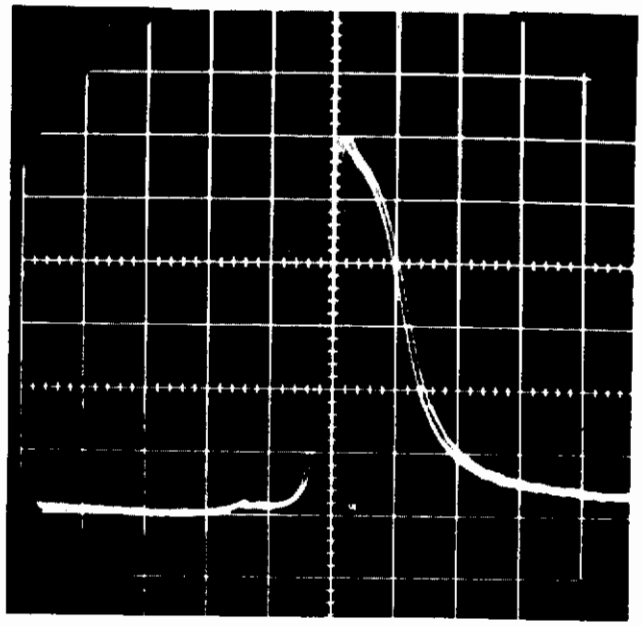

(b) P_h = 116,000 psi
Abscissa scale = 0.0085 in./div
Ordinate scale ≈ 20,000 psi/div
← Direction of Rolling

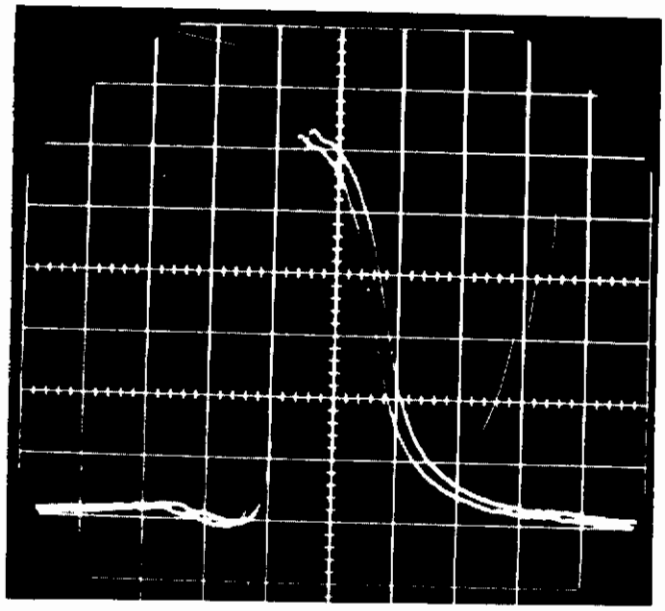

(c) P_h = 128,000 psi/div
Ordinate scale ≈ 20,000 psi/div
← Direction of Rolling

FIGURE 28. PRESSURE MEASUREMENTS BETWEEN STEEL DISKS USING IMPROVED PRESSURE MEASUREMENT TECHNIQUE

T = 115 F; P_h = 104,000, 116,000, and 128,000 psi Hertz; RS = 2100 fpm.

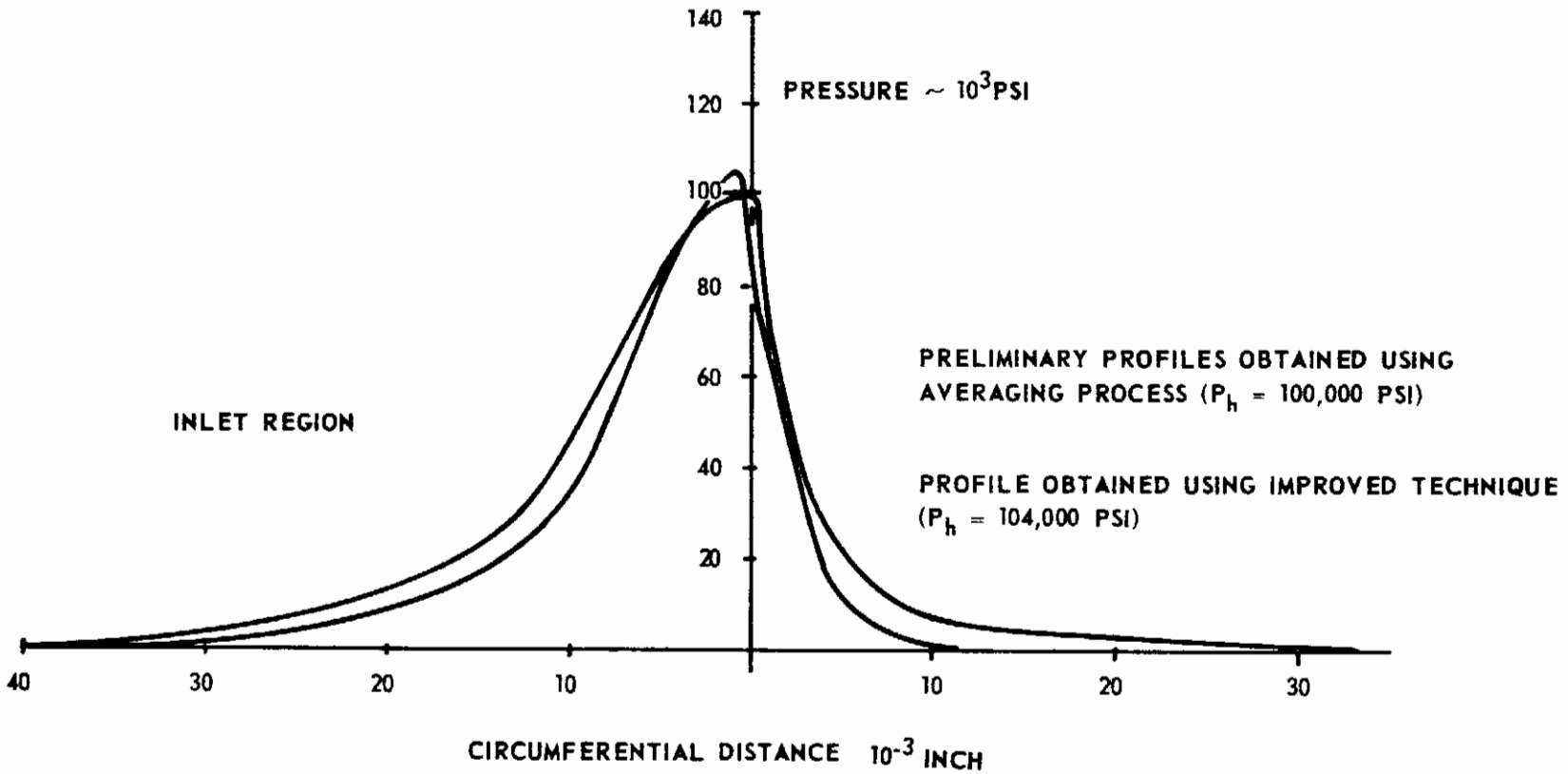

FIGURE 29. COMPARISON OF PRELIMINARY PRESSURE PROFILE OBTAINED WITH THE AID OF AN AVERAGING PROCESS WITH A PROFILE BY DIRECT MEASUREMENTS

T = 115 F; RS = 1400 fpm.

To demonstrate how the pressure patterns vary with loading, pressures obtained for three loadings have been plotted on the same graph in Figure 30. In Figure 31, pressure patterns for T = 115 F, a loading of 128,000 psi Hertz, and three rolling speeds are presented. For the rolling speeds studied here, there is apparently no significant change in the pressure patterns with speed.

ANALYSIS OF PRESSURE DATA

A computer program has been developed, using classical elasticity theory, for inferring deformation and stresses in rolling elements from a knowledge of the film pressures.

Computation of Deformation from Pressures

Although the computation of pressures from measured deformations requires very precise experimental data and mathematical procedures, deformations can be calculated quite readily from pressures and do not seriously reflect errors in the pressure data. Such deformations represent a very convenient means for correlating the measured pressures with the measured deformations.

The equations used for calculating deformations may be obtained directly from reference 10 (first equation of page 21) expressed as follows:

$$\delta(\xi) = \frac{-2a\,(1-\nu^2)}{\pi E} \int_{-1}^{1} p(\zeta)\, \ln \frac{a\,(\xi-\zeta)}{2R}\, d\zeta \quad . \qquad (1)$$

The origin for the tangential position variable x was chosen such that the pressure p would vanish at $x = \pm a$. The dimensionless position variable ξ is given by $\xi = x/a$. The function $p(\xi)$ represents the measured pressure distribution and the quantities R, ν, E and $\delta(\xi)$ represent the cylinder radius, Poisson's ratio, Young's modulus, and the deformation, respectively.

In order to evaluate the integral appearing in the above equation, the interval $-1 \leq \zeta \leq 1$ was divided into a number of equally spaced subintervals. In each of these subintervals, the pressure, $p(\zeta)$, was approximated by the parabola passing through the end points and the midpoint of the subinterval. The integrals were then evaluated analytically and summed over the entire interval $-1 \leq \zeta \leq 1$.

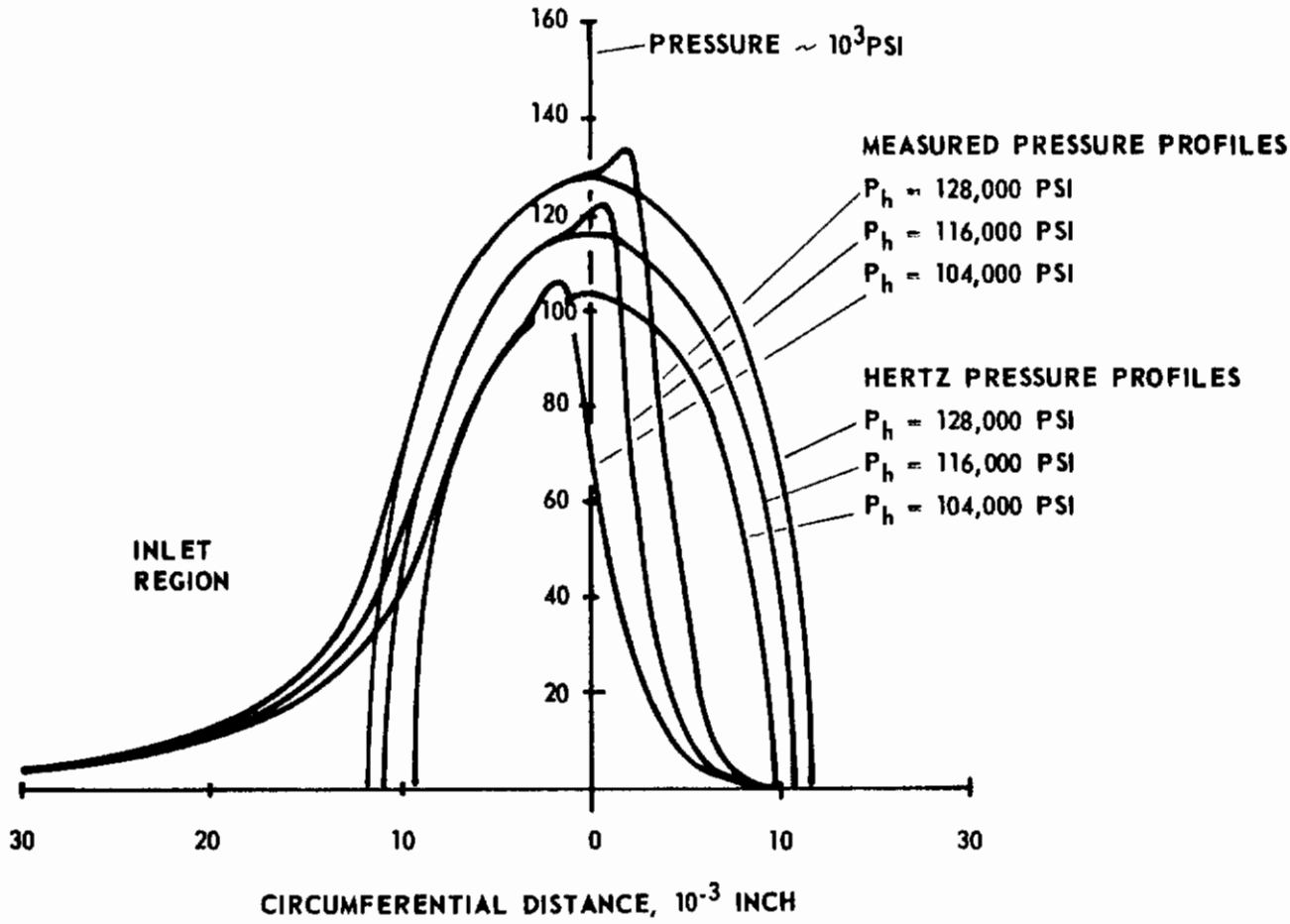

FIGURE 30. MEASURED VARIATION IN PRESSURE PROFILE WITH DISK LOADING

T = 115 F; RS = 1400 fpm.

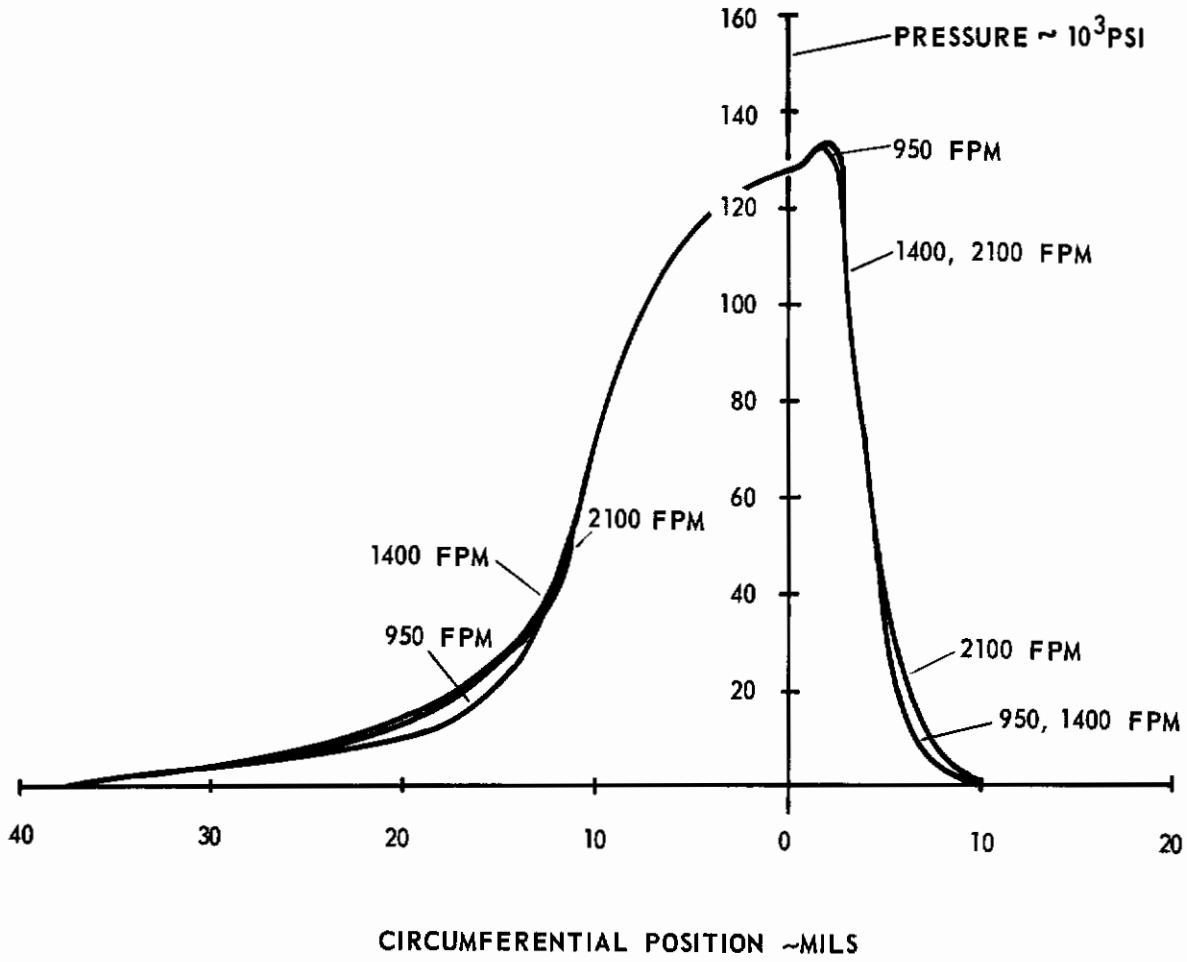

FIGURE 31. VARIATION IN PRESSURE PROFILE WITH ROLLING SPEED
T = 115 F; P_h = 128,000 psi.

Comparison of Measured Deformations with Deformations Computed from Measured Pressures

In Figure 32 a deformation profile of the rolling disk lubricated with polyphenyl ether[5] is given for the operating conditions of T = 175, rolling speed = 2600 fpm, and a Hertz pressure of 100,000 psi. Also given in Figure 32 is a deformation profile computed from the measured pressure distribution given in Figure 24 for similar operating conditions. In the computation of deformation from pressures, there is, of course, no means for determining the absolute magnitude of this film thickness. The vertical location of the computed deformation curve was chosen to yield an optimum fit with the experimental data.

The comparison between the measured and computed deformations is quite encouraging but the agreement is certainly not perfect. The measured profile is somewhat flatter in the center region than the computed profile. There are, however, some slight differences in the operating conditions for the two sets of data. For example, in the X-ray measurements crowned disks are being used whereas cylindrical rollers are used in the study with the manganin-pressure transducer. Also it was not possible to obtain exactly the same rolling speed in the pressure measurements as had been used in deformation profile experiments. Future experiments are to be conducted with both apparatuses so that comparison between the two sets of data can be made for several operating conditions to better determine the consistency between the data of both machines.

Computations of Stresses from Measured Pressures

One basic goal of the program is to determine the effect of lubricant properties in bearing fatigue. Though the mechanics of fatigue are not clearly understood, it is generally accepted that bearing fatigue is directly related to the stresses in the rolling-contact elements. These stresses can be determined from the measured pressures.

The stress function applicable to this analysis was derived by superposition of stress functions (valid for problems of line forces imposed on the surface of a semi-infinite solid) as given in Reference 10 (Equation (a) of page 66). The stress function, $\psi(\xi,\eta)$, so obtained is

$$\psi(\xi,\eta) = -\frac{a^2}{\pi}\int_{-1}^{1} p(\zeta)\,(\xi-\zeta)\,\tan^{-1}\left(\frac{\xi-\zeta}{\eta}\right)\,d\zeta\,, \qquad (2)$$

where η is the radial distance measured from the cylinder surface divided by a. The other notations are consistent with the notation used in the discussion on computing deformations from pressures.

The subsurface stresses are given by

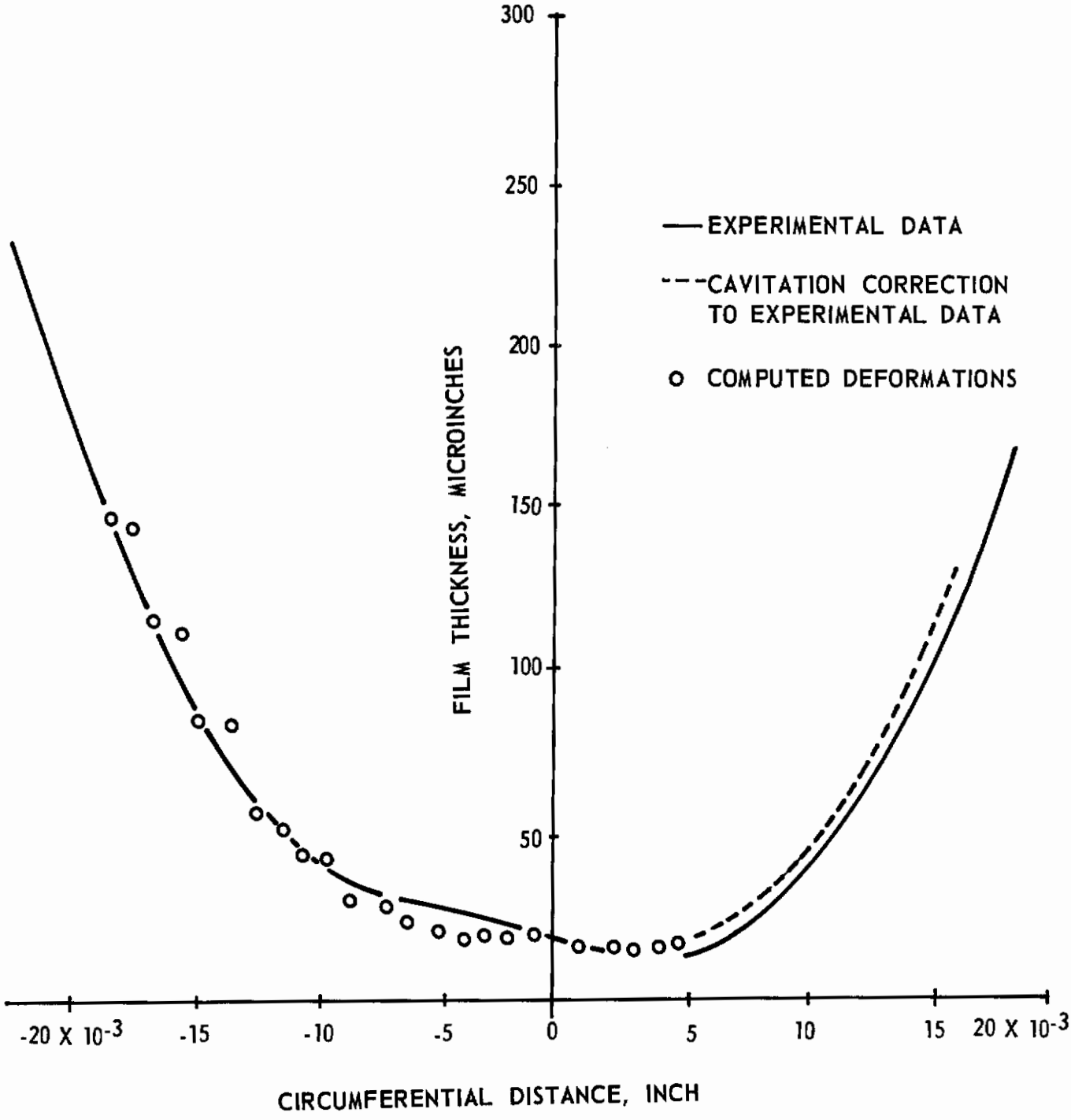

FIGURE 32. COMPARISON OF DEFORMATION PROFILE COMPUTED FROM THE MEASURED PRESSURES OF FIGURE 17 AND MEASURED DEFORMATION PROFILE

$$\sigma_y(\xi,\eta) = \frac{1}{a^2}\frac{\partial^2\psi}{\partial\xi^2} = -\frac{2}{\pi}\int_{-1}^{1}\frac{\eta^3}{[\eta^2+(\zeta-\xi)^2]^2}\,p(\zeta)\,d\zeta \qquad (3)$$

$$\sigma_x(\xi,\eta) = \frac{1}{a^2}\frac{\partial^2\psi}{\partial\eta^2} = -\frac{2}{\pi}\int_{-1}^{1}\frac{\eta(\zeta-\xi)^2}{[\eta^2+(\zeta-\xi)^2]^2}\,p(\zeta)\,d\zeta \qquad (4)$$

$$\tau_{xy}(\xi,\eta) = -\frac{1}{a^2}\frac{\partial^2\psi}{\partial\xi\,\partial\eta} = \frac{2}{\pi}\int_{-1}^{1}\frac{\eta^2(\zeta-\xi)}{[\eta^2+(\zeta-\xi)^2]^2}\,p(\zeta)\,d\zeta \qquad (5)$$

The numerical methods employed in the evaluation of the above integrals are similar to those used in computing deformations from pressure measurements. That is to say that the interval $-1 \leq \zeta \leq 1$ was divided into a number of equally spaced subintervals and quadratic approximations to the pressure data were used in each subinterval.

The output of the subsurface stress computer program contains radial and tangential stresses, shear stresses, principal stresses, maximum shear stress, and orientation of the principal axes as functions of position. In addition, the magnitude of the maximum shear reversal and the depth, and the orientation of the plane upon which it occurs are also included in the output. These computations are believed to provide all the stress information needed for use in conjunction with existing fatigue criteria.

Results have been obtained for the preliminary pressure data obtained using steel disks as well as a Hertzian loading. The magnitude of the maximum shearing stress obtained from the measured pressures is quite similar to the maximum shear stress for dry contact. However, the location of the maximum shear stress as calculated from pressure data is much closer to the surface than that which occurs with a Hertzian loading. In Figure 33, calculated maximum shearing stress is presented as a function depth into the disks for three loading conditions. In Table 2, the magnitude of the peak maximum shearing stress is compared with the computed maximum shear reversal and the maximum shearing stress for dry contact (Hertzian).

THE DETERMINATION OF THE TEMPERATURES IN THE LUBRICANT FILM

A knowledge of the temperatures in the lubricant film is of prime importance to the understanding of the significant properties a fluid should have for effective lubricating characteristics. Film temperatures are being analyzed as a part of the study. The basic approach for determining film temperatures is to measure the temperatures on the surface of one of a pair of rolling-contact disks by using an evaporated resistance thermometer, similar to the manganin pressure transducer, and to infer the temperature across the film.

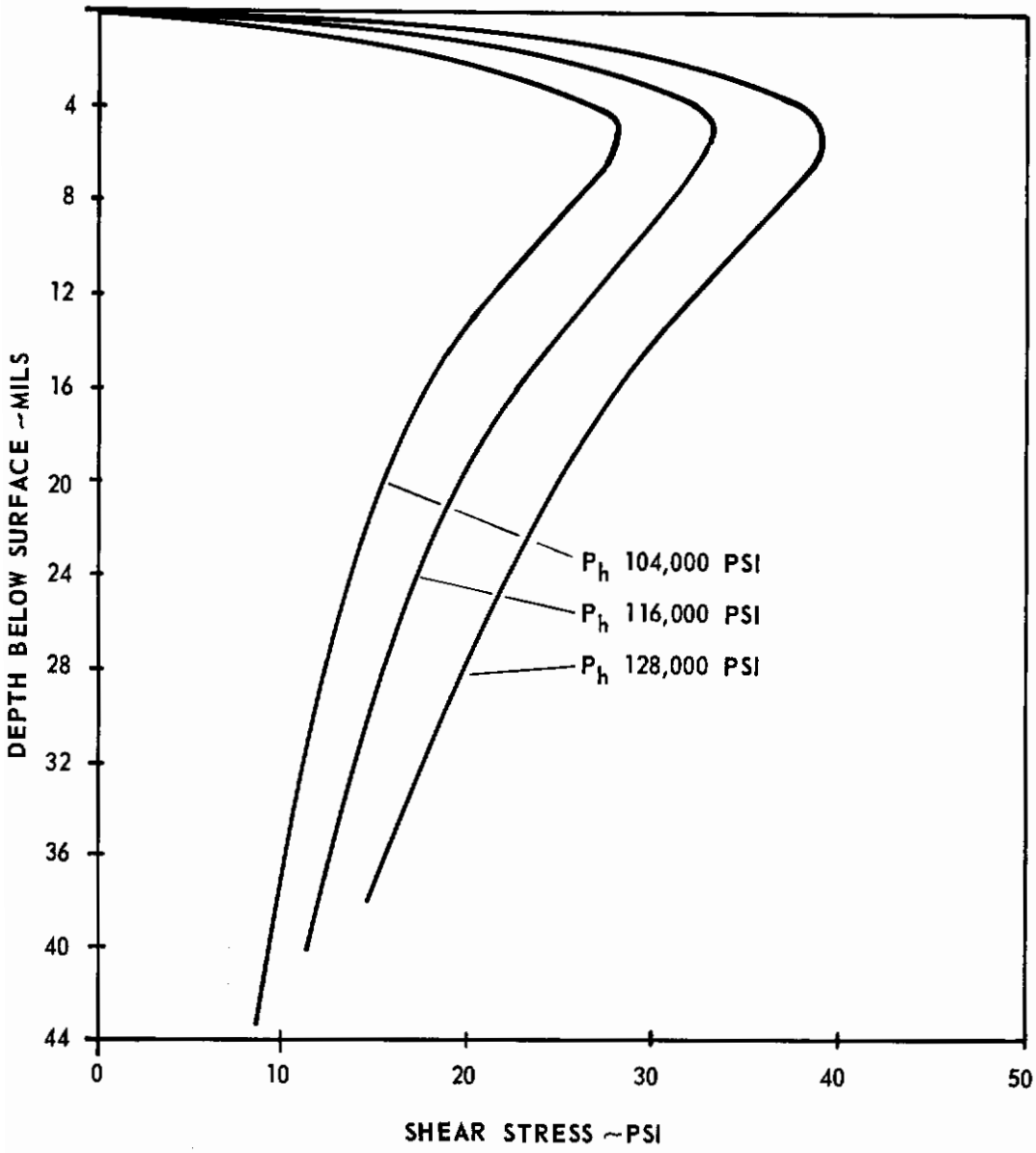

FIGURE 33. VARIATION OF MAXIMUM SHEARING STRESS BELOW SURFACE IN ROLLING ELEMENTS AS CALCULATED FROM PRESSURE MEASUREMENTS

T = 115 F; RS = 1400 fpm.

TABLE 2. MAXIMUM SHEARING STRESSES IN ROLLING DISKS UNDER STATIC AND LUBRICATED DYNAMIC CONDITIONS

Load, psi Hertz	Calculated Maximum Shearing Stress Dry Contact		Calculated Maximum Shearing Stress Dynamic Conditions		Calculated Maximum Shear Reversal Dynamic Conditions
	Magnitude, psi	Depth, inches	Magnitude, psi	Depth, inches	Magnitude, psi
104,000	35,400	0.0084	28,000	~0.0048	37,000
116,000	38,800	0.0092	33,000	~0.0048	48,000
128,000	42,500	0.0102	39,500	~0.0048	56,000

The evaporated resistance thermometer being evaluated consists simply of a thin narrow ($\sim 10^{-6}$ in. x 10^{-2} in.) band of copper.* The copper band is coated axially on the surface of a fused quartz disk. The change in resistance of the copper as it passes through the contact zone is detected by a Wheatstone bridge type of circuit with the voltage change displayed on an oscilloscope.

Discussion of Temperature Experiments

In Figures 34-35, measured temperatures are presented for a range of disk loadings. For these experiments, the resistance of the copper was 100 Ω, the voltage on the bridge was 1.5 VDC, the speed of the disk was 1400 fpm, and the ambient disk temperature was 110 F. Calibration of the temperature transducer was obtained by heating the band in a bath of oil and observing the deflection on the oscilloscope.

Although the temperature data are very preliminary, some interesting observations can be made. The peak temperatures presented are on the order 30-40 F which appears to be quite sizable for the moderate operating conditions. The shape of the temperature profiles is quite similar to the pressure profiles between quartz disks discussed in reference 2 except near the trailing edge.

One possible source of error in temperature measurements is pressure effects, since copper has a pressure coefficient of resistivity very similar to that of manganin. Therefore, pressure effects should be deleted if possible from the temperature measurements. Fortunately, the pressure coefficient of resistivity for copper is negative while its temperature coefficient is positive, so it is possible to distinguish gross temperature effects from gross pressure effects provided they do not merely cancel each other. Entire cancellation appears to be unlikely, since the temperature effects on the resistivity of copper appear greater than the pressure effects for the operating conditions given here. In comparing the pressure traces of reference 2 with the temperature traces given here, it should be remembered that 6 volts were applied to the Wheatstone bridge for the pressure measurements there while only 1.5 volts are being applied here.

Analysis of the Preliminary Temperature Measurements

To understand the measured temperature, a detailed thermal analysis is needed which incorporates the generation of heat in the film due to both compression and shearing of the lubricant and the conduction and convection of the heat by both the lubricant and the steel disks. Such an analysis is being pursued but is quite complicated.

*Orcutt[11] is also conducting temperature experiments using an evaporated temperature transducer similar to the one being described here; a platinum rather than a copper coating is used in his experiments.

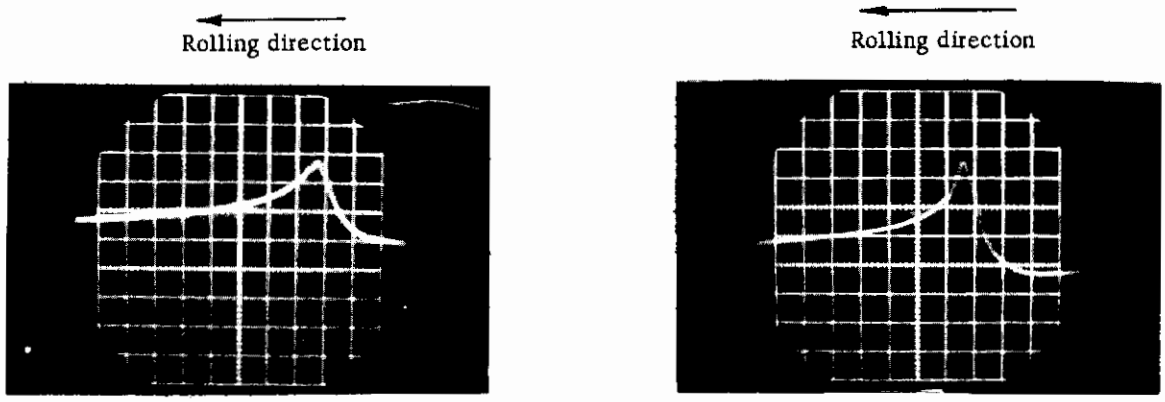

a. 149 lb/in.
(18,000 psi Hertz)

b. 246 lb/in.
(24,000 psi Hertz)

FIGURE 34. PRELIMINARY FILM-TEMPERATURE MEASUREMENTS USING A COPPER TRANSDUCER WITH QUARTZ DISKS. T(AMBIENT) = 110 F, ROLLING SPEED = 1400 FPM, AND LOADING OF 149 AND 246 LB/IN.

Oscilloscope Sweep Speed	100 microsec/div.
Estimated Temperature	10 F/div.
Abscissa Scale	0.028 in./div.

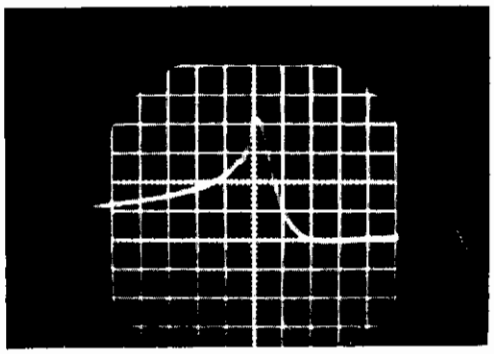

Rolling direction

FIGURE 35. PRELIMINARY FILM-TEMPERATURE MEASUREMENTS USING A COPPER TRANSDUCER WITH QUARTZ DISKS. T(AMBIENT) = 110 F, ROLLING SPEED = 1400 FPM, AND A LOADING OF 390 LB/IN. (30,000 PSI HERTZ)

Oscilloscope Sweep Speed	100 microsec/div.
Estimated Temperature	10 F/div.
Abscissa Scale	0.028 in. /div.

Great simplification of a temperature analysis in the contact region can be had by assuming that the disks present thermally nonconducting walls for the lubricant. Partial justification for such an assumption can be seen in Figures 34 and 35 where there is only a slow temperature decline downstream from the trailing edge of contact where little or no heating should be expected. This slow decline could indicate that quartz is a poor enough thermal conductor so that heat losses through the wall in the contact region should be small compared to the amounts of heat generated there. The temperature does decay to ambient at a distance of several contact widths downstream from the contact region, so that heat generated in each pass of each element of the lubricant through the contact zone is dissipated before that element of fluid re-enters the contact zone.

The basic equation of heat dissipation as taken for pure rolling from reference 3 (Equations 17 and 20), using the modification to the compressive heating term suggested by Burton[12], is

$$J \rho c u \frac{\partial T}{\partial x} - J K \frac{\partial^2 T}{\partial y^2} = \frac{e^{\alpha T - \gamma p}}{\mu_o} [y-h/2]^2 \left(\frac{\partial P}{\partial x}\right)^2 + u \beta T_o \frac{\partial P}{\partial x} . \qquad (6)$$

Here x is the coordinate variable measured circumferentially along the disks; y is the coordinate variable measured normal to the surface; T is the local temperature; T_o is the absolute temperature; β is the coefficient of thermal expansion; u is the rolling velocity; h is the film thickness (assumed constant for the simplified analysis here); μ_o is the base viscosity; γ and α, the pressure and temperature coefficients of viscosity; ρ the lubricant density; K the disk thermal conductivity; c the specific heat of the fluid; and J the factor for converting thermal energy into its mechanical equivalent.

In the analyses being conducted here, the heat conduction by the quartz disk is assumed to be small with respect to the amount of heat generated. Since the lubricant is an even poorer conductor than is quartz, it is consistent to assume that there is little conduction through the lubricant film itself. Thus a not unreasonable simplification of the heat dissipation equation can be had by dropping the conduction term (that is, putting K = 0) and restricting attention to the surface y = 0 where the temperature is measured. This eliminates the second term of equation 6 and makes the third term independent of y. The remaining equation can be integrated numerically by using a simple iteration procedure. Variations in the parameters ρ, c, u, β, and T_o[1] should be small and are ignored in this analysis.

Using measured pressures from reference 2, a temperature profile has been computed for quartz disks using a computer solution to Equation 6 for T = 110, a rolling speed of 1400 fpm, and a loading of 30,000 psi Hertz. The data are given in Figure 36 along with the measured temperatures for the same conditions. The fact that the measured temperatures are apparently spread out more than the computed adiabatic temperature can be attributed at least partially to width of the temperature transducer($\sim 10^{-2}$ inch) which was much wider than the pressure transducer. Future experiments will be conducted with narrower temperature transducers.

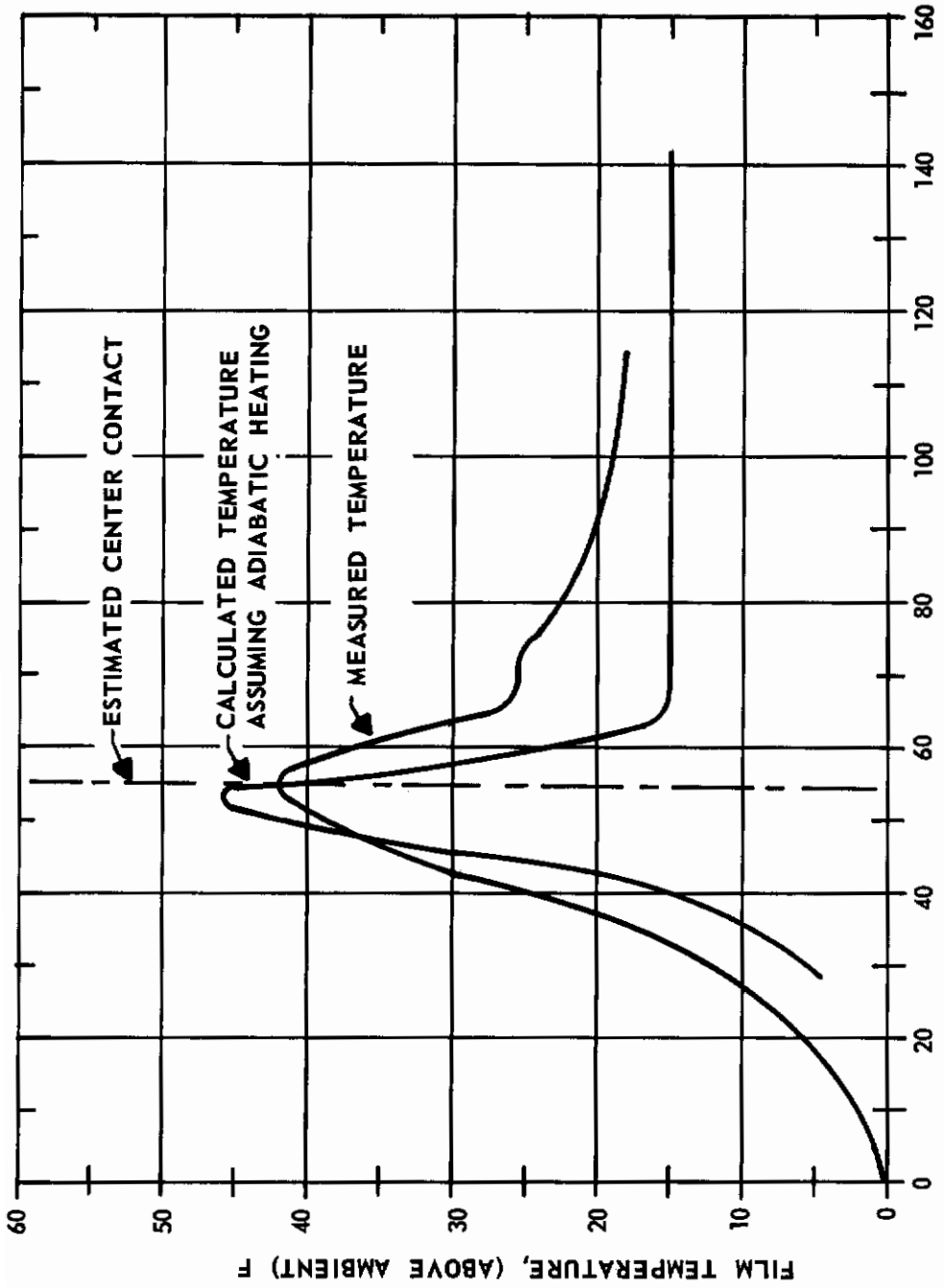

FIGURE 36. COMPARISON OF MEASURED TEMPERATURE PROFILE WITH PROFILE COMPUTED USING AN ADIABATIC ANALYSIS

The center of contact for the computed temperature was taken from the input pressure data. The measured temperature profile was adjusted along the circumferential direction to obtain a reasonable fit with the computed data. On the whole the calculated temperature appears lower than the measured temperature, but at least the order of magnitude is the same in both cases.

Detailed Analysis of Temperatures in Lubricant Films

To better understand the nature of the temperature distributions in the film between rolling elements, a detailed thermal analysis is being conducted. The objective is to perform a more conclusive check on the measured surface temperatures of quartz disks as well as to yield temperature distributions in the lubricant film between steel as well as quartz disks.

In the formulation of the heat-transfer problem, it is assumed that the effect of conduction in the direction of rolling is negligible compared with convection in the rolling direction and conduction in the radial direction. (Such an assumption can be easily justified for the rolling speeds in the range of interest.) Under these conditions, the thermal equation assumes a form that is analogous to a three-region (rolling and sliding) or a two-region (pure rolling) one-dimensional unsteady-state heat-transfer problem with a non-linear heat generation rate in the lubricant. An existing finite different computer program is available for solving multi-region heat-transfer problems of this type. The temperature analysis is to utilize measured film pressures in the computation of heat generation.

The computer program has been modified to make it applicable to the rolling-contact problem. The work involved in the process consists of obtaining workable representations for the pressure, pressure gradient, film thickness profile, and viscosity temperature and pressure relationships. Methods have been developed for dealing with the complicated non-linear heat-generation rate and some of the above-mentioned functional representations have been obtained for particular sets of data.

From the work performed, it appears that the prospects of computing lubricant temperatures from measured film thickness and pressure profiles is very promising.

RHEOLOGY EXPERIMENTS

A knowledge of the rheological properties of the lubricant that controls its effectiveness as a bearing lubricant is of paramount importance to the overall study. Such properties as determined under less severe conditions than exist in the contact zone have been found to be insufficient for predicting bearing behavior. Under this study, rheology data are being obtained by using

the disk machine.[3] Slip is induced between the disks, and measurements of rolling speed, sliding speed, film thickness, and traction in the film are recorded. These data can be put in the form of effective shear stress (traction/contact area) versus effective shear rate (slip/film thickness); these data can be interpreted in terms of fundamental lubricant rheology. A knowledge of the pressures and temperatures in the film will be extremely valuable in interpreting the data.

The early rheology experiments were conducted with a polyphenyl ether lubricant. Rheology experiments have been conducted with a highly refined mineral oil.

Discussion of Experiments with a Highly Refined Mineral Oil

In Figure 37, traction versus mean shear rates are presented for a highly refined mineral oil for conditions where T = 175 F, a loading of 100,000 psi Hertz pressure, and rolling speeds of 4500 and 6800 fpm. In Figure 38 are traction-shear rate curves for a polyphenyl ether[3] for the same operating conditions as the data of Figure 35.

In all the data, linear portions of the traction-shear rate curves exist at low shear rates followed by definite regions of non-linearity. The slope of this linear portion, which, in essence, represents an effective viscosity of the fluid, is significantly lower for the mineral oil than the polyphenyl ether. If it is assumed that the contact areas are essentially the same for all the 140,000 psi Hertz pressure loading conditions then a rough comparison between the effective viscosities on the highly refined mineral oil and polyphenyl ether can be made; that is

$$\frac{\mu_p}{\mu_o} \approx \frac{F_{Tp}\,\bar{s}_o}{F_{To}\,\bar{s}_p} \quad .$$

Here μ is the effective viscosity and the subscripts o and p represent the highly refined mineral oil and polyphenyl ether respectively. For the linear portions of the data of Figures 37 and 38

$$\frac{\mu_p}{\mu_o} = 510 \text{ and } 400$$

for rolling speeds of 4500 and 6800 fpm respectively. This ratio of effective viscosities is much larger than the ratio of the viscosity data obtained for these fluids by conventional viscometers such as given in Table 1.

The increase in the ratio which is probably associated primarily with the high pressures existing in the contact region demonstrates the magnitude of difference to be expected in the behavior of a lubricant under rolling contact conditions then static conditions. It might be anticipated then that the polyphenyl ether would give better lubtication than the mineral oil. This is consistent with the observed variations in deformation profiles given in Figure 16. For both fluids, the rheology data show a marked dependence on rolling speed.

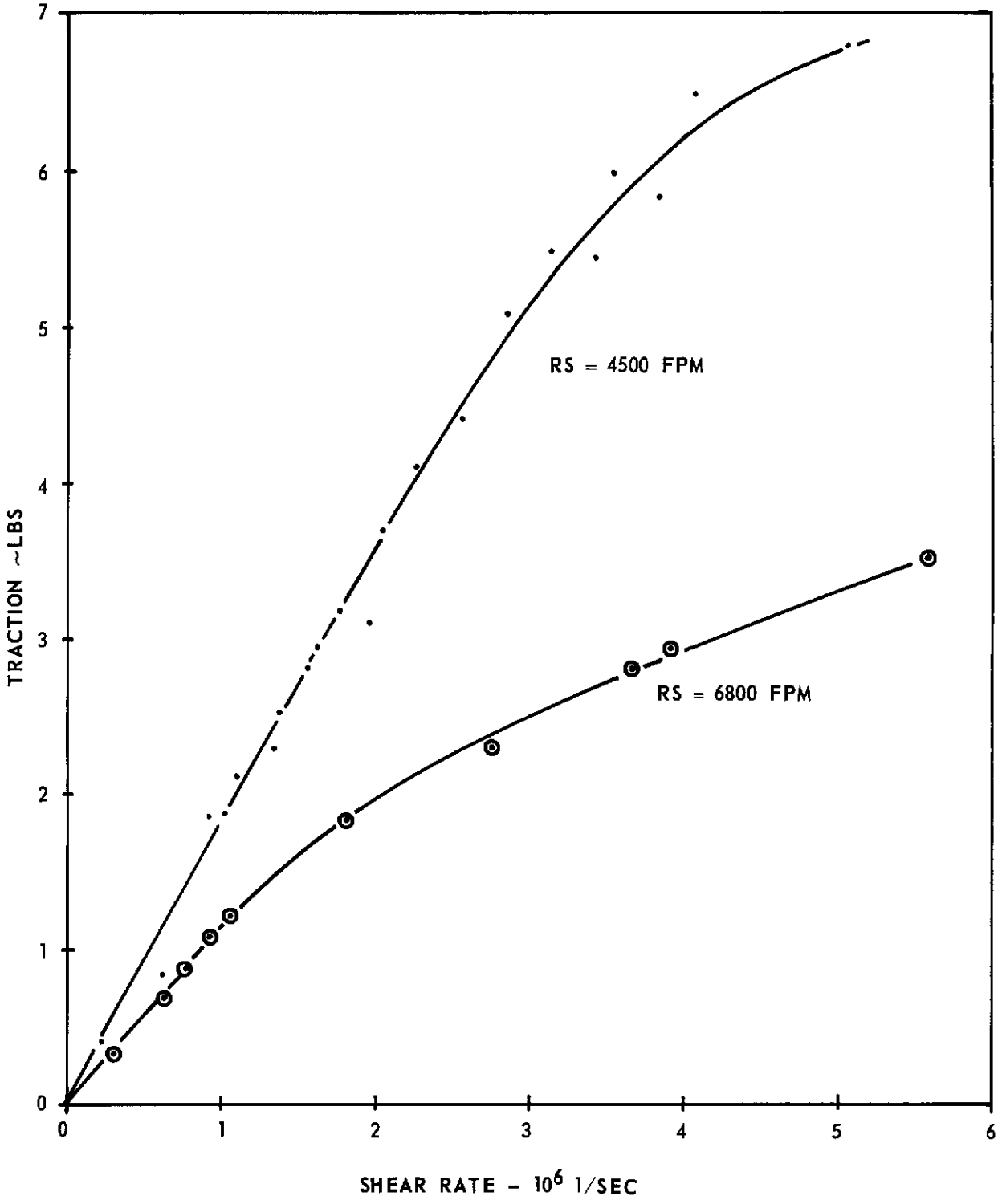

FIGURE 37. TRACTION-SHEAR RATE DATA FOR HIGHLY REFINED MINERAL OIL

P_h = 140,000 psi Hertz; T = 175 F.

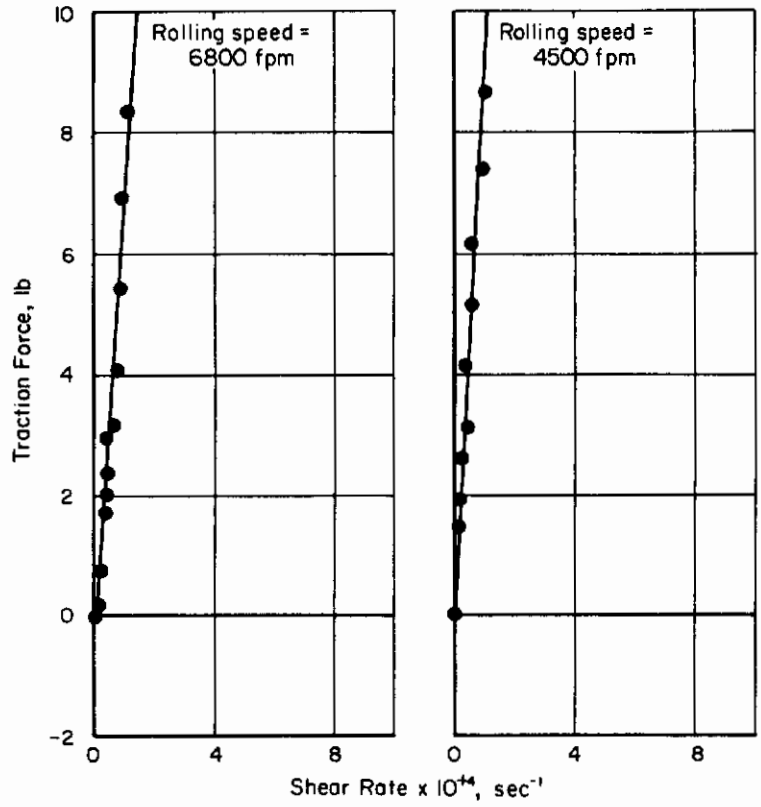

FIGURE 38. TRACTION-SHEAR RATE DATA FOR POLYPHENYL ETHER

P_h = 140,000 psi; T = 175 F.

Analysis of Rheology Data

In reference 3, an equation was derived for expressing the traction in the lubricant film in terms of the load and shape parameters and Newtonian model lubricant characteristics. This equation is given by

$$F_T = - \frac{2\pi a b \mu_o \bar{s}}{\gamma^2 p_h^2} \left[e^{\gamma p_h} (\gamma p_h - 1) + 1 \right] . \qquad (7)$$

Here F_T is the tractive force, b and a are the major and minor axis of the contact ellipse, μ_o is the bane viscosity of the lubricant at operating temperature, $\bar{s}$ is the mean shear rate, γ is the pressure coefficient of viscosity, and p_h is the maximum Hertz contact pressure. In essence this equation implies that for conditions where all parameters except F_T and $\bar{s}$ are constant, the traction-shear rate curve should be linear for a Newtonian fluid, implying, then, that both the highly refined mineral oil and the polyphenyl ether are Newtonian at low shear rates.

The non-linearity in the data could result from thermal disturbances (i.e., a drop in the fluid viscosity due to a temperature rise from sliding friction) or from some non-Newtonian characteristic of the lubricant manifested when a fluid is subjected simultaneously to high pressures and high shear rates. To determine if the non-linear portion of the data can be attributed, Equations 10 and 11 of Reference 3 were derived to yield an expression for the maximum temperature which can exist in a lubricant film. This equation can be given by

$$T_{ms} < \frac{3}{4} \frac{\bar{s} F_T}{u J \rho c b} , \qquad (8)$$

where T_{ms} is the maximum film temperature, u is the rolling speed, ρ is the lubricant density, and c the thermal conductivity. From analysis of the polyphenyl ether data, it was observed that at the point where non-linearity first occurred in the traction shear-rate curve the film temperature due to sliding was quite small. It was subsequently hypothesized that the polyphenyl ether could be non-Newtonian under some conditions of pressure and shear stresses.

Applying a similar analysis to the mineral oil data for the condition where R.S. = 6800 at onset of non-linearity (using Equation 8), it can be observed that

$$T_{ms} < \frac{3}{4} \frac{\bar{s} F_T}{u J \rho c b} \approx 100 \text{ F} . \qquad (9)$$

At the onset of non-linearity for the 4500 fpm condition, the maximum possible temperature could be considerably higher than 100 F.

It is possible then that the non-linearity in the traction-shear-rate data for the highly refined mineral oil could be a result of thermal disturbances rather than some non-Newtonian characteristic of the lubricant. Future and more detailed analyses are needed to clarify the point.

In Reference 3, one unexplained anomaly in the traction-shear-rate curves for the polyphenyl ether was the dependence of the data on rolling speed. Such a dependence is also seen in the highly refined mineral oil data and the exact explanation for such results is still somewhat in doubt. However, from the recent temperature measurements, there appears to exist some possibility that temperatures during pure rolling are quite high. Such temperatures could depend on rolling velocity (especially at high rolling speeds) such that the effective viscosity might change with rolling speed. Another possible reason for the variation in the effective viscosity with rolling speed is attributed to the variation in pressures with rolling speeds. For example, in Reference 4, pressures (computed from deformations) are presented for three rolling-speed conditions. The peak pressures are approximately 90,000 psi, 80,000 psi, and 75,000 psi for the rolling speeds of 2600 fpm, 4500 fpm, and 6800 fpm, respectively. Since the viscosity changes approximately exponentially with pressure, these pressure changes could account for a marked variation in viscosity with rolling speed.

CONCLUSIONS

A program has been conducted to determine the role of lubricant properties in determining the performance of rolling-contact elements.

Experiments have been conducted with a rolling-disk apparatus using an X-ray technique to determine the shapes of elastically deformed lubricated rolling elements. Such deformations are related to the stresses in the elements. Deformation profiles of the disks have been recorded for a range of rolling speeds, temperatures, loadings, and lubricants. From comparisons of the variation in the deformation profiles for various lubricants with existing bearing-fatigue life data for those lubricants, it appears that a general correlation might exist between deformation and performance.

Film pressures have been inferred from the measured deformations. The technique is based on classic elasticity theory and a Fourier series representation of the deformations. Pressure profiles have been obtained for a highly refined mineral oil lubricant. Studies have been made to determine the sensitivity of the inferred pressures to inconsistencies in the measured deformations.

Lubricant film pressures between bearing-steel disks have been measured directly using a manganin pressure transducer located on the surface of one of the disks. The transducer arrangement consists of an insulating coating of silicon-dioxide followed by a thin band coating of manganin; the change in resistance of the manganin due to film pressures is detected. The measured pressures patterns vary notably with loading but not with disk-rolling speeds (for the conditions given here). At high loadings, a slight pressure spike is evident in the data. From stresses inferred from the pressure measurements, it appears that the maximum shearing stress, which is possibly a fatigue-inducing stress, is closer to the surface than for dry contact. The magnitude of the maximum shearing stress is not significantly altered from dry contact. A profile of the rolling disk computed from measured pressures has been compared with a measured disk profile. The agreement between these profiles appears to demonstrate the consistency of both measurement techniques.

The surface temperatures existing in rolling contact have been measured. A band of copper was coated onto a quartz disk and the change in resistance of this copper, due to temperature, was detected as the band passes through contact. The surface temperatures measured by this method have appeared to be reasonably high and have compared favorably with temperatures computed assuming no heat loss to the disk surfaces during the time each fluid element passes through contact.

Studies have been made to determine the rheological behavior of a highly refined mineral oil lubricant in the contact region. A rolling-disk viscometer is used in these studies. Here slip is imposed between the rolling disk and the traction between the disks, the slip and the film thickness is measured. Analysis of the traction effective shear rate (slip divided by film thickness) curves obtained in the experiments appear to show the mineral oil to be a Newtonian fluid at least when the lubricant is subjected to low shear rates. The effective viscosity (traction divided by contact area and shear rate) of the mineral oil appears to be significantly lower (approximately by a factor of 500) than the effective viscosity for polyphenyl ether which had been studied previously for comparable pressure and temperature conditions.

REFERENCES

(1) Sibley, L. B. and Orcutt, F. K., "Elastohydrodynamic Lubrication of Rolling-Contact Surfaces", ASLE Trans., 4, 234-249 (1961).

(2) Bell, J. C., "Lubrication of Rolling Surface by a Ree-Eyring Fluid", ASLE Trans., 5, 160-171 (1962).

(3) Bell, J. C., Kannel, J. W., and Allen, C. M., "The Rheological Behavior of the Lubricant in the Contact Zone of a Rolling-Contact System", Trans. ASME, J. of B. Eng., Vol. 68, Sec D, No. 3, pp 423-435, September, 1964.

(4) Kannel, J. W., Bell, J. C., and Allen, C. M., "Methods for Determining Pressure Distributions Between Lubricated Rolling Contacts", 1964, Preprint 64-LC-23 (to be published as an ASLE paper).

(5) Kannel, J. W., Bell, J. C., and Allen, C. M., "A Study of the Influence of Lubricants on High-Speed Rolling-Contact Bearing Performance", ASD-TDR-61-643, Part IV, Sept., 1964.

(6) Dowson, D. and Higginson, G. R., "A Numerical Solution to the Elastohydrodynamic Problem", J. Mech. Eng. Sci., 1 (1), 6-15 (1959).

(7) Moult, J. F., "Critical Aspects in Bearing Fatigue Testing", ASLE Report No. 63, AM 2A-1, May, 1963.

(8) Dowson, D., Higginson, G. R., and Whitaker, A. V., "Elastohydrodynamic Lubrication: A Survey of Isothermal Solutions", J. Mech. Eng. Sci., 4 (2), 121-126 (1962).

(9) Archard, G. D., Gair, F. C., and Hirst, W., "The Elastohydrodynamic Lubrication of Rollers", Proc. Roy. Soc., A, 262, 51-71 (1961).

(10) Timoshenko, S. and Goodier, J. N., Theory of Elasticity, McGraw-Hill Book Company, Inc., New York (1951).

(11) Orcutt, F. K., "Experimental Studies of Elastohydrodynamic Lubrication", MTI, 64 TR 37 (July, 1964).

(12) Burton, R. A., Discussion of Paper by Bell, J. C., Kannel, J. W., and Allen, C. M., "The Rheological Behavior of a Lubricant in the Contact Zone of a Rolling-Contact System", Trans. ASME, J. of Bas. Eng., Vol. 68, Ser D, No. 3, pp 423-435, September, 1964.

(13) Hamming, R. W., Numerical Methods for Scientists and Engineers, McGraw Hill, New York, 1962.

APPENDIX A

ACCURACY OF PRESSURE FOUND FROM SURFACE DEFORMATION

A Method for Finding Pressure from Surface Deformation

Basic Theory

Consider two cylinders of radius R_1 and R_2 rolling against each other in lubricated contact under sufficient load so that they are elastically deformed. Suppose that the clearance h between them is known at any distance x in the rolling direction from a base line near the center of contact. It is desired to evaluate the pressure p in the lubricant as a function of x from the known clearance h(x). The elastic module of the cylinders E_1 and E_2 are presumed to be known together with their Poisson ratios ν_1 and ν_2.

It is known[4] that the clearance h(x) has the form

$$h(x) = A + \frac{x^2 - 2b\,x}{2R} - \frac{2(1-\nu^2)}{\pi E} \int_{-a}^{+a} p(z) \ln \frac{|x-z|}{2R}\, dz, \tag{10}$$

where A and b are constants,

$$\frac{1}{R} = \frac{1}{R_1} + \frac{1}{R_2}, \quad \frac{1-\nu^2}{E} = \frac{1-\nu_1^2}{E_1} + \frac{1-\nu_2^2}{E_2},$$

and the zone $-a \leq x \leq a$ is taken large enough to contain all the significant pressure region. In terms of dimensionless variables

$$\xi = \frac{x}{a}, \quad \zeta = \frac{z}{a}, \quad g(\xi) = \frac{R}{a^2} h(x), \quad q(\xi) = \frac{2R\,(1-\nu^2)}{aE} p(x),$$

this relation can be expressed as

$$g(\xi) = \frac{AR}{a^2} - \frac{b}{a}\xi + \frac{1}{2}\xi^2 - \frac{1}{\pi} \int_{-1}^{+1} q(\zeta) \ln \frac{|\xi-\zeta|}{2R/a}\, d\zeta. \tag{11}$$

If the clearance profile h(x) is known, it is possible to express it in the form

$$g(\xi) = \frac{1}{2}\alpha_o + \sum_{n=1}^{\infty} \alpha_n T_n(\xi), \tag{12}$$

where $T_n(\xi)$ is a Tchebyshev polynomial of the first kind, that is

$$T_n(\xi) = T_n(\cos\theta) = \cos n\theta$$

where $\cos\theta = \xi$. The coefficients α_n can be found from

$$\alpha_n = \frac{2}{\pi}\int_{-1}^{+1} g(\xi)\, T_n(\xi)\, \frac{d\xi}{\sqrt{1-\xi^2}} \quad . \tag{13}$$

If $g(\xi)$ is represented in this way, then it has been shown[4] that the pressure distribution is given by*

$$q(\xi) = (1-\xi^2)^{1/2}\left\{1-2\sum_{n=2}^{\infty} n\,\alpha_n\, U_{\left[\frac{n-2}{2}\right]}(\xi)\, U_{\left[\frac{n-1}{2}\right]}(\xi)\right\}, \text{ for } -1<\xi<1, \tag{14}$$

where $U_n(\xi) = U_n(\cos\theta) = \frac{\sin(n+1)\theta}{\sin\theta}$ is a Tchebyshev polynomial of the second kind, and $\left[\frac{n}{2}\right]$ denotes the largest integer in $n/2$.

In principle it is thus possible to find the pressure acting on the roller surfaces if the shape of the clearance between them is known. In practice, however, there are important difficulties to be overcome. One can be seen immediately in that the coefficient α_n in the series for the clearance is multiplied by n in the series for the pressure. Thus convergence of the series for the pressure can be significantly slower than that for the film thickness. This means that many of the coefficients α_n which contribute little in the clearance are important in the pressures, that is trivial detail in the clearance may reflect important detail in the pressure. This relationship demands high accuracy in the clearance measurements. Since these measurements, as obtained by the X-ray method, involve noticeable statistical error, real care must be used in making them.

---

*This relationship may be expressed alternatively as

$$q(\xi) = \frac{1}{\sqrt{1-\xi^2}}\left\{(1-\xi^2) - \frac{1}{2} + W + M\,\xi + \sum_{n=2}^{\infty} n\,\alpha_n\, T_n(\xi)\right\},$$

where, with W' being the load per unit length of the cylinders,

$$W = \frac{1}{\pi}\int_{-1}^{+1} q(\xi)\, d\xi = \frac{1}{2} - \sum_{n=2,4,6,\cdots} n\,\alpha_n = \frac{2R(1-\nu^2)\,W'}{\pi a^2 E} \quad .$$

$$M = \frac{2}{\pi}\int_{-1}^{+1} \xi\, q(\xi)\, d\xi = -\sum_{n=3,5,7,\cdots} n\,\alpha_n \quad .$$

A second difficulty arises in that the clearance measurements are made only at discrete locations, at least that is true now. Thus the continuous function $g(\xi)$ needed in the integrations for evaluating the α_n's really is not available unless some method for interpolation of $g(\xi)$ is assumed. A complete interpolation of $g(\xi)$ can be constructed rather effectively for the low order integrations, but as n increases the propriety of the assumed interpolation becomes more and more doubtful. This doubt ultimately limits the number of coefficients α_n which can be calculated from a given set of clearance measurements.

Beyond these problems, it is known of course that X-ray data need to be corrected to allow for the variation that outlet cavitation causes in the absorption of the X-rays. Another factor is that the finite width of the X-ray beam tends to average X-ray counts across what should be several distinct sampling positions, and careful analysis of pressures may require that this averaging should be undone first. It is possible to undo much of this averaging by observing how the X-ray counts vary with each partial shift in the sampled region, but the statistical variations of the X-ray counts make the de-averaging rather uncertain. Even without these problems, the statistical nature of X-ray counting and other possible experimental irregularities make the required fine details in the clearance measurements somewhat uncertain.

In view of such problems, it seems well to investigate how much accuracy can be obtained in pressure distributions calculated from clearance profiles obtained from X-ray counting. Considering the formula which shows the pressure as an infinite series of Tchebyshev polynomials, one may conduct this investigation by seeking first to find how many terms of the series can be justified from a given set of data, and second to find how many terms would be needed to yield the detail that may be required in the pressure calculations. These are the matters to be considered here.

Fitting of Polynomial Series of X-Ray Data

Pursuing the present method for finding lubricant film pressures from X-ray-measured disk clearances, it is required to find coefficients α_n for the dimensionless clearance $g(\xi)$ in (12). The method used previously for finding the α_n's consisted of interpolating a fairly smooth, continuous function for $h(x)$ among the data points, and then integrating that function for many values of n according to the plan shown in equation (13). This method yields coefficients α_n, but it gives little indication of how accurate they are. Therefore, it is desirable to construct some other method for finding them which will account for the discrete character of the data and also their statistical uncertainty.

An immediate thought in fitting data statistically to some function such as the polynomial series in (12) is to choose coefficients for a finite series by minimizing the sum of the squares of residual errors in the fitting. Unfortunately, Tchebyshev polynomials do not lend themselves readily to such a fitting procedure when the data are spaced linearly on the ξ-scale, as the available data are. (For Tchebyshev polynomial series, spacing of the data would be convenient if it were uniform on the θ-scale where $\cos\theta = \xi$. The inconveniences of linear spacing on the

ξ-scale is related to the fact that the orthogonality relation among Tchebyshev polynomials involves a weight function $1/\sqrt{1-\xi^2}$ which is nonlinear.) An ordinary hower series likewise is inconvenient, since for present use many terms would be required, and these become difficult to compute because the determinant of the normal equations for finding the coefficients becomes small very rapidly as its order increases (Cf Reference 13, pp 229-231).

An acceptable procedure for fitting the data can be had, however, by using a different form of orthogonal polynomial series which is for an arbitrary arrangement of data points, including, in particular, points that are uniformly spaced over $-1 \leq \xi \leq +1$ (Cf Reference 13, pp 244-246). This series consists of polynomials $\varphi_n(\xi)$ connected by a recursion formula of the form:

$$\begin{aligned} \varphi_0(\xi) &= 1 \\ \varphi_1(\xi) &= \xi - \gamma_1 , \\ \varphi_n(\xi) &= (\xi - \gamma_n)\,\varphi_{n-1}(\xi) - \delta_n\,\varphi_{n-2}(\xi), \text{ for } n=2,3,4,\ldots. \end{aligned} \tag{15}$$

Having given a set of coordinates ξ_i (with $i = 0,1,---, I$) where measurements are to be made, the definition of the polynomials $\varphi_n(\xi)$ is completed by adding the requirements that

$$\begin{aligned} \sum_{i=0}^{I} \varphi_n(\xi_i)\,\varphi_{n-1}(\xi_i) &= 0 \text{ for } n \geq 1, \\ \sum_{i=0}^{I} \varphi_n(\xi_i)\,\varphi_{n-2}(\xi_i) &= 0 \text{ for } n \geq 2. \end{aligned} \tag{16}$$

From these requirements, it can be shown that

$$\begin{aligned} \gamma_n &= \sum_{i=0}^{I} \xi_i\,\varphi_{n-1}^2(\xi_i) \Big/ \sum_{i=0}^{I} \varphi_{n-1}^2(\xi_i) \text{ for } n \geq 1, \text{ and} \\ \delta_n &= \sum_{i=0}^{I} \xi_i\,\varphi_{n-1}(\xi_i)\,\varphi_{n-2}(\xi_i) \Big/ \sum_{i=0}^{I} \varphi_{n-2}^2(\xi_i) \text{ for } n \geq 2. \end{aligned} \tag{17}$$

The recursion formula in (15) becomes applicable to the case $n = 1$ if it is agreed also that $\delta_1 = 0$. It may be observed that γ_1 is simply the mean value of the ξ_i's, and it vanishes for the case where the ξ_i's are spaced uniformly from $\xi = -1$ to $\xi = +1$.

These functions $\varphi_n(\xi)$ are orthogonal in the sense that

$$\sum_{i=0}^{I} \varphi_n(\xi_i)\,\varphi_m(\xi_i) = 0 \quad \text{for } m \neq n. \tag{18}$$

To prove this, it is sufficient to prove it for $m < n$. Its validity for $n = 1$ and $n = 2$ follows at once from (16). For $n > 2$, it can be shown true by induction. Thus, suppose it holds for $n \leq k$. Then, putting $n = k+1$, and taking $0 \leq m \leq k-1$,

$$\sum_{i=0}^{I} \varphi_{k+1}(\xi_i)\,\varphi_m(\xi_i) = \sum_{i=0}^{I} \left[(\xi_i - \gamma_{k+1})\,\varphi_k(\xi_i) - \delta_{k+1}\,\varphi_{k-1}(\xi_i)\right]\varphi_m(\xi_i)$$

$$= \sum_{i=0}^{I} \varphi_k(\xi_i) \cdot \xi_i\,\varphi_m(\xi_i)$$

$$= \sum_{i=0}^{I} \varphi_k(\xi_i)\left[\varphi_{m+1}(\xi_i) + \gamma_{m+1}\,\varphi_m(\xi_i) + \delta_{m+1}\,\varphi_{m-1}(\xi_i)\right] = 0 .$$

From (16), this sum vanishes also if $m=k-1$ or k. Therefore, (18) holds for $n=k+1$ also, and hence by induction for all $n \geq 1$.

Now let it be required to fit a set of disk separation data taken at points ξ_i (where $i=0,1,2,\text{---},I$) by a finite series of the form

$$g_N(\xi) = \sum_{n=0}^{N} A_n\,\varphi_n(\xi), \qquad N < I , \tag{19}$$

with the coefficients A_n chosen so as to minimize the sum of the square of the residuals

$$s^2 = \frac{1}{I+1} \sum_{i=0}^{I} \left[g_N(\xi_i) - y_i\right]^2, \tag{20}$$

where the y_i are the measured estimates of the dimensionless clearance $g(\xi)$ at $\xi=\xi_i$. Putting $\partial s^2/\partial A_m = 0$, one has

$$\sum_{i=0}^{I} \left[\sum_{n=0}^{N} A_n\,\varphi_n(\xi_i) - y_i\right]\varphi_m(\xi_i) = 0, \text{ for } m = 0,1,2,\text{---},N.$$

Then from the orthogonality relation (18) it follows that

$$A_m = \frac{\sum_{i=0}^{I} y_i\,\varphi_m(\xi_i)}{\sum_{i=0}^{I} \varphi_m^{\,2}(\xi_i)}, \text{ for } m = 0,1,2,\text{---},N. \tag{21}$$

Thus a straightforward calculation quickly yields values for the coefficients A_n from the experimental data, and no large sacrifice of accuracy occurs in the numerical processes.

If estimates are available for the variances to be expected in the measurements y_i, then it is possible to obtain estimates for the variances of the coefficients A_n, and hence of expected variances of pressures calculated from them at various values of ξ. However, a simpler approximate approach to the question of how much pressure calculation is justified by the data can be had by simply computing s^2 from equation (20) and comparing it with σ^2, the average variance expected among individual measurements. When enough terms are included in the series (19) so that $s^2 \leq \sigma^2$, then the series fits the data as well as can be expected, so no further addition of terms to the series is justified.

Once a polynomial series of the Form (19) has been fitted in the least-squares sense to a set of data, a Tchebyshev polynomial series of the same order can also be fitted in the least-squares sense. Getting this second series amounts to rearranging terms in the first series, just as getting a least-squares fitted power series would, but it is not advantageous to perform the rearrangement of terms directly. The disadvantage of direct rearrangement arises from the extensive cancellation of terms that goes on within individual Tchebyshev polynomials, and presumably also within the polynomials $\varphi_n(\xi)$ defined by (15). Direct recombining of coefficients would run the risk of losing most or all of the significant parts of many coefficients. Therefore, an indirect procedure for getting the related Tchebyshev series becomes advantageous. This method is simply to use the series of form (19) to compute estimates of $q(\xi_i)$ at a set of points ξ_i properly spaced for evaluation of a Tchebyshev polynomial series, and then to perform a least-squares fit of a Tchebyshev polynomial series of the same order N to those points. This refitted series, being simply a rearrangement of the first series, should reproduce the values given by the first series very closely (to within small round-off errors) throughout the fitted range. That is, the second series should be effectively the least-squares fitted Tchebyshev polynomial series for the measured clearance data also.

Fitting of a Tchebyshev polynomial series can be more easily described in terms of the variable $\theta = \arccos \xi$. Thus let

$$\xi = \cos \theta, \; T_n(\xi) = T_n(\cos \theta) = \cos n\theta, \; g(\xi) = \bar{g}(\theta) \; . \tag{22}$$

Then, from Equation (12), a finite series of order N for $g(\xi)$ is

$$\bar{g}(\theta) = \frac{1}{2} \alpha_o + \sum_{n=1}^{N} \alpha_n \cos n\theta \; . \tag{23}$$

Now let it be required to find a least-squares fit of this series of $\bar{g}(\theta)$ to a set of values y_i computed from the polynomial series of from (19) at points $\theta = \theta_i$ (that is at $\xi = \cos \theta_i$) where

$$\theta_i = \frac{i\pi}{I} \; , \; i = 0,1,2,---,I \; .$$

The variance to be minimized is

$$\bar{s}^2 = \frac{1}{I+1} \sum_{i=0}^{I} [\bar{g}(\theta_i) - \bar{y}_i]^2 . \qquad (24)$$

Putting $\frac{\partial \bar{s}^2}{\partial \alpha_m} = 0$ for m = 0,1,---,N, one finds

$$\sum_{i=0}^{I} [\frac{1}{2} \alpha_o + \sum_{n=1}^{N} \alpha_n \cos n\theta_i - \bar{y}_i] \cos m \theta_i = 0 ,$$

for all those values of m. Taking the values of the θ_i into account, and letting

$$S_m^I = \sum_{i=0}^{I} y_i \cos i \frac{m\pi}{I} \qquad (25)$$

shows

$$\frac{1}{2} \alpha_o \sum_{i=0}^{I} \cos i \frac{m\pi}{I} + \frac{1}{2} \sum_{n=1}^{N} \{\alpha_n \sum_{i=0}^{I} [\cos \frac{i(m+n)\pi}{I} + \text{cr} \frac{i(m-n)\pi}{I}]\} = S_m^I . \qquad (26)$$

It is advantageous now to observe the Lagrange identity which may be written as

$$\sum_{i=0}^{I} \cos i \theta = \begin{cases} \frac{1}{2} [1 - \frac{\cos (I+1) \theta - \cos I \theta}{1 - \cos \theta}] & \text{if } \theta \neq 2k\pi , \\ I+1 \quad \text{if} \quad \theta = 2k\pi , \end{cases} \qquad (27)$$

and k is any integer. From this it follows that

$$\sum_{i=0}^{I} \cos i \frac{m\pi}{I} = \begin{cases} I+1 & \text{if } m = 0, \\ 0 & \text{if } m = 1,3,5,----, \\ 1 & \text{if } m = 2,4,6,----. \end{cases} \qquad (28)$$

Also

$$\sum_{i=0}^{I} [\cos i \frac{(m+n)\pi}{I} + \cos i \frac{(m-n)\pi}{I}] = \begin{cases} 2(I+1) & \text{if } m=n=0 \\ 0 & \text{if } m=1,3,5,---, \\ 2 & \text{if } m+n=2,4,6,---\text{and } m \neq n, \\ 1+2 & \text{if } m+n=2,4,6,---\text{and } m=n. \end{cases} \qquad (29)$$

Now let E(N) be the largest even integer $\leq$ N, and O(N) the largest odd integer. Then from (26), (28), and (29):

$$\frac{I}{2} \alpha_m = S_m^I - [\frac{1}{2} \alpha_o + \sum_{n=2,4,6,---}^{E(N)} \alpha_n] , \text{ for } m = 0,2,4,---,E(N).$$

Summing all these equations for even values of m, but giving the weight 1/2 to the one for m = 0, one can solve for this last bracketed quantity and find

$$[\tfrac{1}{2}\alpha_o + \sum_{n=2,4,6,---}^{E(N)} \alpha_n] = \frac{2}{I+1+E(N)} [\tfrac{1}{2} S_o^I + \sum_{n=2,4,6,---}^{E(N)} S_n^I] .$$

Substituting this sum into the previous equation shows

$$\alpha_m = \frac{2}{I} \{S_m^I - \frac{2}{I+1+E(N)} [\tfrac{1}{2} S_o^I + \sum_{n=2,4,6,---}^{E(N)} S_m^I]\}, \text{ for } m=0,2,4,---,E(N) . \quad (30)$$

Similarly, from (26) when m is odd,

$$\tfrac{I}{2} \alpha_m = S_m^I - \sum_{n=1,3,5,---}^{O(N)} \alpha_n , \text{ for } m=1,3,5,--- .$$

Adding these equations shows

$$\sum_{n=1,3,5,---}^{O(N)} \alpha_n = \frac{2}{I+1+O(N)} \sum_{n=1,3,5,---}^{O(N)} S_m^I ,$$

and substituting this sum into the preceding equation shows

$$\alpha_m = \frac{2}{I} [S_m^I - \frac{2}{I+1+O(N)} \sum_{n=1,3,5,---}^{O(N)} S_n^I], \text{ for } m=1,3,5,---,O(N). \quad (31)$$

It has been shown here that the fitting of the Tchebyshev polynomial series to the points $(\theta_i, \overline{y}_i)$ derived from the first polynomial series can be accomplished by computing the sums S_m^I from (15), then getting the coefficient α_m from (30) and (31), and by applying these to the series in (23) which is termwise equivalent to the series for $g(\xi)$ in (12). Then equation (23) for evaluation of the coefficients α_n is no longer needed; the pressure function $q(\xi)$ given in (14) now is defined by the coefficients α_n given by (30) and (31).

Computation of Pressure Distributions

In order to evaluate pressure distributions from circumferential profile data, a computing program was prepared for use on an electronic computer (a Control Data G20 computer). With this program, the computer was made to perform the following operations:

(1) For a given set of equally spaced abscissal ξ_i over the interval $-1 \leq \xi \leq 1$, that is for a given value of I, and for $n=0,1,2,---,N < I$, internal coefficients for a set of polynomials $\varphi_n(\xi)$ as (15) are computed using the equation (17), and those polynomials are evaluated at all the points $\xi = \xi_i$, where $i=0,1,2,---,I$.

(2) Using the data points (ξ_i, y_i), coefficients A_n for n=0,1,2,---N are computed according to equation (21).

(3) Taking $\bar{g}(\theta) \equiv g(\xi)$ as given by (19), values of $\bar{y}_i \equiv \bar{g}(\frac{i\pi}{I})$ are computed for i=0,1,2,---,I. Then coefficients α_n, n=0,1,2,---,N, for a Tchebyshev polynomial series are found using equations (25) (30), and (31).

(4) These coefficients α_n are inserted into the series in equation (14) and the series is evaluated at a number of values of ξ sufficient to outline the dimensionless pressure function $q(\xi)$. In most cases evaluations have been made at the points where ξ = -1(0.05)1, but smaller intervals have been used in some cases. The dimensional pressure is then

$$p(x) = \frac{aE\ q(\xi)}{2R\ (1-\nu^2)} \quad . \tag{32}$$

In this calculation, the pressure distribution calculated depends initially on the set of data points (ξ_i, y_i); but it depends also on the choice of N, the number of terms, and more detail can be expected to appear in the pressure curve as N increases. If the data are experimental, then the number of terms justified is approximately only that which is large enough to make s^2 in (20) as small as σ^2, the expected variance among individual measurements. If interpolation of data points is regarded as acceptable, then many more terms can be included, but, as will be seen later, the usable number of terms is still limited by the number and quality of the interpolated points: beyond some number of terms the addition of more terms leads to spurious calculated pressures. More will be said about this in connection with the examples that follow.

Examples of Pressure Calculations

Data Selected for Analysis

In order to illustrate the plan described above for calculation of pressure acting between rolling disks, and to gauge its capability for revealing sharp detail in the pressure distribution, a few sets of experimental data were selected for analysis. The data selected involve highly refined mineral oil as the lubricant. In order to make them usable, a necessary first step is to develop a plan for converting the data into film thicknesses. For this purpose, a calibration experiment was performed, using unloaded, stationary disks with the space between them flooded with lubricant. X-ray counts were made at intervals of 0.001 inch across the central region. The results are shown in Figure 39. The symmetric parabola in the figure shows what measurements would have been correlated by a simple proportionality between the X-rays and the clearance, and it can be seen to serve very well except for readings 0.005 inch or more beyond the center on the outlet side. Beyond that point, the disparity may be explained (as it was in earlier work[4]) by the estimate that the intensity of the incoming X-ray beam fell off linearly with position, so that beginning 0.004 in. beyond the center it decreased at a rate of 25/11 per cent per 0.001 inch toward the outlet.

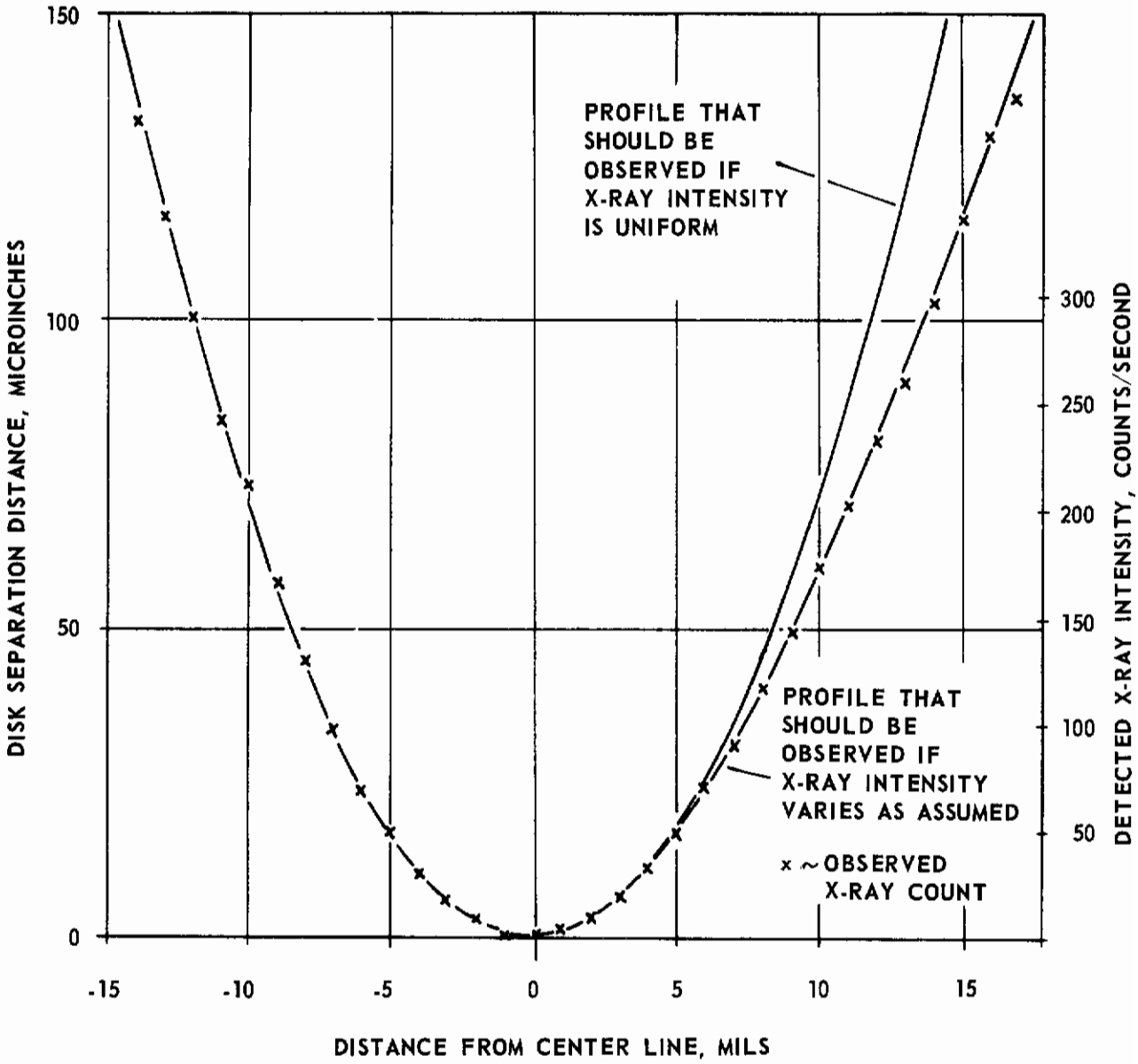

FIGURE 39. STATIC PROFILE OF UNLOADED DISKS USED FOR CALIBRATION OF X-RAY MEASUREMENTS OF DISK SEPARATION BY A FILM OF HIGHLY REFINED MINERAL OIL

When the disks roll, the lubricant film separates on the outlet side, and X-ray absorption by the lubricant differs from that in the calibration experiment. Therefore, X-ray counts from the experiment illustrated in Figure 39 were compared with counts from an experiment where no lubricant was present. It was found thus that flooding the space between the disks with highly refined mineral oil cut the X-ray transmission to about 58/108 of that between dry disks.

In order to correct clearance reading in the outlet region for absorption, it was assumed that the thickness of the minimum clearance is also the thickness of the lubricant film which adheres to the disks' surfaces in the outlet region, and that the rest of the clearance between the disks in the outlet region is occupied by a cavity. Thus, if h_m is the minimum clearance, and $h(x)$ is the actual clearance at point x in the outlet region, the effective clearance for X-ray transmission is

$$h_m + \frac{108}{58} [h(x)-h_m] .$$

If $I(x)$ is the intensity of the X-ray beam directed toward position x, and I_o is the intensity on the upstream side (where it was presumably uniform), then the nominal film thickness $h_{nom}(x)$ in the outlet, if calibrated on the same scale as that in the inlet region, is

$$h_{nom}(x) = \frac{I(x)}{I_o} \{h_m + \frac{108}{58} [h(x)-h_m]\} .$$

Solving this for $h(x)$ shows

$$h(x) = \frac{50}{108} h_m + \frac{58}{108} \frac{I(x)}{I_o} h_{nom}(x) . \qquad (33)$$

Thus, if $h_{nom}(x)$ is film thickness apparently measured at some position x in the outlet region, the $h(x)$ from (33) is an estimate of the true thickness calibrated compatibly with the measured thicknesses in the inlet and central regions.

For one set of operating conditions, three complete circumferential profiles were measured at increments of 0.001 inch. The conditions consisted of a nominal maximum Hertz pressure of 100,000 psi, disk temperature 175 F, and rolling speed 9100 ft/min (that is, 12,000 rpm). The actual load probably should have produced a maximum Hertz pressure of 107,000 psi, with a dry contact area half width equal to 0.00950 in. The existence of three replicate experiments, all of them seemingly favorable, provided a good starting point for careful analysis, so these experiments were adopted as a starting point.

Analyses of Direct Experimental Data

Disk clearances as read at various positions for the three replicated experiments after correction according to Equation (33) are shown in Figure 40. Values of the clearance h at each point in each experiment were read and tabulated.

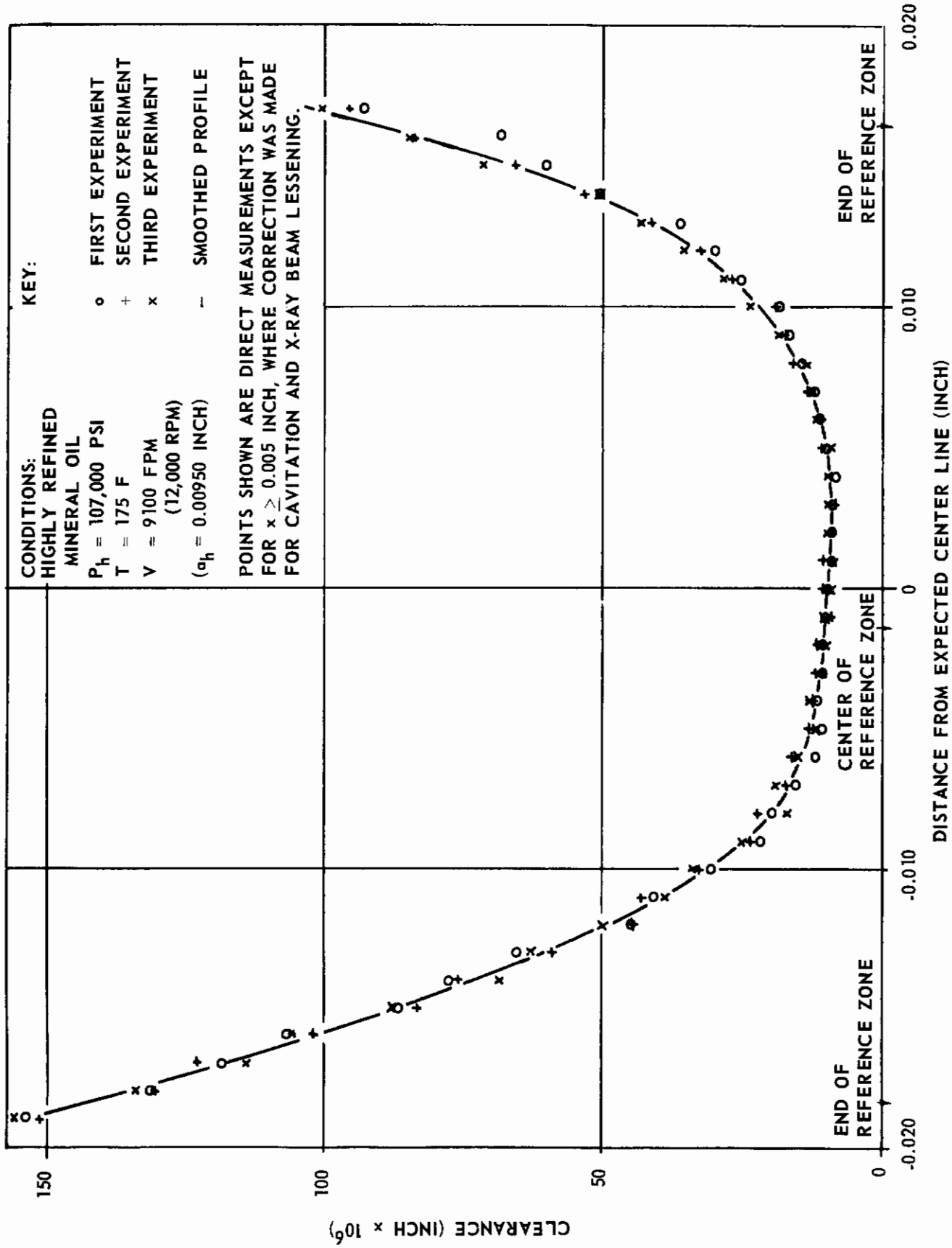

FIGURE 40. CIRCUMFERENTIAL CLEARANCE PROFILE DATA USED IN PRESSURE ACCURACY STUDY

Then the average $\bar{h}$ among the readings at each position was tabulated, as was the variance among the readings at each position. The over-all average variance among individual readings (after deletion of one erratic reading in the next to last position on the right) is 3.58×10^{-12} in.^{2}, though it may be observed that the variance is generally greater at the ends of the graph than it is in the middle. Since the relative radius of curvature of the undeformed disks is R = 0.72 in., ($\frac{1}{R} = \frac{1}{R_1} + \frac{1}{R_2}$), and since the half-width of the reference zone was taken to be a = 0.018 in., the dimensionless clearance $g(\xi) \equiv \frac{R}{a^2} h(x)$ here is $\frac{2}{900}$ times the dimensional clearance h in microinches. That is, the variance in individual readings of $g(\xi)$ is

$$\sigma^2 = 3.58 \left(\frac{2}{900}\right)^2 = 0.177 \times 10^{-4}.$$

This is the σ^2 to be compared with the s^2 of Equation (20) in deciding whether a given orthogonal polynomial fit to $g(\xi)$ for a particular experiment is of too low or too high order. If a fit is made to the average clearance $\bar{h}$ at each position, then a proper σ^2 would seem to be one-half of the above σ^2, since the variance in the estimate of a mean based on n points is 1/n-1 times the variance among the individual values.

Figure 40 also shows a smooth curve drawn in with the aid of visual interpolation, eliminating irregularities in the end sections which are surely unrealistic. In its end sections, this curve also closely approaches the exterior Hertz profile, suitably adjusted vertically as is reasonable, thus showing its reasonability as a deformed clearance profile.

Figures 41 and 42 show the pressure curves derived by fitting these data with Tchebyshev polynomial series, according to the method described above. It can be seen that the curves based on 11-term expansions are reasonably consistent among themselves, but the curves based on 21-term expansions are fairly widely scattered. Curves based on 31-term expansions were computed for the second experiment, the average readings $\bar{h}(x)$, and the smoothed readings, but the pressures they predict are so far wrong that they could not be plotted on Figures 41 and 42. This scattering was to be expected on the basis of the variances s^2 among the fits to individual data points, computed from Equation (20). A comparison of s^2 and σ^2 for the various cases is shown in Table 3. For the sake of later comparisons, it should be noted that for each of these pressure calculations, the clearance data had been tabulated at 37 points.

The fair consistency among the solutions using 11-term expansions is understandable here since s^2 is not much smaller than σ^2 in any case. With 21-term expansions, s^2 was much smaller, so the solutions scattered noticeably; and with 31-term expansions s^2 was so much smaller that the solutions lost all semblance of reasonability. It should be remarked that comparison of s^2 with σ^2 was a more successful indicator of the quality of the solution for the cases of individual experiments than for the case using averages of experiments. For the case using smoothed data, there is no σ^2 available for ready comparison with s^2.

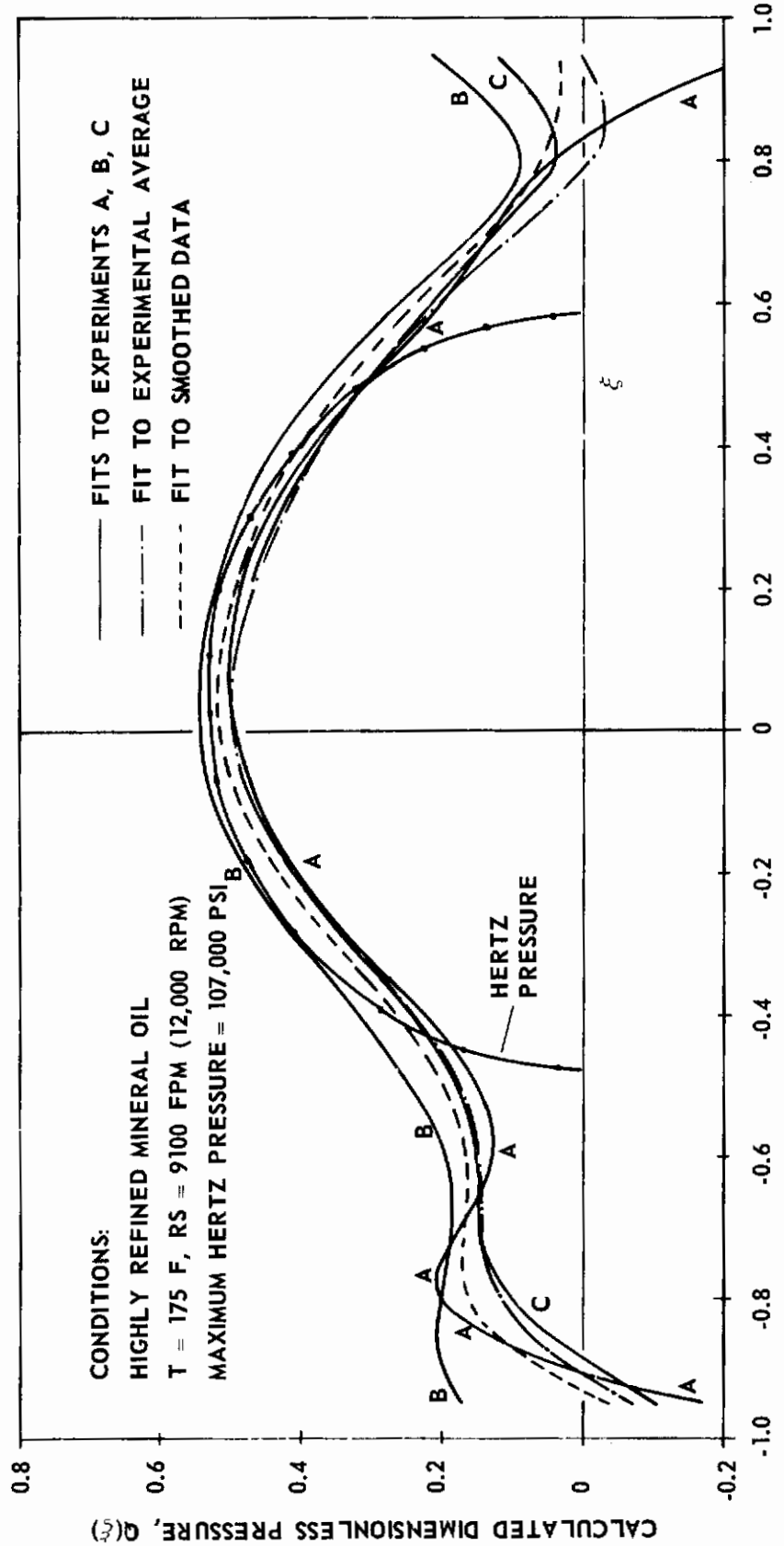

FIGURE 41. CALCULATED PRESSURE DISTRIBUTIONS BASED ON 11-TERM FITS TO 37-POINT TABLES OF PARTICULAR EXPERIMENTAL DATA, AVERAGED DATA, AND SMOOTHED DATA

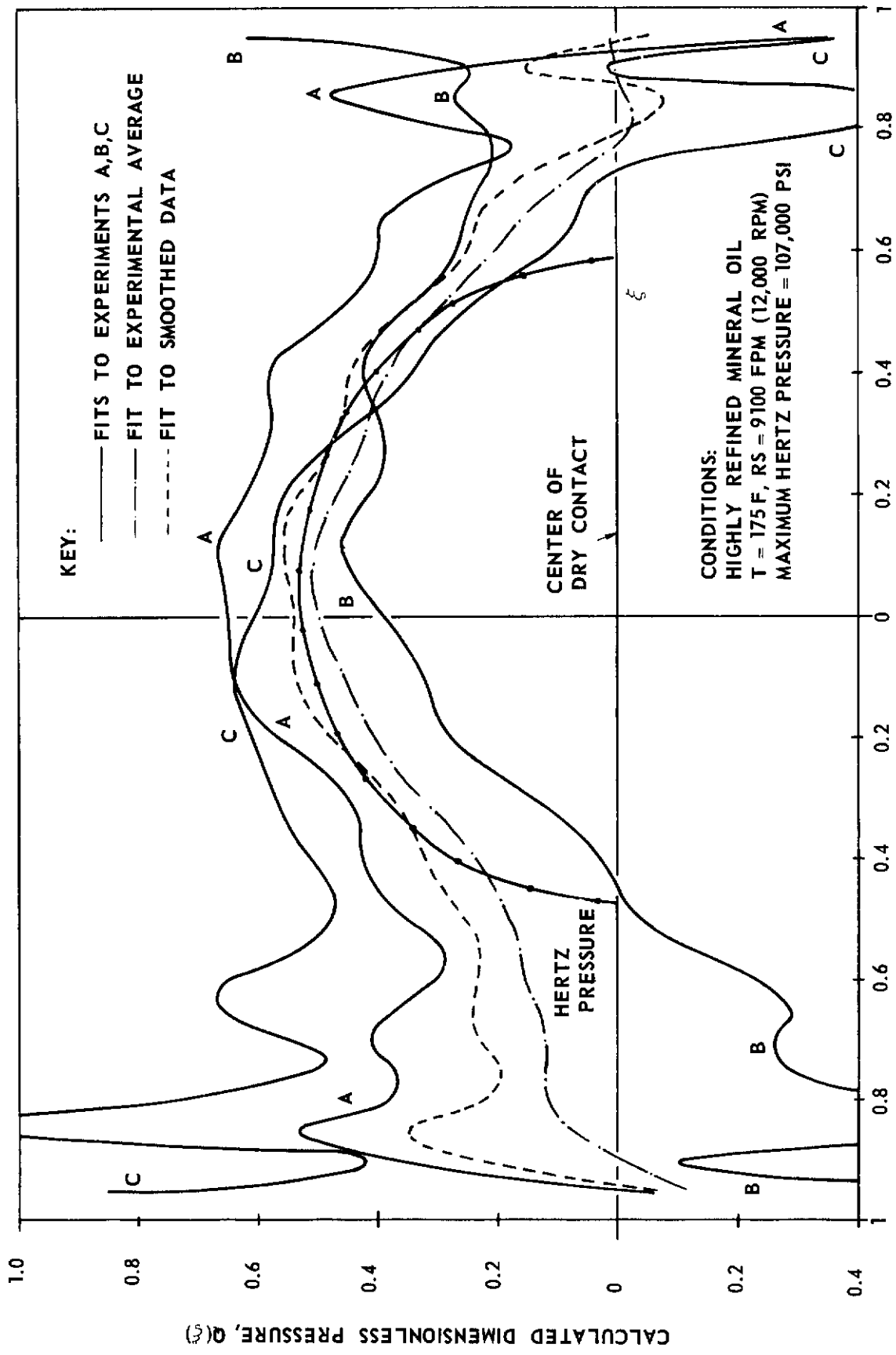

FIGURE 42. CALCULATED PRESSURE DISTRIBUTIONS BASED ON 21-TERM FITS TO 37-POINT TABLES OF PARTICULAR EXPERIMENTAL DATA, AVERAGED DATA, AND SMOOTHED DATA

TABLE 3. VARIANCES AMONG POLYNOMIAL FITS TO EXPERIMENTAL DATA

Source of Data	Number of Points	Number of Terms in (14)	Variance in Fit, $s^2 \times 10^4$	Variance of Data, $\sigma^2 \times 10^4$	Appearance of Pressure
First experiment	37	11	0.169	0.177	Good
	37	21	0.0829	0.177	Poor
Second	37	11	0.167	0.177	Good
Experiment	37	21	0.0882	0.177	Poor
	37	31	0.00645	0.177	Bad
Third	37	11	0.124	0.177	Good
Experiment	37	21	0.0677	0.177	Poor
Average of	37	11	0.0480	0.0883	Good
Experiments	37	21	0.0317	0.0883	Fair
	37	31	0.000708	0.0883	Bad
Smoothed Data	37	11	0.00218	--	Good
	37	21	0.000348	--	Good
	37	31	0.0000535	--	Bad

Effect of Smoothing and Interpolating

It may be seen by comparing Figures 41 and 42 that with smoothed data, read at 37 points from the continuous curve in Figure 40, there was little change in the calculated pressure distribution when the length of the Tchebyshev polynomial expansion was increased from 11 terms to 21 terms. In this respect, the smoothed data definitely excelled even the averaged data. It appears, in fact, that the principal effect of the smoothing was to stabilize the pressure calculation by making it more independent of the length chosen for the polynomial expansion. However, this stabilization was not unlimited, for with 31 terms even the smoothed data gave bad results.

The general phenomenon that seems to be at work here is that when too many terms are used in the expansion (23) there is a strong risk that some high order terms will be improperly large. To put it differently, as the number of terms increases, the wiggles in the expansion (23) between the data points become more and more uncontrolled. Therefore, one may well wonder what would happen if more data points were read off the curve in Figure 40. To examine this matter, points were interpolated midway between each pair of the original 37 data points read from the curve in Figure 40, thus providing a 73-point table. Then this operation was repeated, producing a 145-point table. Then pressure calculations were made, using polynomial expansions with more and more terms based on each of these expanded tables. In each case the computed pressure distribution remained much the same as those shown for the smoothed data in Figures 41 and 42, until finally the number of terms became too great and the computed pressures deteriorated badly. The quality of these experimental calculations was as follows:

	11 terms	21 terms	31 terms	41 terms	51 terms	61 terms
37 points	good	good	bad			
73 points	good	good	good	bad	bad	bad
145 points	good	good	good	good	good	poor

In order to understand why long series may give bad results, it should be remembered that the coefficients α_n for the series (14) are now being found by a least-squares fitting procedure instead of by the integration shown in (4). Thus a particular coefficient α_k changes as more terms are added to the series. Eventually the expansion tries to fit even irrelevant irregularities in the data, and in so doing produces many unduly large coefficients α_n os high order which predict spurious pressure. Expanding the number of data points serves to postpone this difficulty.

These calculations show that both smoothing and interpolation of the data serve to stabilize the pressure calculations, making it possible to handle longer polynomial expansions. This fact can be of considerable value when a long expansion is needed in order to examine some sharp detail of a pressure distribution. However, the precise length of pressure series obtainable from clearances at a given number of points may depend also on the particular set of clearances, so the above tabulation does not provide an absolute guide to the length of series derivable in all cases.

Calculations Based on Modified Clearance Patterns

A Pressure Spike. The preceding discussion has been concerned with how long a series expansion for the pressure distribution may be justified by the data, but it is equally relevant to inquire how long a series may be needed to describe a pressure distribution adequately. In order to examine this matter, a modified version of the smoothed profile of Figure 40 was selected, which was expected to correspond to a sharp peak or spike in the pressure distribution. This modification, together with two others selected for other purposes, is shown in Figure 43, where it is identified as modification 1. It should be observed that modification 1 introduces changes in h of only slightly more than one microinch, that is to say changes that are almost within the scattering of the data shown in Figure 40.

In order to make detailed analysis of the pressure corresponding to modification 1 possible, it was expected that many terms would be needed in the expansion. Therefore, a table of interpolated clearances was prepared containing 289 points. Polynomial expansions of lengths 11, 21, 31, 41, 51, 61, and 71 were fitted to these points, and the pressure distributions corresponding to each of these expansions were computed at intervals of length 0.025 in ξ between $\xi = -1$ and $\xi = +1$. The results of these pressure calculations are shown in Figure 44.

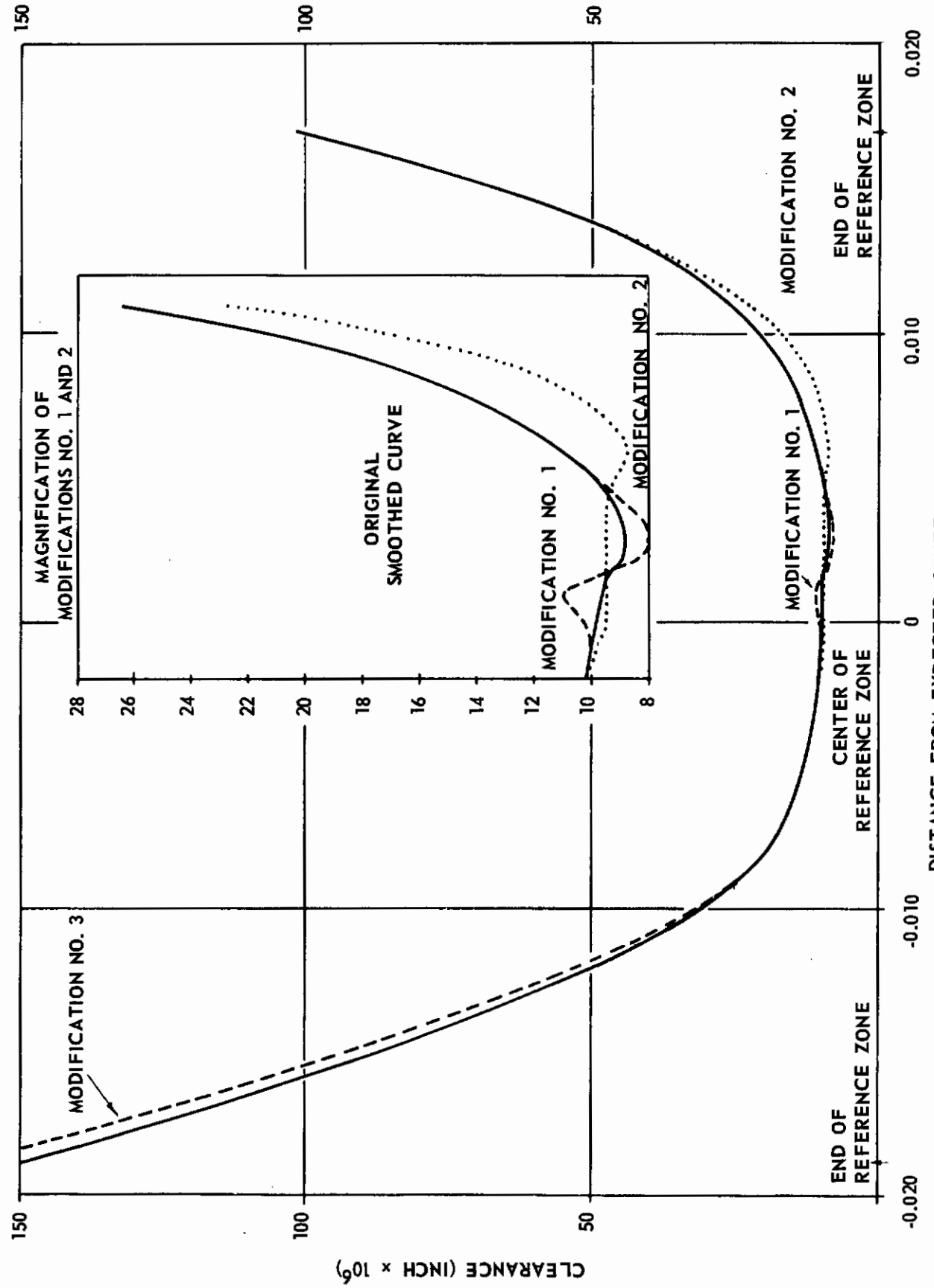

FIGURE 43. MODIFIED CIRCUMFERENTIAL CLEARANCE PROFILE USED FOR PRESSURE SENSITIVITY STUDY

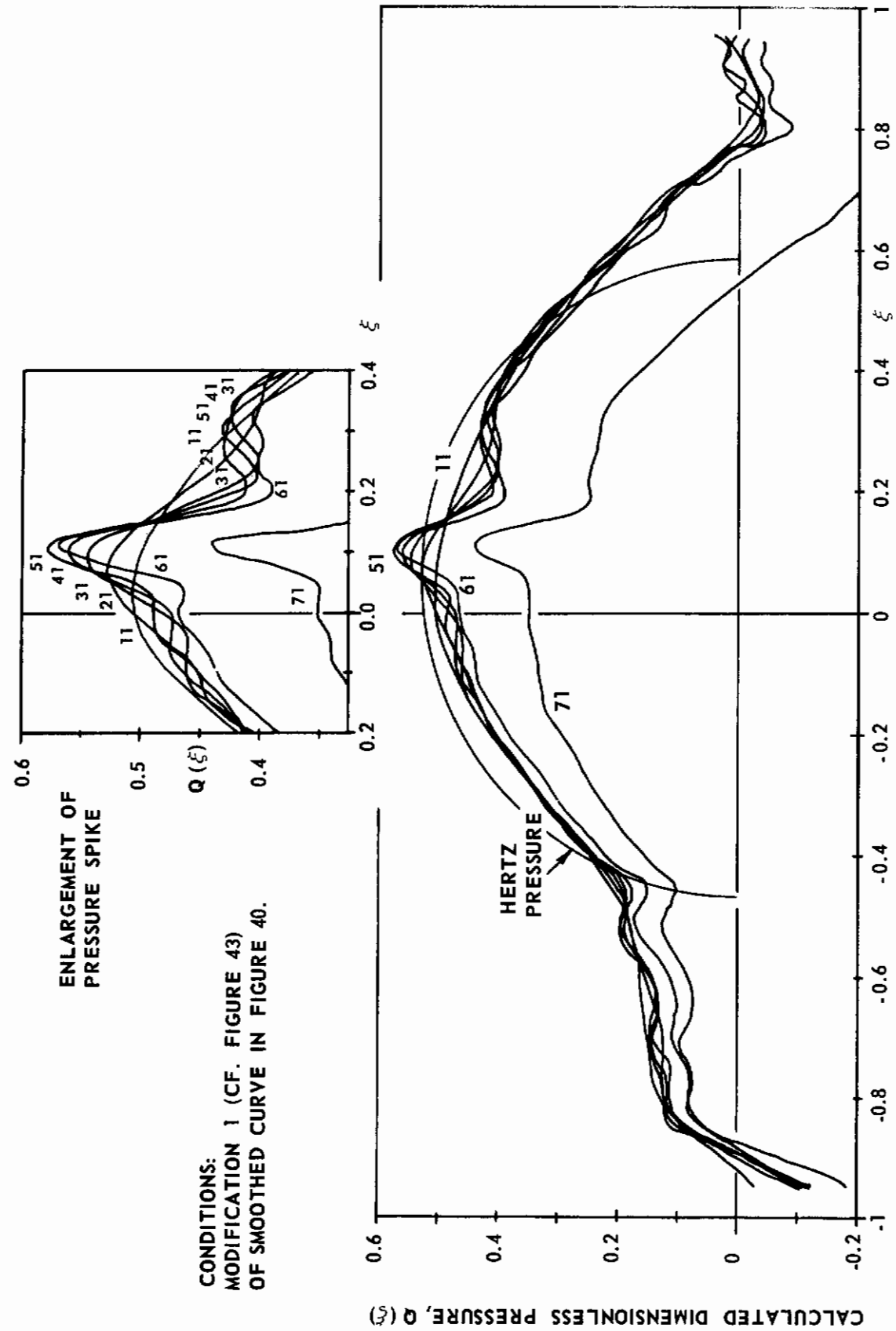

FIGURE 44. A PRESSURE DISTRIBUTION CONTAINING A SPIKE, AS COMPUTED FROM SERIES OF VARIOUS LENGTHS BASED ON A SMOOTHED 289-POINT TABLE (MODIFICATION 1)

Examination of Figure 44 shows that modification 1 does indeed imply a pressure spike which increases the maximum pressure by about 15 per cent. The 11-term series gives no indication of the spike, and the 21-term series shows it only feebly. The sharpness of the spike continues to grow with increasing length of the series up to 51 and perhaps even to 61 terms. Series of those lengths seem to have converged moderately well in showing the details of pressure around the spike, but when 71 terms are used the series expansion begins to fail because it is excessively long for the 289 point table that was used, which specified smoothed values of h to within a tenth of a microinch.

This calculation of a pressure spike shows that clearance data analyzed according to the present plan can indeed show pressure spikes, even though very sharp spikes may cause much difficulty. If a pressure spike is to be analyzed, clearance readings in the spike region need to be made at intervals which are substantially less than one per cent of the width of the dry contact area. (Elsewhere, coarser intervals may be used and the data table may be amplified with interpolated values, which have been observed previously to be harmless and which serve to keep the high-order terms of the expansion under control.) If a given table of data is pressed to excessive length of the polynomial expansion without first converging satisfactorily to a pressure distribution, then it becomes necessary to expand the table in order to pursue the pressure analysis further. In the region of the spike, the expansion of the table should be based on actual measurements of the clearance performed accurately enough so that the data vary quite smoothly. Fortunately, it appears that tables with probably attainable detail should provide interesting pressure detail.

In the analysis of pressure spikes, it may become desirable to revise the pressure calculation method by using non-uniformly spaced data with denser readings in the spike region. It can be noted that this is possible, though some changes would be needed in the computing program. In minimizing the sum of the squared residuals, as in (11), it may be desirable to weigh the residuals according to the expected accuracy at their individual locations. One plausible weighting is in proportion to the inverse square of the standard deviation at each location, and this would emphasize fitting near the central part of the contact region, where spikes are more apt to occur. Both these modifications, and perhaps others, eventually may prove to be useful in pressure spike analysis.

Minor Modifications. A second modification of the smoothed curve of Figure 40 was selected as representing another attribute of clearance profiles found by elastohydrodynamic theory. It is shown as modification 2 in Figure 43. It has a longer flat region in the center, followed by a steeper rise at the outlet than the original curve has. The pressure distribution calculated with a 21-term expansion derived from a 73-point table of this modification 2 is shown in Figure 45. The pressure drop in the outlet side is somewhat steeper than the drop calculated from the original clearance curve, but the change is not very drastic.

Modification 2 may be viewed also as representing a possible ambiguity of the data on account of an uncertain correction for absorption at the beginning of the outlet region. The fact that it affected the calculated pressure as little as it did is mildly reassuring in that it suggests that miscalibration in this region may not cause as drastic errors in the calculated pressures as might have been feared.

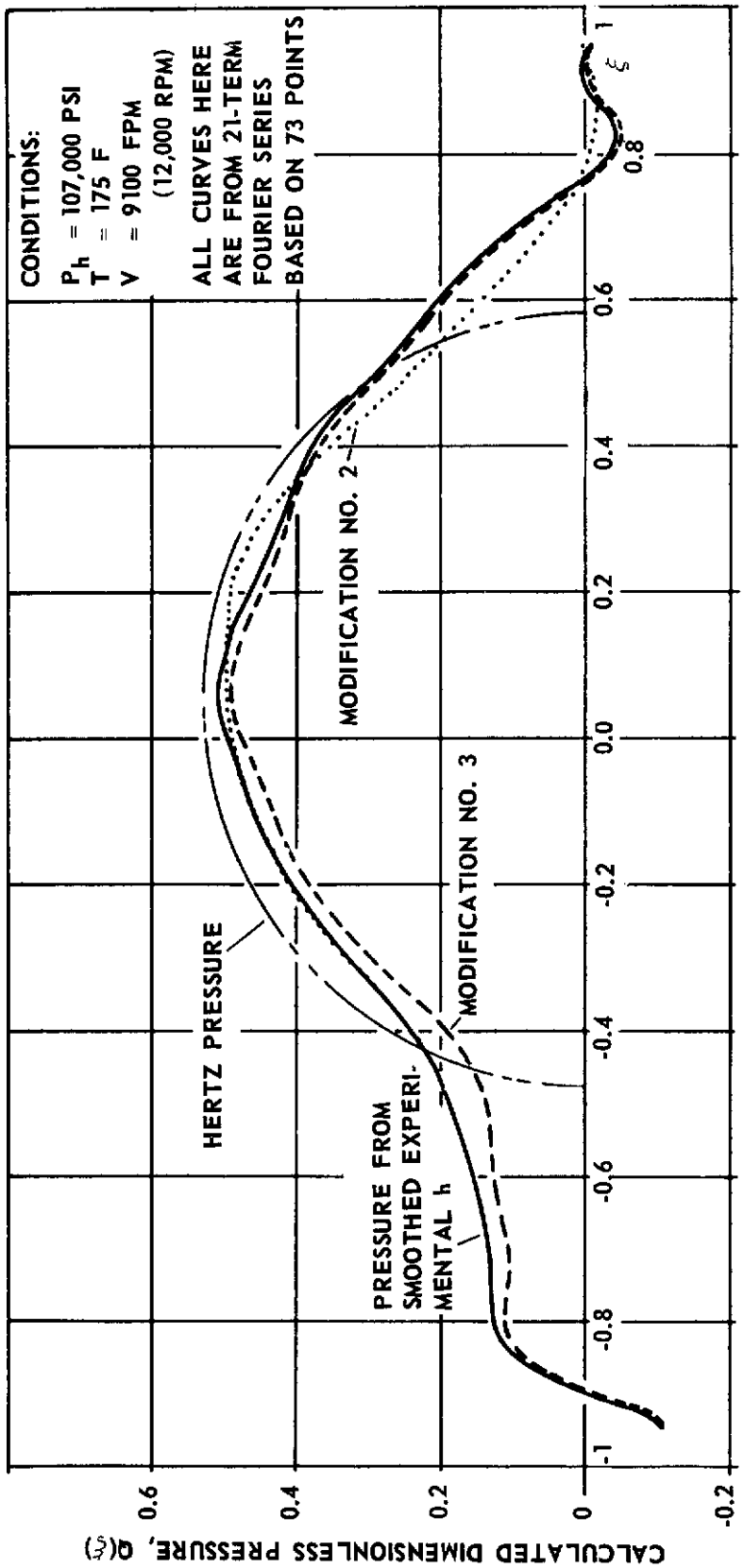

FIGURE 45. EFFECT OF MINOR CLEARANCE CHANGES ON CALCULATED PRESSURE DISTRIBUTION

A third modification was tried to indicate what difficulties might be associated with measuring errors in the inlet region. (X-ray data at the far inlet and outlet regions have shown so much scatter that smoothing of data in those regions has on occasion been governed largely by the exterior Hertz profile that it was believed the data should approach.) This third alteration of the clearance profile is shown as modification 3 in Figure 43, and the pressure distribution derived from it is shown in Figure 45. (The calculation employed a series of 21 terms based on a 73-point table.) Surprisingly, one principal effect of this modification seems to be a slight lowering of the entire pressure curve; in addition, there is a somewhat larger drop near the edge of the dry-contact area on the inlet side. This suggests that when the over-all load predicted by a pressure calculation differs substantially from the known applied load (as has been observed in past calculations), the trouble may lie in the asymptotic behavior of the clearance data in the end regions. This is a reminder that clearance data should extend a substantial distance beyond the dry-contact area, especially in the inlet region where comparison with an exterior Hertz profile is more ambiguous than in the outlet region.

With attention drawn to the inlet region as it is by Modification 3, it should be remarked that the present calculations probably would have been more satisfying if the experimental data had extended farther into the inlet region. The sharp drop in the calculated pressure beyond $\xi = -0.9$ for all the cases treated here suggests that more clearance data were needed beyond that point. If they had been available, they could have been included in the analysis simply by enlarging the reference zone used in the pressure calculation.

Conclusions Concerning Accuracy of Pressure Calculations

An objective and even mechanized method has been evolved for computing pressure distributions acting between lubricated rolling disks from measurements of the disk separation at a discrete set of points. It appears that X-ray measurements of this separation should be quite useful in getting moderately well detailed pressure calculations, though the measurements now available support only first order estimates of the pressure distributions.

The study of accuracy of these calculations was based on the structure of the solution in terms of a series of Tchebyshev polynomial. The study was divided essentially in two parts: how long a series can a given set of data justify, and how long a series is needed to attain the kind of solution that should be desired.

The length of series which is justified is governed both by the number of positions where disk separation is measured and by the accuracy of those measurements. With current accuracy of measurements, readings at 37 positions justify only about 10 terms. Readings at more positions would justify more terms, but the ratio of the number of justifiable terms to the number of reading positions probably would not increase. Repetition of readings likewise should justify more terms, but the extent of this improvement needs further study. Smoothing and interpolation of the data may make evaluation of many more terms possible (indeed more than 60 terms

have been computed reasonably on this basis), but eventually the irregularities in any set of inexact data produce unduly large high-order terms which predict badly erroneous pressures.

Two methods are available for judging the length of series to be used. One is to truncate the series when the variance of its fit to the data becomes as small as the average variance in the data. (This method could be improved by using residuals weighted according to location of the reading.) The other method is to compute pressure distributions from series of increasing length, seeking a limiting distribution which hopefully will be attained before the series deteriorates because of excessive length (that is, overfitting of the data).

Some notion of the length of series needed was sought on the basis of a modified profile thought to correspond to a pressure spike. Calculations based on series up to 71 terms long did show the presence of a spike about 15 per cent as large as the maximum Hertz pressure. The series of lengths 51 and 61 appeared to be fairly satisfactory. It is possible that equally useful results could have been attained with shorter series based on readings concentrated near the spike region. (It would have been possible to analyze these by reprogramming the calculation modestly.) It is possible also that better results could have been obtained by using weighted residuals in the calculation. Thus it appears it should be possible to make measurements which should give at least fair indication of the presence of a pressure spike.

Unclassified

Security Classification

DOCUMENT CONTROL DATA - R&D

(Security classification of title, body of abstract and indexing annotation must be entered when the overall report is classified)

1. ORIGINATING ACTIVITY (Corporate author) Battelle Memorial Institute	2a. REPORT SECURITY CLASSIFICATION Unclassified 2b. GROUP --

3. REPORT TITLE "A Study of the Influence of Lubricants on High-Speed Rolling Contact Bearing Performance. Part V. Research on Elastohydrodynamic Lubrication on High-Speed Rolling Contacts"

4. DESCRIPTIVE NOTES (Type of report and inclusive dates)
Final report, February 1964 - February 1965

5. AUTHOR(S) (Last name, first name, initial)
Kannel, Jerrold; Bell, J. Clarence; Walowit, J. A.; et al.

6. REPORT DATE	7a. TOTAL NO. OF PAGES	7b. NO. OF REFS
July 1965	84	13

8a. CONTRACT OR GRANT NO.	9a. ORIGINATOR'S REPORT NUMBER(S)
AF 33(615)-1311 b. PROJECT NO. 3044 c. Task No. 304401 d.	ASD-TDR-61-643, Part V 9b. OTHER REPORT NO(S) (Any other numbers that may be assigned this report) --

10. AVAILABILITY/LIMITATION NOTICES
Qualified requesters may obtain copies of this report from DDC.

11. SUPPLEMENTARY NOTES	12. SPONSORING MILITARY ACTIVITY
	Air Force Aero Propulsion Laboratory Wright-Patterson Air Force Base, Ohio

13. ABSTRACT

The effects of lubricants on the performance of heavily loaded rolling-contact elements have been studied experimentally and theoretically. Measurements of the deformations of lubricated rolling elements have been made using an X-ray technique for a range of loadings, temperatures, rolling speeds, and lubricants. A qualitative agreement appears to exist between variations in deformation profiles with lubricant types and variations in existing fatigue life with lubricant type. Efforts have been made to infer film pressures from the deformation measurements. Film pressures have been measured between steel as well as quartz disks using a manganin pressure transducer. For the heavily loaded conditions, a slight pressure spike appears in the measurements of pressures between steel disks. Stresses in the rolling elements have been inferred from the pressure measurements. The magnitudes of the maximum stresses do not deviate significantly from the Hertzian stresses although the location of the maximum shearing stress is much closer to the surface. The temperature on the surface of a pair of quartz disks has been measured using an evaporated resistance thermometer type transducer. The magnitude of the measured apparent temperature appears to be higher than anticipated resembling the peak temperature predicted assuming no heat loss from the lubricant to the disk for the pass of each fluid element through contact. Some rheology experiments have been conducted with a highly refined mineral oil.

DD FORM 1 JAN 64 1473

Unclassified

Security Classification